ATLAS Note

ATL-COM-PHYS-2016-485

Draft version 0.4

Search for Higgs pair production in the final state of $WW^*WW^*(\to \ell^\pm \nu \ell^\pm qqqq)$ using 36.1 fb^{-1} pp collision data recorded at $\sqrt{s}$ = 13 TeV with the ATLAS detector

Xinchou Lou[a,e], Yaquan Fang[a], Weiming Yao[b], Liang Li[c], Xiaohu Sun[d], Xingguo Li[c], Maosen Zhou[a]

[a]*Institute of High Energy Physics, Chinese Academy of Sciences*
[b]*Lawrence Berkeley National Laboratory and University of California, Berkeley*
[c]*Shanghai Jiao Tong University, China*
[d]*University of Alberta, Canada*
[e]*University of Texas at Dallas, USA*

9th July 2017

A search is performed for resonant and non-resonant Higgs pair production with each Higgs boson decaying to a W boson pair using 36.1 fb^{-1} of proton-proton collision data at $\sqrt{s}$ = 13 TeV recorded by the ATLAS detector at the Large Hadron Collider. The final state considered in this analysis contains two same-electric-charge leptons, missing energy and jets. In this case, both electroweak and QCD backgrounds are strongly suppressed. The data are found to be consistent with the expectation of the backgrounds and an upper limit at 95% C.L. is set for the production cross section. For the non-resonant Higgs pair production, the observed (expected) upper limit on $\sigma(gg \to hh)$ is xxx pb (151.45 pb). For resonant Higgs pair production($gg \to X \to hh$), the observed (expected) upper limits range from xxx pb (24.74 pb) to xxx pb (3.88 pb) as a function of resonant mass in the range 260 GeV < m_X <500 GeV. Additionally, observed (expected) limits are set on a model($gg \to X \to SS$) that introduces a new Higgs-like scalar, S, that has the same coupling as the Standard Model Higgs boson. The limits on this model range from xxx pb (0.29 pb) to xxx pb (5.25 pb) as a function of m_X and m_S in the ranges 280 GeV $\leq m_X \leq$ 340 GeV and 135 GeV $\leq m_S \leq$ 165 GeV. The narrow-width approximation is assumed for all heavy-Higgs models used in this analysis.

Contents

1 Change Log

1.1 Version 0.X

- To include trigger SF uncertainty(plan to use v29 samples(running), which has complete uncertainty);
- To include theoretical uncertainty.

1.2 Version 0.4

22/06/2017, updated v04 from v03

- Included HSS production and results.

1.3 Version 0.3

19/06/2017, updated to v03 from v02:

- Updated to v27.01 samples;
- Included di-lepton triggers;
- Retrieved all experimental uncertainties.

1.4 Version 0.2

v26.02 nutples being used.
16/03/2017, updated to v02 from v01:

- Updated to results using v26.02;
- Implemented comments on CDS;
- Added new variable(`ChargeIDBDTTight`) to suppress QmisID.

1.5 Version 0.1

v23.02 nutples being used.
24/02/2017, updated to v01 from v00:

- Re-arranged the order of plots;
- Completed event yields of all resonant search;
- Included limits;
- Included (un)blinding strategy;
- Included change log itself.

2 (Un)blinding strategy

To avoid the effect of the data on the optimisation strategy, the following strategy has been used.

- Data are not used in any way in the optimisation strategy from preselection to the signal region.
- The optimisation is based on the existing MC samples and on the sample of fakes estimates. Additional checks are done to avoid statistical fluctuations in the MC (extremely low signal efficiencies are not considered).
- Data events are removed from all plots and tables if it fulfils the signal region cuts for any of the optimisation points. This restriction is applied to data only, in order to be able to contemplate the signal region expectations in cut-flows, efficiency determinations etc.

The unblinding will include 36.1 fb^{-1} data collected from 2015 to 2016.

3 Introduction

A Higgs boson was discovered by the ATLAS and CMS collaborations [1, 2] in 2012 and has been subsequently studied by spin and coupling measurements, which have established that its properties are very similar to the ones of the SM Higgs boson. These measurements are based on Higgs production via gluon-fusion, vector-boson-fusion and in association with a W or Z boson.
The Standard Model predicts production of Higgs boson pairs via top loops as well as through self-coupling. Although this production cross section is expected to be well below the sensitivity of the current data. However, the Higgs pair production can be significantly enhanced either by altering the Higgs boson self-coupling λ_{hhh} or in extended Higgs sectors such as 2-Higgs-Doublet Model (2HDM).
In RUN I, various channels were explored with the ATLAS detector, such as $bb\gamma\gamma$ [3], $bbbb$ [4], $bb\tau\tau$ and $WW\gamma\gamma$ [5]. $WWWW$ channel with two same-signed leptons or three leptons have been studied phenomenologically [6, 7].
In addition to the hh production mechanisms described above, this analysis searches for evidence of an additional extended Higgs sector model that introduces two new heavy Higgs bosons, X and S [8]. In this model, X couples strongly to both S and h. S couples weakly to SM particles, suppressing direct production, but has the same mass-dependent branching ratios as h. The process considered in this analysis is $X \to SS$.

Because the channel of $X \to SS \to 4W$ has the highest production rate in this model for the mass ranges $2m_h < m_X < 2m_t$ and 135 GeV $< m_S < 2m_t - m_h$. Values of m_X greater than $2m_t$ are not considered because above this value, $X \to t\bar{t}$ is expected to be the dominant decay mode. Furthermore, m_S is assumed to be greater than 135 GeV such that $S \to WW^{(*)}$ is the dominant decay mode.

This note provides supporting material for the search of Higgs pair production with the decay of $hh \to WWWW$ where a pair of the same-signed Ws decay to leptons and the rest to hadrons. The multi-lepton selection can strongly suppress the QCD backgrounds. In addition, the same-signed leptons requirement can further reduce the standard model backgrounds, such as $t\bar{t}$, Drell-Yan, and W^+W^- processes. The analysis for different processes but with similar event signature have been studied by other groups at ATLAS, such as SUSY, $t\bar{t}h$, and the same-signed W pair searches [9, 10].

This note is organized as follows. A brief introduction on the ATLAS detector is given in Section 4. In Section 5, the current data and the MC samples relevant for this analysis are described. Section 6 defines the objects such as lepton, jet etc. used in this analysis. In Section 7.1 the pre event selections and signal topology are summarized. The estimations of the different backgrounds are discussed in Section 8. After background estimations, signal optimizations are performed in section 9. All the systematical uncertainties are discussed in Section 10. Section 11 documents the statistical procedure used to extract the sensitivity of the analysis. Finally, section 12 summarizes the results and conclusions of the study in this note.

4 The ATLAS detector

The ATLAS detector [11] at the LHC covers nearly the entire solid angle around the collision point. It consists of an inner tracking detector surrounded by a thin superconducting solenoid, electromagnetic and hadronic calorimeters, and a muon spectrometer incorporating three large superconducting toroid magnets. The inner-detector system (ID) is immersed in a 2 T axial magnetic field and provides charged particle tracking in the range $|\eta| < 2.5$.

The high-granularity silicon pixel detector covers the vertex region and typically provides three measurements per track, the first hit being normally in the innermost layer. It is followed by the silicon microstrip tracker which usually provides four two-dimensional measurement points per track. These silicon detectors are complemented by the transition radiation tracker, which enables radially extended track reconstruction up to $|\eta| = 2.0$. The transition radiation tracker also provides electron identification information based on the fraction of hits (typically 30 in total) above a higher energy deposit threshold corresponding to transition radiation.

The calorimeter system covers the pseudorapidity range $|\eta| < 4.9$. Within the region $|\eta| < 3.2$, electromagnetic calorimetry is provided by barrel and endcap high-granularity lead/liquid-argon (LAr) electromagnetic calorimeters, with an additional thin LAr presampler covering $|\eta| < 1.8$, to correct for energy loss in material upstream of the calorimeters. Hadronic calorimetry is provided by the steel/scintillating-tile calorimeter, segmented into three barrel structures within $|\eta| < 1.7$, and two copper/LAr hadronic endcap calorimeters. The solid angle coverage is completed with forward copper/LAr and tungsten/LAr calorimeter modules optimised for electromagnetic and hadronic measurements respectively.

The muon spectrometer (MS) comprises separate trigger and high-precision tracking chambers measuring the deflection of muons in a magnetic field generated by superconducting air-core toroids. The precision chamber system covers the region $|\eta| < 2.7$ with three layers of monitored drift tubes, complemented by cathode strip chambers in the forward region, where the background is highest. The muon trigger system covers the range $|\eta| < 2.4$ with resistive plate chambers in the barrel, and thin gap chambers in the endcap regions.

A two-level trigger system is used to select events. The first-level trigger is implemented in hardware and uses a subset of the detector information to reduce the accepted rate to a design maximum of 100 kHz. This is followed by a software-based trigger with a maximum average accepted event rate of 1 kHz.

5 Data set and Monte Carlo samples

5.1 Data set

This analysis uses the complete set of $\sqrt{s} = 13$ TeV pp data collected by ATLAS in 2015 and 2016. The data must pass the `All_Good` GRL, which uses only data in which there are no major detector defects. This corresponds to a total integrated luminosity of 36.1 fb^{-1}. The data set was produced with xAOD format, and followed HIGG8D1 derivation, which provides a reduction model specifically optimised for the $t\bar{t}H$ analysis with multiple leptons in the final states. These reductions contain slimming (removing unneeded variables), thinning (removing entire objects from events) and skimming (removing whole events with very loose preselections). The skimming is performed such that events are required to contain at ≥ 2 loose electrons or muons with $|\eta| < 2.6$ and $p_{\mathrm{T}} > 5$ GeV such that the leading electron has $p_{\mathrm{T}} > 15$ GeV or to contain ≥ 1 loose electron or muon and ≥ 2 loose τ candidates.

5.2 Monte Carlo samples

5.2.1 Signal samples

Signal samples of $gg \to hh$ were generated by MadGraph5 and Herwig++. For non-resonant signal, the event generation was performed using a next-to-leading order SM Higgs pair model [12] in MadGraph5. For resonant signal samples, the event generation was also performed using a next-to-leading order heavy resonant model [12] called `2HDMCP_EFT` in MadGraph5. The heavy scalar, X, is assumed to have narrow width with respect to the experimental resolution. The decay width of the X boson in the simulation is set to 10 MeV for the following mass points: 260 GeV, 300 GeV, 400 GeV and 500 GeV. The card used in MadGraph5 for signal event generations is attached in Appendix A. Subsequently, the X boson is required to decay into a pair of SM Higgs bosons, both of which decay into a pair of W bosons using Herwig++. Finally, two $W^+(W^-)$ are forced to decay leptonically (taus included), while the other two $W^-(W^+)$ hadronically. All the signal samples are list in Tab. 1. It has been decided that the samples provide sufficient statistics for the analysis. Non-resonant hh production is assumed to have a production cross-section of $\sigma^{\mathrm{NLO}}_{gg\to hh} = 33.41$ fb [13] and resonant production is assumed to have a production cross-section of $\sigma_{gg\to X\to hh} = 1$ pb for all values of m_X. In both resonant and non-resonant production, a branching ratio of $\mathrm{BR}(hh \to 4W \to \ell^{\pm}\nu\ell^{\pm}\nu qqqq) = 4.4\times 10^{-3}$ is used.

The $H \to SS$ samples are produced at LO using Pythia8 [14] with the A14NNPDF2.3LO PDF set [15]. The Pythia8 HiggsBSM:gg2A3 model is used. X is constrained to decay only to SS and S is constrained to decay to a pair of W-bosons. Both X and S are assumed to have a narrow decay width with respect to the experimental resolution and are therefore set to 1% of their pole masses. An event-level filter is used to only accept events in which two same-signed W-bosons decay leptonically (τs included), while the remaining two W-boson decays hadronically. In order to maximise the event generator efficiency, events are split into two samples by lepton charge: the + samples have two positive leptons and the − samples have two negative leptons. A set of mass points is used to test the sensitivity across the full range of m_X and m_S to which the 4W analysis is expected to be sensitive. The set is chosen such that m_X can be fixed to measure the sensitivity as a function of m_S and vice versa. A summary of the $X \to SS$ samples used is given in Table 2. All $X \to SS$ samples are assumed to have a production cross-section of $\sigma_{gg\to X\to SS} = 1$

DSID	lepton charge	m_X [GeV]	Num. Events	Simulation	e/a/s/r/p-tags
344133	(+)	Non-res	500000	AFII	e5060, a766, a821, r7676, p2949
344134	(-)	Non-res	500000	AFII	e5060, a766, a821, r7676, p2949
343704	(+)	260	100000	AFII	e5234, a766, a821, r7676, p2949
343712	(-)	260	100000	AFII	e5234, a766, a821, r7676, p2949
343706	(+)	300	100000	AFII	e5234, a766, a821, r7676, p2949
343714	(-)	300	100000	AFII	e5234, a766, a821, r7676, p2949
343709	(+)	400	100000	AFII	e5153, a766, a821, r7676, p2949
343717	(-)	400	100000	AFII	e5153, a766, a821, r7676, p2949
343711	(+)	500	100000	AFII	e5153, a766, a821, r7676, p2949
343719	(-)	500	100000	AFII	e5234, a766, a821, r7676, p2949

Table 1: Summary of the MC hh samples which have been produced for study.

pb and branching ratio into the final state based on the mass-dependent expected branching ratios of the SM Higgs boson [16].

In the analysis, the two charge sides are considered simultaneously.

Charge	m_X	m_S	BR(SS two SS leptons)	DSID	N_{events}
	280 GeV	135 GeV	1.47×10^{-2}	344927	25000
	300 GeV	135 GeV	1.535×10^{-2}	344928	25000
	320 GeV	135 GeV	1.535×10^{-2}	344930	25000
+	340 GeV	135 GeV	1.535×10^{-2}	344933	25000
	340 GeV	145 GeV	3.454×10^{-2}	344934	25000
	340 GeV	155 GeV	6.049×10^{-2}	344935	24000
	340 GeV	165 GeV	8.842×10^{-2}	344936	25000
	280 GeV	135 GeV	1.47×10^{-2}	344937	25000
	300 GeV	135 GeV	1.535×10^{-2}	344938	25000
	320 GeV	135 GeV	1.535×10^{-2}	344940	25000
−	340 GeV	135 GeV	1.535×10^{-2}	344943	25000
	340 GeV	145 GeV	3.454×10^{-2}	344944	24000
	340 GeV	155 GeV	6.049×10^{-2}	344945	25000
	340 GeV	165 GeV	8.842×10^{-2}	344946	25000

Table 2: Summary of the MC $X \to SS$ signal samples used.

5.2.2 Background samples

Diboson, Z+jets and W+jets events are generated with Sherpa v2.1. The CT10 PDF set is used for these samples. $t\bar{t}$ background events are generated with Powheg v2.0 [17] and interfaced with Pythia6 for the parton showering and fragmentation. The Perugia 2012 (P2012) parameter set (tune) with the CTEQ6L1 PDF set is used for the underlying event (UE) description. A filter requiring at least one lepton is included. The $t\bar{t}$ cross section is 832 pb at $\sqrt{s} = 13$ TeV. Powheg is also used to model other top backgrounds such as single top t-channel, s-channel and Wt. $t\bar{t}V$ background events are generated with MadGraph, interfaced with Pythia8. Three $t\bar{t}W$ background samples, with 0, 1 and 2 additional partons are generated. The total $t\bar{t}W$ cross section is 566 fb at $\sqrt{s}$ = 13 TeV. The $t\bar{t}Z$ ($Z \to ll, l = e, \mu$) samples generated with 0 and 1 additional partons. The total $t\bar{t}Z$ cross section is 760 fb at $\sqrt{s}$ = 13 TeV. All $t\bar{t}V$ samples use A14NNPDF2.3LO PDF set. A summary of the background samples used is given in Table 3.

Background	DSID	Process	Generator	cross-section(pb)	K-factor	Simulation
VV	342284	$WH125\_inc$	Pythia8	1.1021	1.0	Full
	342285	$ZH125\_inc$	Pythia8	0.60072	1.0	Full
	361063	$llll$	Sherpa	12.583	0.91	Full
	361064	$lllvSFMinus$	Sherpa	1.8446	0.91	Full
	361065	$lllvOFMinus$	Sherpa	3.6235	0.91	Full
	361066	$lllvSFPlus$	Sherpa	2.5656	0.91	Full
	361067	$lllvOFPlus$	Sherpa	5.0169	0.91	Full
	361069	$llvvjj\_ss\_EW4$	Sherpa	0.02575	0.91	Full
	361070	$llvvjj\_ss\_EW6$	Sherpa	0.043375	0.91	Full
	361071	$lllvjj\_EW6$	Sherpa	0.042017	0.91	Full
	361072	$lllljj\_EW6$	Sherpa	0.1279	0.91	Full
	361073	$ggllll$	Sherpa	0.02095	0.91	Full
VVV	361620	WWW_3l3v	Sherpa	0.008343	1.0	Full
	361621	WWZ_4l2v	Sherpa	0.001734	1.0	Full
	361623	WZZ_5llv	Sherpa	0.00021783	1.0	Full
	361624	WZZ_3l3v	Sherpa	0.000855458	1.0	Full
	361625	ZZZ_6l0v	Sherpa	1.7059×10^{-5}	1.0	Full
	361626	ZZZ_4l2v	Sherpa	9.9467×10^{-5}	1.0	Full
$t\bar{t}V$	410155	ttW	aMC@NLO+Pythia8	0.5483	1.1	Full
	410156	$ttZnunu$	aMC@NLO+Pythia8	0.15499	1.11	Full
	410157	$ttZqq$	aMC@NLO+Pythia8	0.52771	1.11	Full
	410218	$ttee$	aMC@NLO+Pythia8	0.036888	1.12	Full
	410219	$ttmumu$	aMC@NLO+Pythia8	0.036895	1.12	Full
	410220	$tttautau$	aMC@NLO+Pythia8	0.036599	1.12	Full
	410081	$ttbarWW$	MadGraph+Pythia8	0.0080975	1.2231	Full
tV	410013	$Wt\_inclusive\_top$	Powheg	34.009	1.054	Full
	410014	$Wt\_inclusive\_antitop$	Powheg	33.989	1.054	Full
	410050	$tZ\_4fl\_tchan\_noAllHad$	Madgraph+Pythia	0.24013	1.0	Full
	410215	$tWZDR$	Pythia8+EvtGen	0.015558	1.0	Full
$t\bar{t}H$	341177	$ttH \to ll + H$	aMC@NLO+Herwig++	0.05343	1.0	Full
	341270	$ttH \to ljets + H$	aMC@NLO+Herwig++	0.22276	1.0	Full
	341271	$ttH \to allhad + H$	aMC@NLO+Herwig++	0.23082	1.0	Full
$3/4t$	304014	$3top\_SM$	MadGraph+Pythia8	0.0016398	1.0	Full
	410080	$4topSM$	MadGraph+Pythia8	0.0091622	1.0042	Full

Table 3: Summary of the MC background samples for the prompt background. The prompt background includes $t\bar{t}V$, $VV(W^{\pm}W^{\pm}, W^{\pm}Z, ZZ)$, tV and $t\bar{t}H$ and VVV.

5.2.3 Detector simulation

All background Monte Carlo samples are processed through a detector simulation of the ATLAS detector response [18] based on Geant4 [19]. All signal Monte Carlo samples are processed through the ATLAS fast simulation framework [18] that uses a parameterised calorimeter response which has been extensively validated against Geant4. Additional simulated pp collisions generated with Pythia8 and the MSTW2008LO [20] PDF set are overlaid to model the effects of both in- and out-of-time pileup, from additional pp collisions in the same and nearby bunch crossings. The average number of primary interactions per bunch crossing ($\langle\mu\rangle$) in the simulation is reweighed to match the $\langle\mu\rangle$ distribution observed in data. All simulated events are processed using the same reconstruction algorithms and analysis chain for data. Additional corrections are applied to simulated samples such that the object reconstruction, identification and isolation efficiencies, energy scales and energy resolutions in the simulation match those determined from data.

6 Object definition

This section outlines the lepton, jet, and $E_{\mathrm{T}}^{\mathrm{miss}}$ selections used in this analysis. Both loose and tight definitions are given for leptons and all leptons are required to pass the loose requirements. The signal region is defined using tight leptons.

6.1 Electrons

- $E_{\mathrm{T}} > 10$ GeV
- $|\eta| < 2.47$ and the crack region $1.37 < |\eta| < 1.52$ is excluded.
- Loose selection:
  - ID: `LooseLH`[1] electron quality requirement
  - Isolation: Two isolation variables are computed: $E_{\mathrm{T}}^{\mathrm{cone20}}/p_{\mathrm{T}}$[2] and $p_{\mathrm{T}}^{\mathrm{varcone20}}/p_{\mathrm{T}}$[3]. Flat efficiencies of 99% in $\eta - p_{\mathrm{T}}$ plane are achieved for electrons by applying cuts on those two isolation variables. The `Loose` isolation working point is used.
  - $|z_0 \sin\theta| < 0.5$ mm[4] and $d_0/\sigma(d_0) < 5$[5]
- Tight selection:
  - ID: `TightLH` electron quality requirement
  - Isolation: `FixedCutTight` ($E_{\mathrm{T}}^{\mathrm{cone20}}/p_{\mathrm{T}}$ <0.06, $p_{\mathrm{T}}^{\mathrm{varcone20}}/p_{\mathrm{T}}$ <0.06) working point

[1] A likelihood-based discriminant, based on shower shapes in electromagnetic calorimeter and track qualities from inner detector, is used to separate electrons from fakes due to hadron decays and photon conversions. The LooseLHElectron working point is used, which gives an approximate 95% electron selection efficiency.

[2] $E_{\mathrm{T}}^{\mathrm{cone20}}/p_{\mathrm{T}}$ is based on the energy of calorimeter topological clusters in a cone of $\Delta R < 0.2$ around the lepton candidate(with energy from itself being subtracted)divided by its transverse momentum.

[3] $p_{\mathrm{T}}^{\mathrm{varcone20}}/p_{\mathrm{T}}$ is the scaler sum of all track momentum in a cone of $\Delta R < 0.2$ (with excluding the tracks associated to itself)around the candidate, divided by its transverse momentum.

[4] The longitudinal impact parameter of the lepton track with respect to the selected event primary vertex, multiplied by the sine of the polar angle.

[5] The transverse impact parameter divided by the estimated uncertainty on its measurement

6.2 Muons

- $p_T > 10$ GeV
- $|\eta| < 2.5$
- Loose selection:
  - ID: `Loose` muon quality requirement
  - Isolation: Similar with electron, E_T^{cone20}/p_T and $p_T^{\text{varcone20}}/p_T$ are computed, and `Loose` working point is used
  - $|z_0 \sin\theta| < 0.5$ mm and $d_0/\sigma(d_0) < 3$
- Tight selection:
  - ID: `Tight` muon quality requirement
  - Isolation: `FixedCutTightTrackOnly` ($p_T^{\text{varcone20}}/p_T < 0.06$) working point

6.3 Jets

- Jets are reconstructed using the anti-k_T algorithm with a radius parameter of $R = 0.4$ from topological clusters calibrated to the electromagnetic scale. Jets arising from the beam background or firing calorimeter noise flags are removed.
- $p_T > 25$ GeV
- $|\eta| < 2.5$
- To discriminate hard scattering jets from pile-up, jets with $p_T < 60$ GeV and $|\eta| < 2.4$ are required to satisfy the criteria based on a multivariate variable called the jet-vertex-tagger (JVT), which gives about 92% efficiency and about 2% fake rate. The requirement for these jets is $|\text{JVT}| < 0.59$.
- The MV2c10 algorithm is used to tag jets containing b-hadrons. This algorithm is based on the long lifetime, high decay multiplicity, hard fragmentation and high mass of b-hadrons. A tight b-tagging working point is used that gives 70% efficiency to tag a jet containing a b-hadron.

6.4 Missing transverse energy

The missing transverse momentum, with magnitude E_T^{miss}, is defined as the transverse momentum imbalance in the detector. It is calculated as the negative vector sum of the transverse momenta of the user-selected calibrated objects, such as electrons, muons, jets and soft contributions, which are reconstructed from the tracks and calorimeter clusters not associated with any hard objects. In this analysis, E_T^{miss}, is reconstructed with the METMakerTool, using calibrated electrons and muons passing the baseline selection before overlap removal is done and calibrated jets before any selection (full jet container). Pile-up degrades the resolution of the calorimeter-based measurement of the soft term. Following the group recommendations the track-based measurement of the soft term, denoted as $E_T^{\text{miss,TRK}}$, is used in this analysis, in which the selected ID tracks satisfy the following requirements:

Keep	Remove	Cone size (ΔR)
muon	electron	0.1
electron	electron(lower p_T)	0.1
electron	jet	0.3
jet	muon	min(0.4, 0.04+10[GeV]/$p_T(\mu)$)

Table 4: Table of overlap removal.

- $p_{\mathrm{T}}^{\mathrm{track}} > 500$ MeV
- ≥ 7 hits in the silicon detector and ≤ 2 holes in the silicon layers or 1 hole in the pixel layers.
- $|z_0 \sin\theta| < 3$ mm and $d_0/\sigma(d_0) < 2$

It has been found that $E_{\mathrm{T}}^{\mathrm{miss,TRK}}$ is robust against high-level pile-up.

6.5 Overlap removal

In absence of a coherent particle flow algorithm implemented at reconstruction level, an ad-hoc overlap removal is performed among objects, on top of above loose selection. A detailed explanation has been documented in [21]. The procedure of overlap removal in this analysis is summarized in Tab. 4. The electron candidate is removed if it is nearby a muon candidate within ΔR <0.1. Then if two electron candidates are close to each other within ΔR <0.1, the electron with lower p_T is removed. Later if one jet is near to one remaining electron within ΔR <0.3, the jet is removed. Lastly, any muon is removed if it is close to any remaining jet within ΔR <min(0.4, 0.04+10[GeV]/$p_T(\mu)$).

7 Event selection

7.1 Pre-selections

The events are required to pass the following pre-selection:

- **GRL**:
  2015 data: `data15_13TeV.periodAllYear_DetStatus-v79-repro20-02 _DQDefects-00-02-02_PHYS_StandardGRL_All_Good_25ns.xml`
  2016 data: `data16_13TeV.periodAllYear_DetStatus-v88-pro20-21 _DQDefects-00-02-04_PHYS_StandardGRL_All_Good_25ns.xml`
- **Event cleaning criteria**: cleaning for Tile corrupted events, LAr noise bursts and corrupted data
- **Vertex criteria**: events are required to contain at least one primary vertex with ≥ 2 associated tracks. The detailed selection on the vertex can be found in [22]
- **Trigger**:
  For 2015 data set: the following triggers are used with an "OR" boolean operator:
  - Single lepton triggers:
    * HLT_mu20_iloose_L1MU15

- * HLT_mu50
- * HLT_e24_lhmedium_L1EM20VH
- * HLT_e60_lhmedium
- * HLT_e120_lhloose

  - Dilepton triggers:
    - * HLT_2e12_lhloose_L12EM10VH
    - * HLT_e17_lhloose_mu14
    - * HLT_mu18_mu8noL1

For 2016 data set: the following triggers are used with an "OR" boolean operator:

  - Single lepton triggers:
    - * HLT_mu24_ivarmedium
    - * HLT_mu50
    - * HLT_e24_lhtight_nod0_ivarloose
    - * HLT_e60_lhmedium_nod0
    - * HLT_e140_lhloose_nod0
  - Dilepton triggers:
    - * HLT_2e17_lhvloose_nod0
    - * HLT_e17_lhloose_nod0_mu14
    - * HLT_mu22_mu8noL1

- **Object definitions**: select objects after object definitions and OLR.

To suppress fakes from background, two tight same-signed leptons are required. There is one additional variable introduced since v26.02 samples, called `ChargeIDBDTTight`, used to suppress charge-mis-identification of electrons. Current WP. is `ChargeIDBDTTight>0.067`. More details can be found in App. F.2. There must be at least one lepton which matches any lepton trigger used. In addition, p_T of the lepton matched trigger must be larger than 30 GeV. The p_T of sub leading lepton is required to be at least 20 GeV. This requirement on sub leading lepton is to suppress fakes(jet faking lepton). In order to suppress background from top quark associated processes, b veto is applied which means rejecting any events containing at least one b jet. And due to the fact that Drell-Yan is not well modeled, the invariant mass of two tight leptons has to be larger than 15 GeV. And to suppress charge-mis-identification from Zjets, Z veto is applied for ee channel. Finally, for pre-selection level, the number of jets is required at least 2. All the pre-selections are summarized in Tab. 5.

Pre-selection	GRL Event clean criteria Pass any trigger applied Select objects following object definitions Overlap removal Two tight same-signed leptons, with at least one trigger matched $p_T(\ell_1) > 30$ GeV, $p_T(\ell_2) > 20$ GeV b veto E_T^{miss} >10 GeV $M(\ell\ell)$ >15 GeV $\lvert M(\ell\ell) - M(Z)\rvert$ >10 GeV in ee channel $N_{\rm jet} \geq 2(3)$

Table 5: Summary of pre-selection.

Cut flow	Event yield			Eff.		
Evgen	-			100%		
HIGG8D1	83.33			56.34%		
Event cleaning	83.33			56.34%		
Trigger	63.25			44.84%		
Channel	ee	$\mu\mu$	$e\mu$	ee	$\mu\mu$	$e\mu$
OB, OLR	8.80	8.66	17.08	5.86%	6.23%	11.96%
Tight leptons, trigger match	4.14	6.12	9.84	2.33%	3.46%	5.68%
$p_T(\ell)$	3.26	4.56	7.33	1.93%	2.70%	4.53%
b veto	3.08	4.27	6.90	1.79%	2.49%	4.18%
MET	3.00	4.17	6.70	1.76%	2.45%	4.10%
Drell-Yan cut	3.00	4.17	6.70	1.76%	2.44%	4.10%
Z veto	2.53	4.17	6.70	1.58%	2.44%	4.10%
$N_{\rm jet} \geq 3$	1.45	2.76	4.13	1.03%	1.92%	2.99%

Table 6: The cutflow of pre-selection for non-resonant hh signal. The cross-section of $pp \to hh$ is 1 pb, and the luminosity is 36.1 fb^{-1}.

7.1.1 Cut flow at pre-selection level

The corresponding cut-flow for non-resonant signal is presented through Tab. 6. The event yield column is normalized to current luminosity, with the cross-section assumption of 1 pb($pp \to hh$). And all Eff. are divided by number of Evgen. events. The cut flow for the remaining signal mass points and prompt backgrounds can be found in App. B. Similarly, we present the cut flow for background processes from Tab. 79 to Tab. 82. In the analysis, events are split into three categories based on lepton favors: $e^\pm e^\pm$, $\mu^\pm\mu^\pm$, $e^\pm\mu^\pm$.

7.2 Signal topology

7.2.1 The hh production

The signature of 2LSS is two same signed leptons plus jets. Initially, two SM higgs tends to be in two opposite semi-sphere. Subsequently, both SM higgs decay to two W bosons, one of which is off-shell.

The off-shell W will contribute quite soft jets. In Fig. 1, we present p_T distribution of jet for signal before object definition(25 GeV threshold on jet). The fourth jet tend to be lower than 25 GeV, even for signal with high mass. So most signal events have only 3 jets harder than 25 GeV. Then we present the number of jet distribution after object definition in Fig. 1(f), it is obvious that signal is dominant in N_{jet}=2 region, for mX=260 GeV case. And as mass increases, the signal tend to be dominant in N_{jet}=4 region. So, in this analysis, we divide the signal region to two categories based on number of jets. For 400 GeV, 500 GeV and non-res search, we require at least 3 jets; while for remaining mass points, i.e, 260 GeV and 300 GeV, at least 2 jets are required. In addition, it has been checked that, including all backgrounds, each mass point does show the highest sensitivity in each individual category(more details are presented in App. D). Considering the decay products of SM Higgs close to each other in most cases, certain discriminating variables are further reconstructed: $\Delta R_{min}(\ell, j)$ and $M_{\ell_1 jj}$, which corresponds to ΔR distance between lepton and the closest jet, invariant mass of leading lepton and two closest jets, respectively. These kinematic variables are summarized below:

- $M(ll)$, the invariant mass of two same-signed leptons;
- MET, missing transverse energy;
- $M(l_1 jj)$, the invariant mass of leading lepton and two closest jets;
- $M(all)$, the invariant mass of all selected objects;
- Mt, the transverse mass of all selected objects;
- $\Delta R_{min}(\ell_1, j)$, ΔR distance between leading lepton and the closest jet;
- $\Delta R_{min}(\ell_2, j)$, ΔR distance between sub leading lepton and the closest jet;

All of their distributions can be found in Fig. 5 and Fig. 6.

7.2.2 The SS production

The S scalar is higgs-like, whose mass ranges from 135 GeV to 165 GeV. And the resonance, X ranges from 280 GeV to 320 GeV. The SS model shares quite similar kinematics with hh model. It has been checked that SS signal holds the N_{jet} division. Similarly, we divide all the mass points into two categories:

- Fixing m_S = 135 GeV: m_X = 280 GeV, m_X = 300 GeV and m_X = 320 GeV; where N_{jet} ≥2 is applied.
- Fixing m_X = 340 GeV: m_S = 135 GeV, m_S = 145 GeV, m_S = 155 GeV and m_S = 165 GeV; where N_{jet} ≥3 is applied.

The variables discussed in Sec. 7.2.1 also distinguish signal from backgrounds well.

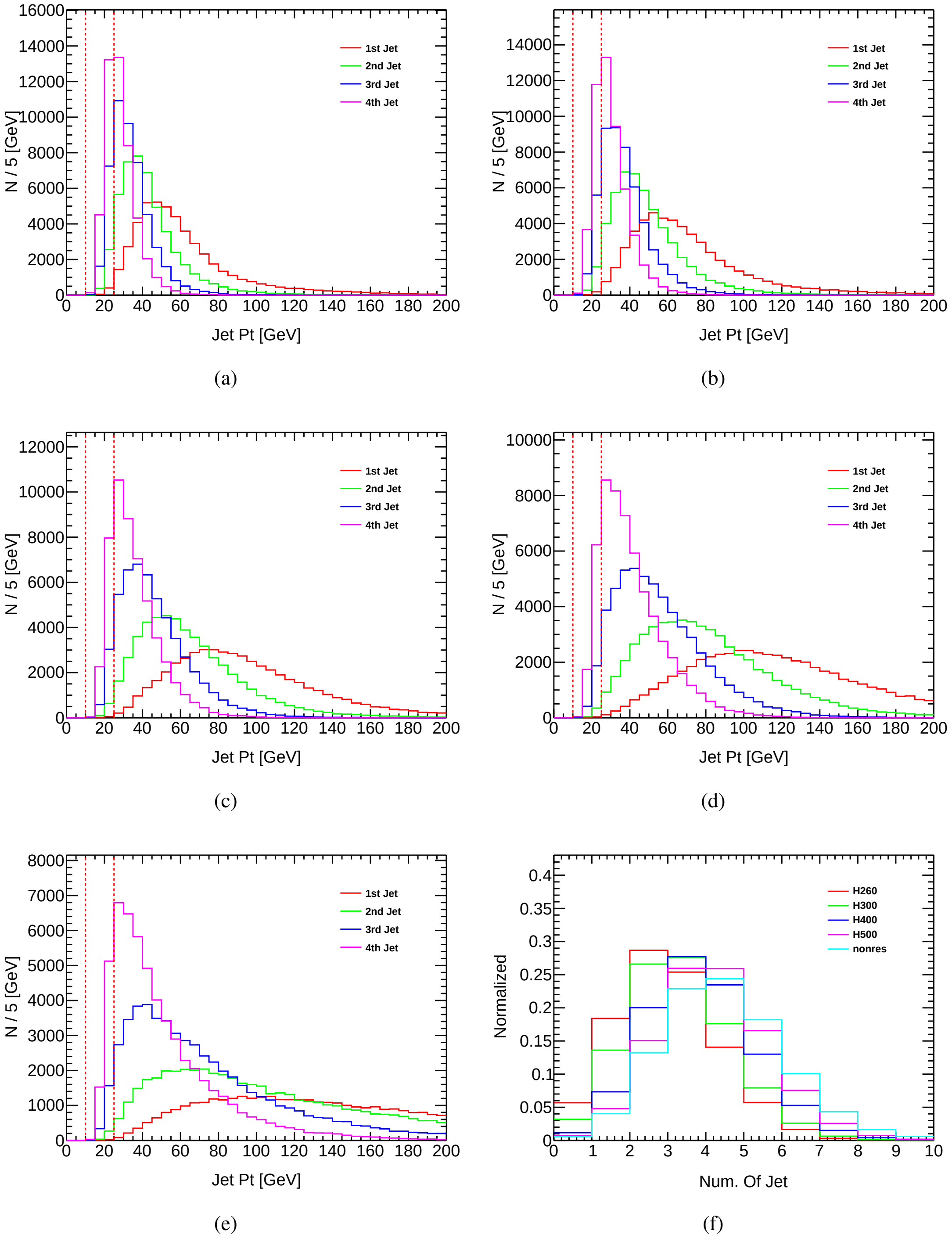

Figure 1: Distributions of p_T and number of jet for signal. Fig. (a) to Fig. (e) are distributions of p_T of jet before 25 GeV cuts, corresponding for mX=260, 300, 400, 500 GeV and non-resonant signal; Fig. (f) is number of jet distribution after 25 GeV cuts.

8 Background estimation

There are several kinds of backgrounds: Prompt same-signed processes(promptSS), Charge-mis-identification (QmisID) and jet faking lepton(fakes). PromptSS are from those processes which contribute two prompt SS leptons, and are estimates with simulated samples. In this analysis, promptSS background consists of ttV, VV($W^{\pm}W^{\pm}$, WZ, ZZ), tV and $t\bar{t}H(H \rightarrow W^{\pm}W^{\mp},\ \tau\tau,$ and $ZZ)$. QmisID is mainly from Z+jet and $t\bar{t}$(fully leptonical), in which one lepton is mis-identified with wrong charge. And jet fakes come from W+jet and $t\bar{t}$(semi-leptonical), in which one jet is mis-identified to lepton. The comparisons between pure MC and data are shown in Fig. 2. Large discrepancy can be see seen in three channels, which indicates the fact that QmisID and jet fakes are not well modeled with MC samples. So both QmisID and jet fakes are estimated with data-driven methods. In addition, there is small fraction of background that comes from $W\gamma$ process, where one photon is mis-identified as a lepton. This will be estimated by simulated samples. Both data-driven methods will be performed at pre-selection level, because of enough statistics and systematics estimations.

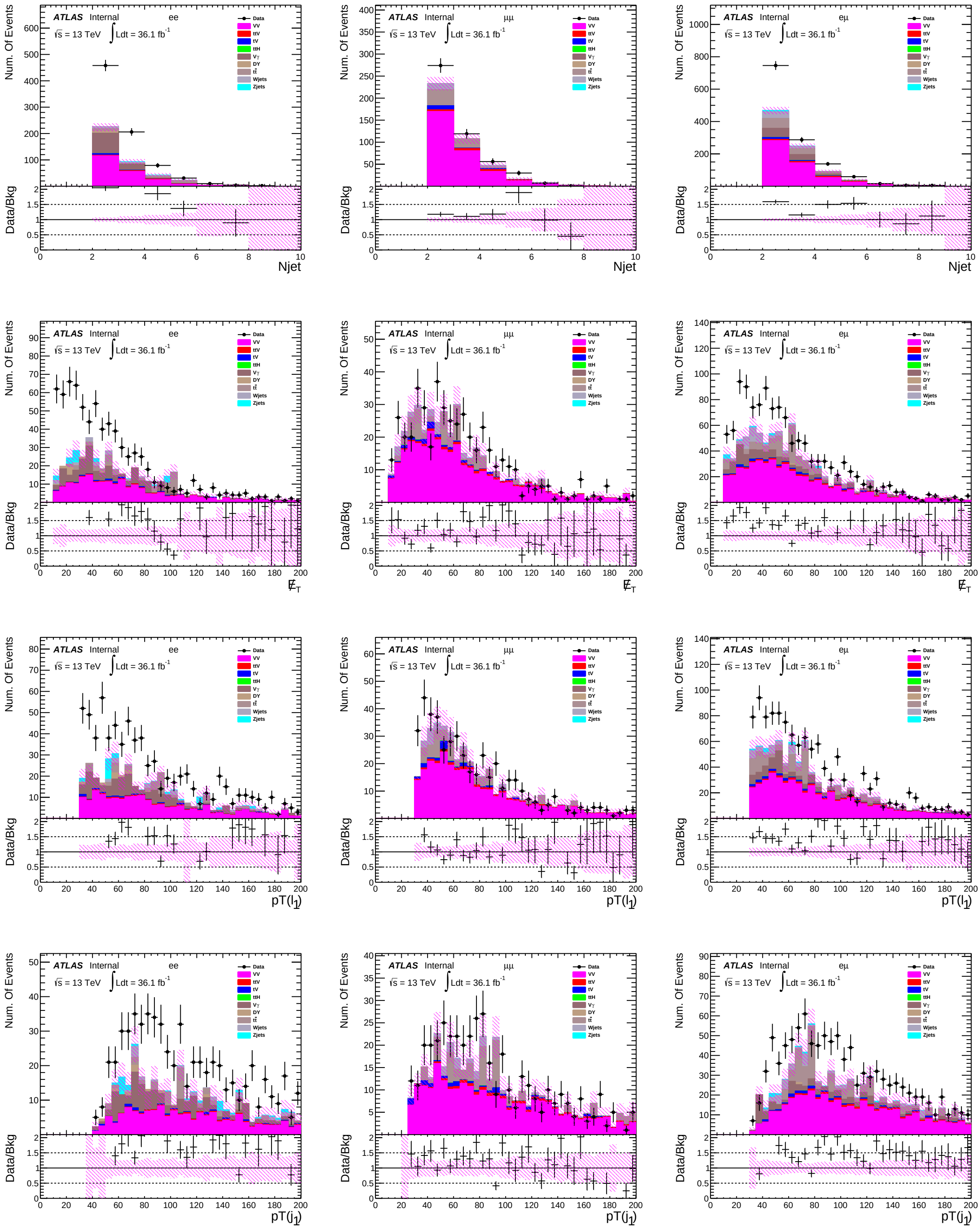

Figure 2: The comparison between data and pure MC at pre-selection level. Left: ee, middle: $\mu\mu$, right:$e\mu$.

8.1 QmisID estimation

The event selection requires two same sign leptons which rejects most of the background contributions. Still, there are some reducible backgrounds coming from the fact that one of the leptons can have the QmisID. According to previous 8 TeV ATLAS studies, muon QmisID is generally below 10^{-5} [23][6], therefore we only consider electron QmisID in this analysis.

There are two main contributions for electron QmisID. The main contribution comes from the radiation of a hard photon (hard Bremsstrahlung process) when the electron passes through materials. This photon then converts into e^+e^- pair and when the EM cluster is associated with the wrong electron's track, an electron of the opposite charge with respect to the original electron maybe reconstructed, leading to QmisID. The hard Bremsstrahlung process depends on the amount of interaction materials in the detector, which in turn depends on $|\eta|$, thus the QmisID rates are expected to have a strong $|\eta|$ dependence. The second and minor contribution comes from the measurement error for a lightly curved track or when the track-cluster association is wrong. This effect is important at high transverse momentum, thus the QmisID rates are also expected to have a small dependence on p_T.

Electrons coming from the leptonical decay of the Z boson are used to measure the QmisID rates in data using a Likelihood technique [24]. The QmisID rates are measured selecting events with two tight electrons originating from a Z decay. Events are selected with the pre-selections requiring two tight leptons with an invariant mass within ±20GeV of the Z mass window . These events are then divided into same sign events (SS) and opposite sign events (OS) depending on the charges of two tight leptons. These events are dominated by Z boson decay events and the small remaining backgrounds are subtracted using side-band method. The two dimensional likelihood method defines the bin boundaries as [0., 0.60, 1.1, 1.37, 1.52, 1.70, 2.00, 2.47] on electron η and [10, 60, 90, 130, 1000] GeV on electron p_T. Based on simulated electron samples from Z decays, closure test has been done by comparing the charge flip rates estimated with both likelihood method and truth-matching method. More details can be found in this note [25].

8.2 Jet fakes estimation with fake factor method

Mis-identification is an important source of background for physics analysis using particle-level identification criteria. In the case of the di-lepton analysis presented in this analysis, this background arises from $t\bar{t}$(semi-leptonical) and W+jet events in which a jet is misidentified as a lepton. The motivation to use fake factor method is the rate of lepton-mis-identification may not be accurately modeled in the MC.

8.2.1 Estimation strategy

This measurement is based on the assumption that the fake factor is stable with respect to the jet multiplicity which was tested in ttH analysis in run-I [26]. The fake factor is defined as the ratio of number of SS events with two tight leptons over events with one tight lepton and one anti-tight lepton:

$$\theta_\ell = \frac{N_{\ell\ell}}{N_{\ell\not\ell}} \tag{1}$$

[6] The rate of charge mis-identification for muons is only affected by the track curvature. Because of the long lever arm to the muon system and the fact that the charge is measured in both the inner detector and muon spectrometer the mis-identification rates of the muon charge are very low, making this background negligible compared to the other sources of background

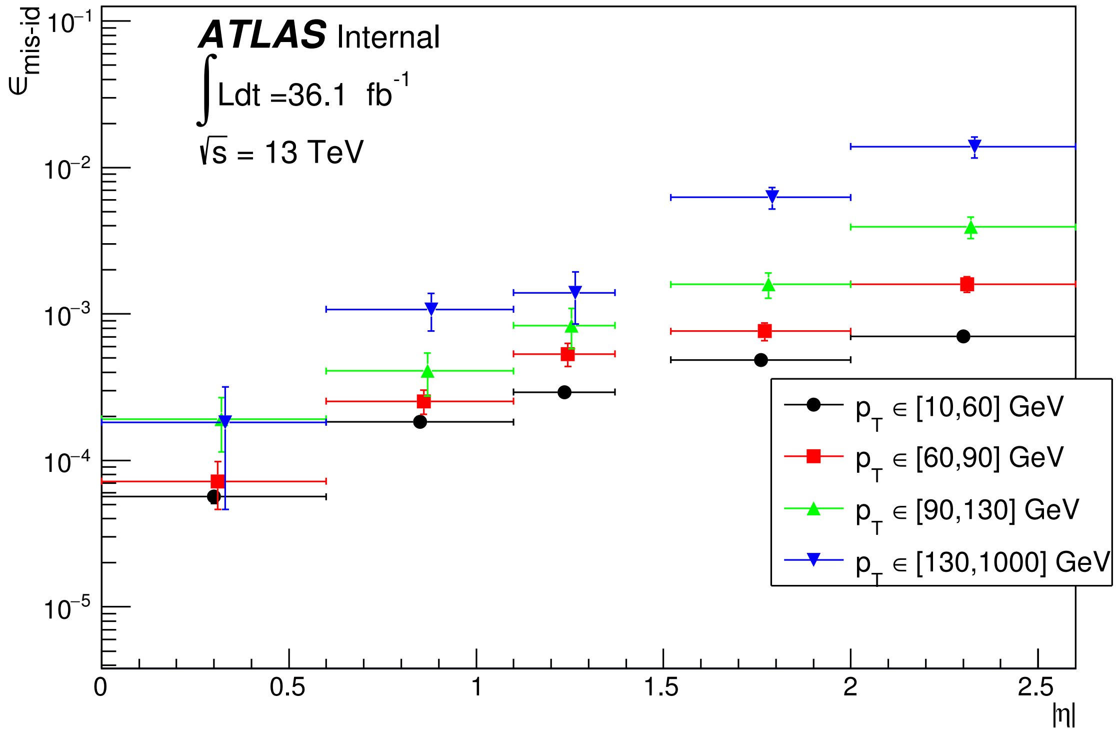

where ℓ is tight e or μ, $\not\ell$ anti-tight lepton which is not used for trigger matching. Then the following is the denominator definition. This is often the most challenging aspect of the method. The denominator selection is chosen such that the contribution from real leptons is suppressed, and the contribution from misidentified jets is enhanced. This is achieved by relaxing or reversing identification criteria used to suppress mis-identification. There is a trade off in terms of uncertainties when specifying these criteria. The tighter the denominator, the smaller the systematics associated with extrapolation. On the other hand, the tighter the denominator definition, the fewer number of jets are reconstructed as denominators. This increases statistical uncertainty. Optimizing the overall background uncertainty requires balancing these competing effects. The primary means to reduce electron mis-identification is through the identification and isolation, while for muon, requirements on isolation and impact parameters are the primary ways [27]. In this analysis, the definitions of ℓ and $\not\ell$ are shown below:

	tight electron	anti-tight electron
ID	TightLH	fail TightLH
isolation	isolationFixedCutTight	-
QmisID	ChargeIDBDTTight>0.067	ChargeIDBDTTight>0.067

Table 7: definitions of tight electrons and anti-tight electrons. In addition to the inverted ID requirement, anti-tight electrons are required to pass the loose selection criteria.

Below demonstrates how to estimate jet fakes using fake factor method, please note that: since there are two categories in signal region, fake factor method is repeated two times. For mX=260 and 300 GeV,

	tight muon	anti-tight muon
ID	Tight	-
isolation	isolationFixedCutTightTrackOnly	fail isolationFixedCutTightTrackOnly

Table 8: definitions of tight muons and anti-tight muons. In addition to the inverted isolation requirement, anti-tight muons are required to pass the loose selection criteria.

fake factor is estimated in $N_{\text{jet}} == 1$ region, and apply fake factor to $N_{\text{jet}} \geq 2$ region; while for mX=400, 500 GeV and non-res, fake factor is estimated in $1 \leq N_{\text{jet}} \leq 2$ region, and apply it in $N_{\text{jet}} \geq 3$ region. Below only demonstrates fake factor method which is corresponding to the high mass search. Fake factor is estimated from low jet multiplicity region and can be written as:

$$\theta_e(\leq 2\text{jets}) = \frac{N_{ee}^{\text{data}} - N_{ee}^{\text{prompt SS}} - N_{ee}^{V\gamma} - N_{ee}^{\text{QmisID}}}{N_{e\not{e}}^{\text{data}} - N_{e\not{e}}^{\text{prompt SS}} - N_{e\not{e}}^{V\gamma} - N_{e\not{e}}^{\text{QmisID MC}}}(\leq 2\text{jets}) \tag{2}$$

$$\theta_\mu(\leq 2\text{jets}) = \frac{N_{\mu\mu}^{\text{data}} - N_{\mu\mu}^{\text{prompt SS}} - N_{\mu\mu}^{V\gamma}}{N_{\mu\not{\mu}}^{\text{data}} - N_{\mu\not{\mu}}^{\text{prompt SS}} - N_{\mu\not{\mu}}^{V\gamma}}(\leq 2\text{jets}) \tag{3}$$

There are three kinds of subtractions. Prompt SS consists of ttV, VV, tV and ttH, which are estimated by MC. Truth matching($\Delta R < 0.2$) is always applied in prompt SS background. The $V\gamma$ backgrounds are estimated using MC, without truth matching. And the prompt opposite-sign events with QmisID(for electrons only) are estimated with data and noted N_{ee}^{QmisID}. In $\ell\not{\ell}$ events, $N_{e\not{e}}^{\text{QmisID MC}}$ is estimated using MC, in which two electrons(in $e^\pm e^\pm$) or the electrons(in $e^\pm\mu^\pm$) match real prompt leptons($\Delta R < 0.2$). Because of these subtractions, there is no overlap between QmisID and jet fakes estimation. Following tables present various numbers of events in different fake factor control regions.

Selections		VV	$t\bar{t}V$	tV	$t\bar{t}H$	$V\gamma$	QmisID	Data
N_{jet} ==1	ee	211.22±19.17	1.09±0.08	5.08±0.93	0.03±0.01	135.94±12.84	164.46±0.65	976
	$e\not{e}$	45.26±3.56	0.13±0.03	8.25±1.32	0.00±0.00	67.33±10.49	28.84±19.23	1116

Table 9: Observed number of data and expected events yields in low jet multiplicity region, which is used for fake factor calculation of electron in low mass search. Uncertainties are statistical.

Selections		VV	$t\bar{t}V$	tV	$t\bar{t}H$	$V\gamma$	Data
N_{jet} ==1	$\mu\mu$	300.76±9.76	1.92±0.11	5.91±1.01	0.02±0.02	0.00±0.00	455
	$\mu\not{\mu}$	57.82±5.03	0.13±0.03	20.80±2.34	0.00±0.00	0.63±0.45	378

Table 10: Observed number of data and expected events yields in low jet multiplicity region, which is used for fake factor calculation of muon in low mass search. Uncertainties are statistical.

In summary, the fake factors of electron and muon with different N_{jet} requirements are found in Tab. 13.

Selections		VV	$t\bar{t}V$	tV	$t\bar{t}H$	$V\gamma$	QmisID	Data
$1 \leq N_{\text{jet}} \leq 2$	ee	326.06±19.83	3.67±0.16	11.27±1.47	0.10±0.02	213.30±17.29	230.40±0.81	1434
	$e\not{e}$	69.67±5.26	0.39±0.06	15.85±1.89	0.02±0.01	104.00±12.71	45.68±22.70	1591

Table 11: Observed number of data and expected events yields in low jet multiplicity region, which is used for fake factor calculation of electron in high mass search. Uncertainties are statistical.

Selections		VV	$t\bar{t}V$	tV	$t\bar{t}H$	$V\gamma$	Data
$1 \leq N_{\text{jet}} \leq 2$	$\mu\mu$	480.96±11.73	6.14±0.21	15.20±2.26	0.17±0.03	0.01±0.01	729
	$\mu\not{\mu}$	75.63±5.44	0.45±0.06	43.59±3.37	0.02±0.01	1.62±0.74	658

Table 12: Observed number of data and expected events yields in low jet multiplicity region, which is used for fake factor calculation of muon in high mass search. Uncertainties are statistical.

Selections	Fake factor	Value
N_{jet} ==1	θ_e	0.4742±0.0269
	θ_μ	0.4902±0.0495
$1 \leq N_{\text{jet}} \leq 2$	θ_e	0.4790±0.0229
	θ_μ	0.4221±0.0334

Table 13: Summary of fake factors of electron and muon with different N_{jet} requirements. Uncertainties are statistical.

Then to predict number of jet fakes in high jet multiplicity region, following calculations will be used:

$$N_{ee}^{\text{fakes}}(\geq 3\text{jets}) = (N_{e\not{e}}^{\text{data}} - N_{e\not{e}}^{\text{prompt SS}} - N_{e\not{e}}^{V\gamma} - N_{e\not{e}}^{\text{QmisID MC}})(\geq 3\text{jets}) \times \theta_e \tag{4}$$

$$N_{\mu\mu}^{\text{fakes}}(\geq 3\text{jets}) = (N_{\mu\not{\mu}}^{\text{data}} - N_{\mu\not{\mu}}^{\text{prompt SS}} - N_{\mu\not{\mu}}^{V\gamma})(\geq 3\text{jets}) \times \theta_\mu \tag{5}$$

$$\begin{aligned} N_{e\mu}^{\text{fakes}}(\geq 3\text{jets}) = {} & (N_{e\not{\mu}} - N_{e\not{\mu}}^{\text{prompt SS}} - N_{e\not{\mu}}^{V\gamma} - N_{e\not{\mu}}^{\text{QmisID}})(\geq 3\text{jets}) \times \theta_\mu \\ & + (N_{\not{e}\mu} - N_{\not{e}\mu}^{\text{prompt SS}} - N_{\not{e}\mu}^{V\gamma} - N_{\not{e}\mu}^{\text{QmisID MC}})(\geq 3\text{jets}) \times \theta_e \end{aligned} \tag{6}$$

Tab. 14 and Tab. 15 present number of events with different N_{jet} requirements in control regions.

After all the subtractions, and multiply with corresponding fake factors, the number of jet fakes in three channels are summarized in Tab. 16. The uncertainty is only statistical here, which is due to size of high multiplicity control region and approximated by $\theta_\ell \times \sqrt{N_{\ell\not{\ell}}^{\geq 2\text{jet}(3\text{jet})}}$ [27].

8.2.2 Systematics

There are several sources of systematic uncertainties on estimated fake factors:

Selections		VV	$t\bar{t}V$	tV	$t\bar{t}H$	$V\gamma$	QmisID	Data
$N_{\mathrm{jet}} \geq 2$	$e\not e$	40.79 ± 4.31	1.67 ± 0.12	11.55 ± 1.62	0.19 ± 0.04	51.74 ± 8.67	33.20 ± 12.82	829
	$\mu\not\mu$	33.56±2.85	1.44±0.15	38.97±3.15	0.12±0.03	1.01±0.59	-	583
	$\not e\mu$	43.69 ± 3.15	2.02 ± 0.17	15.46 ± 2.13	0.19 ± 0.04	53.50 ± 9.21	60.73 ± 9.35	708
	$e\not\mu$	18.17 ± 2.50	0.42 ± 0.10	17.00 ± 1.99	0.03 ± 0.02	0.75 ± 0.39	0.00 ± 0.00	267

Table 14: Observed number of data and expected events yields in high jet multiplicity region, which is used to predict fakes in low mass search. Uncertainties are statistical.

Selections		VV	$t\bar{t}V$	tV	$t\bar{t}H$	$V\gamma$	QmisID	Data
$N_{\mathrm{jet}} \geq 3$	$e\not e$	16.38±1.90	1.41±0.11	3.96±0.90	0.17±0.03	15.07±4.85	43.72±21.69	354
	$\mu\not\mu$	15.75±1.96	1.12±0.13	16.18±2.01	0.10±0.03	0.03±0.03	-	303
	$\not e\mu$	19.74±2.11	1.60±0.16	6.71±1.62	0.18±0.04	17.98±5.18	71.77±16.23	287
	$e\not\mu$	4.88±1.07	0.36±0.09	7.68±1.24	0.02±0.02	0.44±0.27	0.00±0.00	149

Table 15: Observed number of data and expected events yields in high jet multiplicity region, which is used to predict fakes in high mass search. Uncertainties are statistical.

Selections	$N_{\mathrm{jet}} \geq 2$			$N_{\mathrm{jet}} \geq 3$		
	ee	$\mu\mu$	$e\mu$	ee	$\mu\mu$	$e\mu$
Event yield	327.13±8.58	248.97±7.73	365.53±13.23	130.91±5.43	113.90±5.23	138.20±5.65

Table 16: Estimated jet fakes in three channels with different selections. Uncertainties are statistical.

- **Statistics**: Statistical uncertainty in low multiplicity region will propagate to θ_e and θ_μ.
- **QmisID**: The contribution of charge-mis-identification is significant in ee channel, the full uncertainty on this background is propagated to θ_e. Therefore, the uncertainty on QmisID background in ee and $e\mu$ are counted on estimated jet fakes.
- **θ_ℓ syst.(closure test)**: There should be some uncertainty on extrapolation from low jet multiplicity region to high jet multiplicity region. This is estimated by simulated W+jets, and the difference between predicted number of fakes and that of real fakes are considered as systematics, which will be translated on θ_e and θ_μ. Both fake factor regions share the same uncertainty on θ_ℓ syst.
  - Compute fake factor in N_{jet}=1 region:
    θ_e=0.1875±0.0443, θ_μ=0.2060±0.0366;
  - Predict fakes in N_{jet} ≥2 region.

	predicted	real	uncer.
ee	11.83±0.90	9.84±1.89	16.80%
$\mu\mu$	22.79±1.06	20.59±2.18	9.68%

Table 17: Non-closure uncertainty on θ_e and θ_μ. To reduce the statistical error, drop SS, $p_T(\ell)$ and $M(\ell\ell)$ >15 GeV requirements in pre-selections.

- **Sample dependence**: The fake factor method assumes that the rate of the background mis-identification in the fake factor control region(low Njet region) is the same as the rate of background mis-identification in the background control region(high Njet region). In reality, the fake factor assumption is an approximation; different types of jets will have different fake factors. In our case, the biggest source arises from difference between fake rate of heavy flavor and light flavor jets, which are produced in ttbar and W+jets, respectively. Due to the fact that jets in W+jets are softer than that in ttbar sample, as Njet increases, the fraction of ttbar becomes bigger, which causes different fake factor(Tab. 18). In this case, the fake factor estimated in low Njet region with b

Pre-selection	N_{jet}=1	N_{jet}=2	N_{jet} ≥3
`Sherpa` W+jets	221.599	68.327	29.036
`Sherpa` ttbar(semi-lep)	17.163	109.917	103.494
$t\bar{t}/Wjets$	0.077	1.61	3.56

Table 18: The contribution from $t\bar{t}$ becomes bigger as more jets are required. W+jets and ttbar(semi-lep) MC samples are produced with here same generator(`Sherpa`).

veto, which is expected to be W+jets dominant is different with that in high Njet region, where $t\bar{t}$ contributes more to backgrounds. So $t\bar{t}$ process is being underestimated in our standard fake factor calculations. In order to estimate such uncertainty, fake factor method is repeated without b veto [7], and the bigest variations are considered as uncertainty on θ_ℓ for both fake factor regions(Tab. 19).

N_{jet}=1	with b veto	without b veto	uncer.
θ_e	0.4742±0.0269	0.3563±0.0841	24.86%
θ_μ	0.4902±0.0495	0.3422±0.0853	30.19%
≤ N_{jet} ≤2	with b veto	without b veto	uncer.
θ_e	0.4790±0.0229	0.4637±0.0613	3.19%
θ_μ	0.4221±0.0334	0.3031±0.0411	28.19%

Table 19: The fake factors of with and without b veto.

All the systematics on θ_e and θ_μ are summarized in Tab. 20 and Tab. 21,respectively.

	N_{jet} ==1	1 ≤ N_{jet} ≤ 2
Statistics	5.67	4.78
QmisID	33.0	30.0
θ_ℓ syst.	16.80	16.80
Sample dependence	24.86	24.86
Total	44.96	42.70

Table 20: Summary of systematic uncertainty on θ_e with different N_{jet} selections(in %).

[7] In principle, the optimal way is to perform a closure test, i.e. compare W+jets MC and ttbar MC. However, the statistics is very low in low N_{jet} region for ttbar(semi-lep), which causes the uncertainty not reliable.

	N_{jet} ==1	$1 \leq N_{\text{jet}} \leq 2$
Statistics	10.10	7.91
θ_ℓ syst.	9.68	9.68
Sample dependence	30.19	30.19
Total	33.27	32.68

Table 21: Summary of systematic uncertainty on θ_μ with different N_{jet} selections(in %).

8.2.3 Event yields at pre-selection level with data-driven methods

After performing all the methods discussed above, we present the event yields at pre-selection level. Assuming statistical uncertainty(the one due to size of high jet multiplicity control region)is independent with systematical uncertainty on θ_ℓ, the total error on estimated jet fakes is: $\sqrt{(\theta_\ell^{\text{sys.}} \times N_{\text{jet fakes}}^{\text{nominal}})^2 + \theta_\ell \times N_{\text{jet fakes}}^{\text{nominal}}}$, where $\theta_\ell^{\text{sys.}}$ is the systematical uncertainty on θ_ℓ, and $N_{\text{jet fakes}}^{\text{nominal}}$ number of jet fakes using median θ_ℓ. Tab. 22 and Tab. 23 show event yields by the requirement of $N_{\text{jet}} \geq 2$ and $N_{\text{jet}} \geq 3$, respectively. And corresponding distributions of N_{jet} are shown in Fig. 3 and Fig. 4. Good agreements are observed between data and total estimated backgrounds within uncertainties. Each region is divided into three channel considering the different flavor pairs of leptons, i.e. ee, $\mu\mu$ and $e\mu$.

	ee	$\mu\mu$	$e\mu$
Jet fakes	327.13±129.68	248.97±83.57	365.53±107.31
PromptSS	228.03±6.84	361.97±8.95	600.76±10.92
$V+\gamma$	105.39±12.43	0.01±0.01	107.99±15.17
QmisID	101.47±0.60	0.00±0.00	18.21±0.23
Total backgrounds	762.02±130.46	610.95±84.04	1092.49±108.92
Observed	790	487	1257

Table 22: Event yields at pre-selection level, corresponding to $N_{\text{jet}} \geq 2$. Uncertainties include all systematics.

	ee	$\mu\mu$	$e\mu$
Jet fakes	130.91±38.86	113.90±31.87	138.20±29.34
PromptSS	104.34±4.46	168.12±5.80	283.98±7.28
$V+\gamma$	28.03±4.52	0.01±0.01	51.62±13.75
QmisID	35.60±0.38	0.00±0.00	8.38±0.16
Total backgrounds	298.87±39.37	282.02±32.39	482.18±33.21
Observed	332	213	511

Table 23: Event yields at pre-selection level, corresponding to $N_{\text{jet}} \geq 3$. Uncertainties include all systematics.

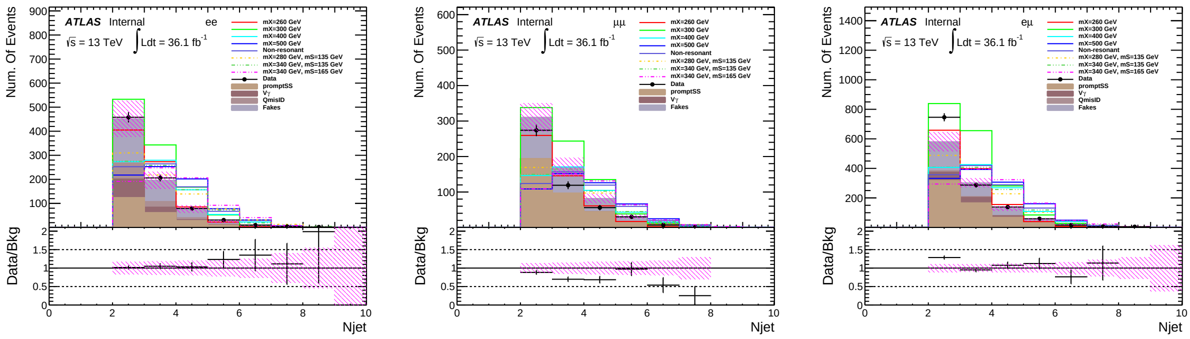

Figure 3: The comparisons between data and backgrounds at pre-selection level, corresponding to $N_{\mathrm{jet}} \geq 2$. Left: ee, middle: $\mu\mu$, right: $e\mu$. Uncertainties include all systematics.

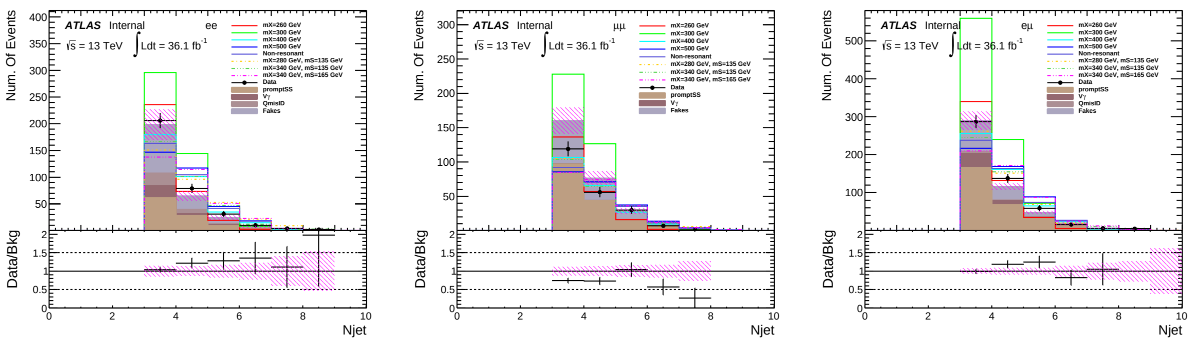

Figure 4: The comparisons between data and backgrounds at pre-selection level, corresponding to $N_{\mathrm{jet}} \geq 3$. Left: ee, middle: $\mu\mu$, right: $e\mu$. Uncertainties include all systematics.

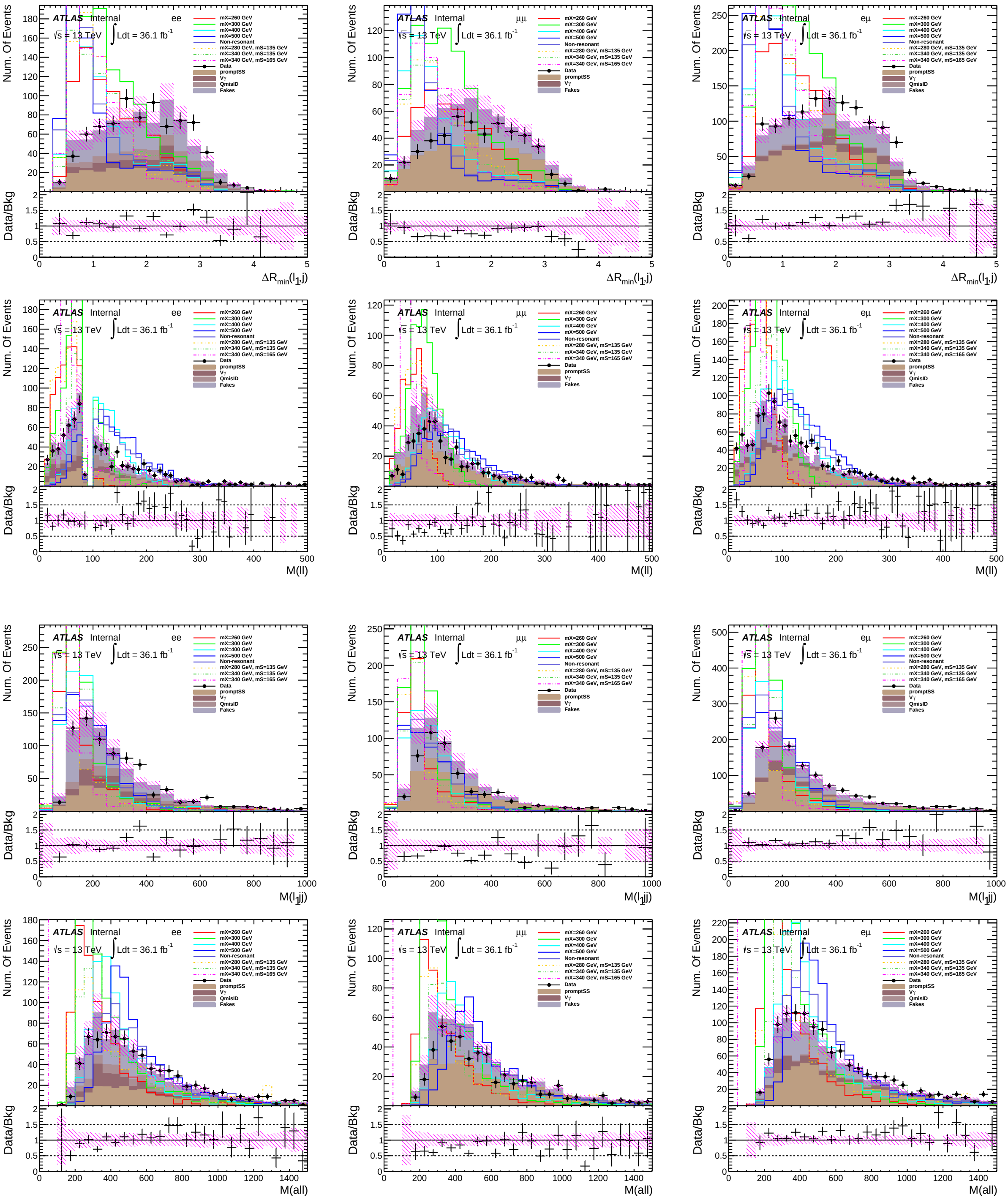

Figure 5: The distributions of kinematic variables that are used to form optimization selections at pr-selection level, corresponding to $N_{\text{jet}} \geq 2$. Left: ee, middle: $\mu\mu$, right: $e\mu$.

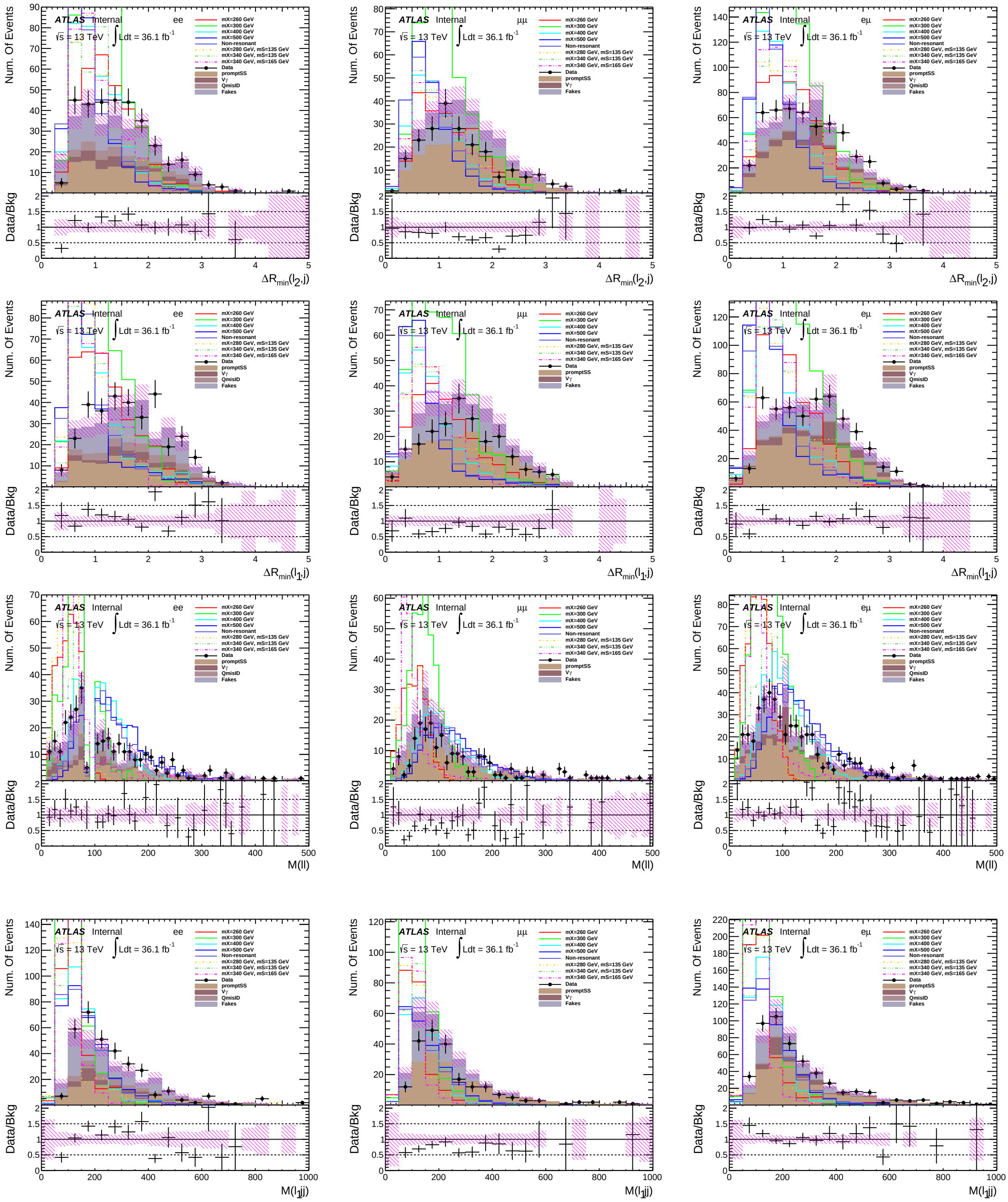

Figure 6: The distributions of kinematic variables that are used to form optimization selections at pre-selection level, corresponding to $N_{\text{jet}} \geq 3$. Left: ee, middle: $\mu\mu$, right: $e\mu$.

9 Signal optimization

After pre-selections, the significant contributions of backgrounds come from prompt same-signed processes and fake leptons. In order to enhance signal sensitivity, optimizations are performed at pre-selection level.

9.1 Optimizations for resonant and non-resonant hh production

A MVA method was used to determine the separating power of different kinematic variables. And correlations between all the variables are taken into account. Eventually, top five kinematic variables are used to form optimization selections. The five optimization variables are $M(\ell\ell)$, $\Delta R_{min}(\ell_2, j)$, $\Delta R_{min}(\ell_1, j)$, $M_{\ell_1 jj}$ and $M(all)$, which have strong separating power and low correlations between them(Fig. 7). In general, $M(\ell\ell)$ and $M_{\ell_1 jj}$ are sensitive to low mass points, while the remaining are sensitive to high mass and non-res signal. Based on this knowledge, $\Delta R_{min}(\ell_1, j)$, $M(\ell\ell)$, $M_{\ell_1 jj}$ and $M(all)$ are used to form optimization cuts in low mass search, while $\Delta R_{min}(\ell_2, j)$, $\Delta R_{min}(\ell_1, j)$, $M(\ell\ell)$ and $M_{\ell_1 jj}$ in high mass search. Their corresponding distributions are found in Fig. 5 and Fig. 6, respectively.

9.1.1 Strategy

The TMVA package(CutsSA option) [28] is used to achieve optimal cuts. All the backgrounds: promptSS, $V\gamma$, QmisID and fakes are included in the training. In order to reduce the dependence on the order of cuts, the framework is used to train only 2 cuts each time. Then assigning a common signal efficiency working point, signal and all background samples are evaluated(pass or not) event by event. For each signal efficiency WP., significance($S/\sqrt{B}$) is calculated. Finally, the signal efficiency WP. that has highest significance is selected. Based on this common WP., optimal cut values can be achieved. Fig. 9.1.1 shows the significance scan as a function of signal efficiency WP. for $\mu\mu$ in the non-resonant signal optimizations. It is repeated for remaining channels and other mass points.
Eventually considering continuity of cut values from low to high(and non-res)mass points, some tuning are performed. The selections are summarized in Tab. 24 and Tab. 25, corresponding to low and high mass search, respectively. In general, it is the most sensitive in $\mu\mu$ channel, as there is negligible QmisID background, as well as much less fakes.

	Channel	$\Delta R_{min}(\ell_1, j)$	$M(ll)$	$M_{\ell_1 jj}$	$M(all)$
mX260	ee	0.35, 1.85	-1, 100	-1, 145	-1, 1100
	$\mu\mu$	0.25, 2.10	-1, 80	-1, 115	-1, 700
	$e\mu$	0.25, 1.80	-1, 85	-1, 135	-1, 650
mX300	ee	0.35, 1.75	-1, 120	-1, 160	-1, 1400
	$\mu\mu$	0.20, 1.75	-1, 115	-1, 185	-1, 1000
	$e\mu$	0.20, 1.80	-1, 135	-1, 160	-1, 800

Table 24: Summary of optimization selections for the search of $X \rightarrow hh(m_X$=260, 300 GeV). -1 means there is no lower cuts. All mass cuts are in GeV.

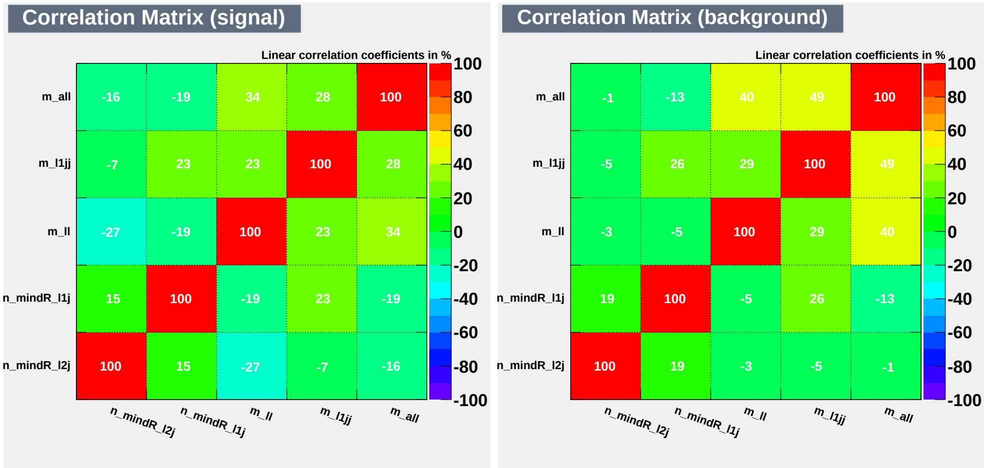

Figure 7: Correlation check of input training variables.

	Channel	$\Delta R_{min}(\ell_2, j)$	$\Delta R_{min}(\ell_1, j)$	$M(ll)$	$M_{\ell_1 jj}$
	ee	0.35, 1.50	0.30, 1.25	45, 235	40, 285
mX400	$\mu\mu$	0.20, 1.20	0.20, 1.20	40, 215	30, 260
	$e\mu$	0.20, 1.50	0.20, 1.05	35, 195	30, 235
	ee	0.20, 1.15	0.20, 1.15	100, 270	40, 285
mX500	$\mu\mu$	0.20, 1.05	0.20, 0.75	60, 250	30, 310
	$e\mu$	0.20, 1.00	0.20, 0.80	75, 250	35, 350
	ee	0.20, 1.40	0.20, 1.15	55, 270	40, 285
Non-res	$\mu\mu$	0.20, 1.05	0.20, 0.75	60, 250	30, 310
	$e\mu$	0.20, 1.15	0.20, 0.80	75, 250	35, 350

Table 25: Summary of optimization selections for the search of $X \to hh(m_X$=400, 500 GeV and non-resonant). All mass cuts are in GeV.

9.2 Optimizations for resonant SS production

The optimizations for resonant SS searches follows the strategy introduced in Sec. 9.1. For SS searches, $\Delta R_{min}(\ell_2, j)$, $\Delta R_{min}(\ell_1, j)$, $M(\ell\ell)$ and $M_{\ell_1 jj}$ are used to form the optimization cuts. Since the kinematics of SS signal samples studied are close, we focus on two mass points:

- Fixing m_S = 135 GeV: m_X = 280 GeV, m_X = 300 GeV and m_X = 320 GeV; the optimizations done in the case of m_S = 135 GeV, m_X = 300 GeV.
- Fixing m_X = 340 GeV: m_S = 135 GeV, m_S = 145 GeV, m_S = 155 GeV and m_S = 165 GeV; the optimizations done in the case of m_X = 340 GeV, m_S = 145 GeV.

The results are summaried in Tab. 26.

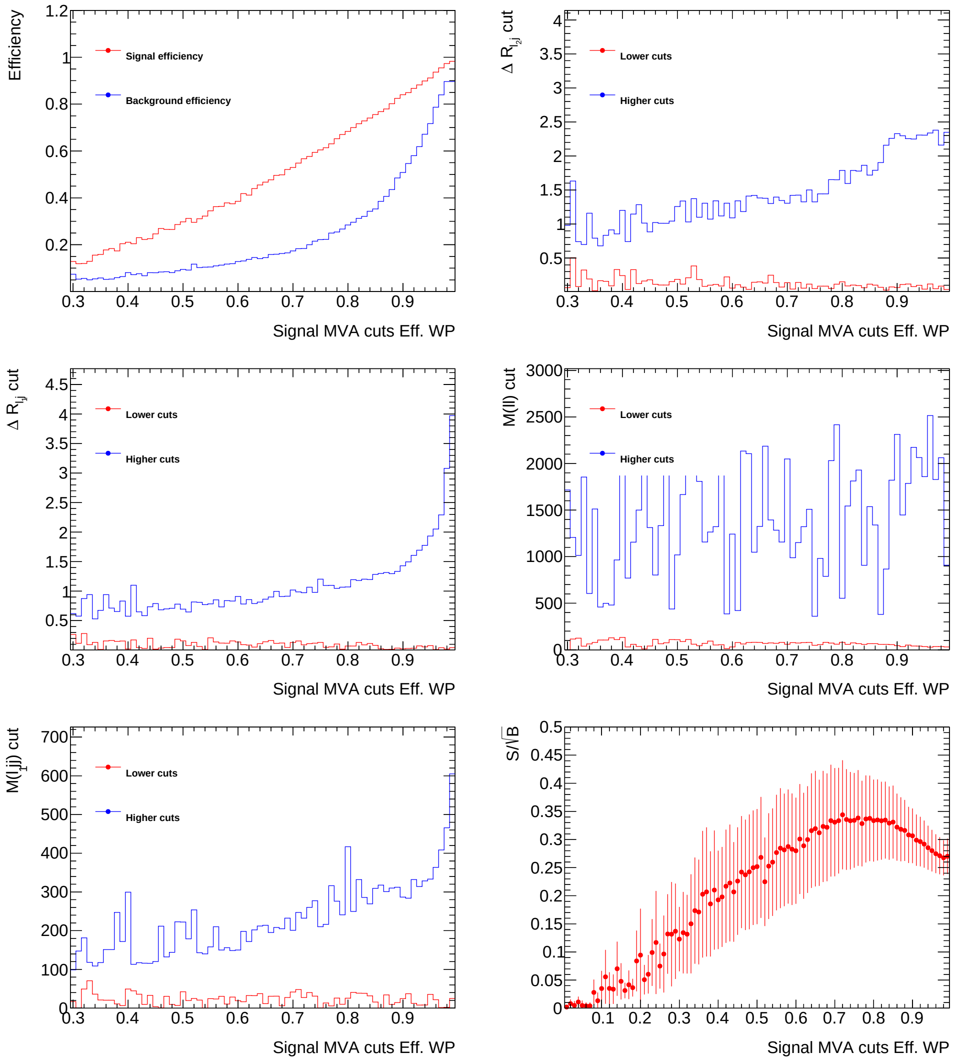

Figure 8: The significance scan as a function of efficiency for $\mu\mu$ in non-resonant signal search. Statistical uncertainties on the background and the signal are considered. The 0.72 working point is chosen for $\mu\mu$ channel in the non-resonant signal optimizations.

	Channel	$\Delta R_{min}(\ell_2, j)$	$\Delta R_{min}(\ell_1, j)$	$M(ll)$	$M_{\ell_1 jj}$
m_X=300 GeV, m_S=135 GeV	ee	0.35, 2.5	0.4, 1.65	-1, 80	50, 150
	$\mu\mu$	0.25, 2.05	0.2, 1.85	-1, 95	50, 150
	$e\mu$	0.25, 1.7	0.25, 1.65	-1, 95	50, 150
m_X=340 GeV, m_S=145 GeV	ee	0.35, 1.85	0.2, 1.65	-1, 130	50, 190
	$\mu\mu$	0.2, 2.0	0.2, 1.65	-1, 115	50, 185
	$e\mu$	0.25, 1.6	0.25, 1.6	-1, 150	50, 150

Table 26: Summary of optimization selections for the search of $X \to SS$. -1 means there is no lower cuts.

9.3 Event yields after optimization selections

The (un)Blinded results are presented from Tab. 27 to Tab. 62. The signal($pp \to hh \to WW^*WW^* \to \ell^\pm \nu \ell^\pm \nu qqqq$)column is corresponding to ee, $\mu\mu$ and $e\mu$ channel. Here the cross-section for each mass point($pp \to hh(SS)$) is assumed 1pb, with SM branching ratios considered. And the luminosity is 36.1 fb^{-1}. The total predicted column mean total backgrounds plus signal. The error on fakes contain all statistical and systematical uncertainties. The other components only include statistical uncertainties. While for QmisID component, its systematical uncertainties have been imported to fakes, which is discussed in Sec. 8.2.2.

9.3.1 Non-resonant results

	promptSS	$V+\gamma$	QmisID	Fakes	Total bkg	signal	Total predicted	Observed
$\Delta R_{min}(l_2, j)$	51.39±3.00	16.25±3.99	15.60±0.24	67.85±20.53	151.09±21.12	1.24±0.04	152.34±21.12	0
$\Delta R_{min}(l_1, j)$	17.57±1.85	2.89±1.04	5.23±0.13	24.08±7.78	49.77±8.06	0.97±0.04	50.74±8.06	0
$M(\ell\ell)$	12.32±1.66	0.95±0.34	3.38±0.10	17.44±5.83	34.09±6.08	0.90±0.03	34.99±6.08	0
$M(l_1jj)$	8.82±1.06	0.54±0.24	2.61±0.09	15.42±5.24	27.39±5.35	0.83±0.03	28.22±5.35	0

Table 27: (un)Blinded results of non-res search in ee channel.

	promptSS	$V+\gamma$	QmisID	Fakes	Total bkg	signal	Total predicted	Observed
$\Delta R_{min}(l_2, j)$	51.91±2.81	0.01±0.01	0.00±0.00	34.85±10.26	86.76±10.64	1.95±0.05	88.71±10.64	0
$\Delta R_{min}(l_1, j)$	10.49±1.23	0.00±0.00	0.00±0.00	5.12±2.03	15.61±2.37	1.20±0.04	16.81±2.37	0
$M(\ell\ell)$	6.85±1.03	0.00±0.00	0.00±0.00	3.68±1.60	10.54±1.91	1.07±0.04	11.61±1.91	0
$M(l_1jj)$	5.05±0.82	0.00±0.00	0.00±0.00	3.30±1.49	8.36±1.69	1.01±0.04	9.37±1.70	0

Table 28: (un)Blinded results of non-res search in $\mu\mu$ channel.

	promptSS	$V+\gamma$	QmisID	Fakes	Total bkg	signal	Total predicted	Observed
$\Delta R_{min}(l_2, j)$	102.30±4.09	15.89±4.14	3.46±0.11	48.29±11.13	169.95±12.56	3.17±0.08	173.12±12.56	0
$\Delta R_{min}(l_1, j)$	21.01±1.84	1.88±0.94	0.68±0.05	8.38±2.83	31.94±3.50	1.86±0.07	33.80±3.50	0
$M(\ell\ell)$	12.30±1.32	0.24±0.21	0.34±0.03	4.59±1.89	17.47±2.31	1.51±0.06	18.98±2.31	0
$M(l_1jj)$	9.74±1.17	0.24±0.21	0.27±0.03	4.25±1.78	14.50±2.14	1.46±0.06	15.95±2.14	0

Table 29: (un)Blinded results of non-res search in $e\mu$ channel.

9.3.2 Resonant hh results

	promptSS	$V+\gamma$	QmisID	Fakes	Total bkg	signal	Total predicted	Observed
$\Delta R_{min}(l_1, j)$	121.55±4.81	37.23±6.02	39.43±0.35	159.83±63.66	358.03±64.13	0.59±0.03	358.62±64.13	0
$M(\ell\ell)$	41.60±2.92	21.34±4.74	17.43±0.18	100.11±40.10	180.48±40.49	0.58±0.03	181.06±40.49	0
$M(l_1jj)$	12.65±1.74	3.34±1.26	4.78±0.06	36.42±14.96	57.18±15.11	0.44±0.03	57.62±15.11	0
$M(all)$	11.95±1.71	3.34±1.26	4.68±0.06	35.97±14.78	55.95±14.94	0.44±0.02	56.38±14.94	0

Table 30: (un)Blinded results of mX=260 GeV search in ee channel.

	promptSS	$V+\gamma$	QmisID	Fakes	Total bkg	signal	Total predicted	Observed
$\Delta R_{min}(l_1, j)$	228.31±6.96	0.01±0.01	0.00±0.00	176.60±59.49	404.91±59.89	1.21±0.04	406.12±59.89	0
$M(\ell\ell)$	78.38±4.42	0.00±0.00	0.00±0.00	88.89±30.30	167.27±30.62	1.07±0.04	168.34±30.62	0
$M(l_1jj)$	10.63±1.53	0.00±0.00	0.00±0.00	17.33±6.46	27.96±6.64	0.56±0.03	28.52±6.64	0
$M(all)$	9.08±1.48	0.00±0.00	0.00±0.00	14.53±5.52	23.61±5.72	0.54±0.03	24.14±5.72	0

Table 31: (un)Blinded results of mX=260 GeV search in $\mu^+\mu^-$ channel.

	promptSS	$V+\gamma$	QmisID	Fakes	Total bkg	signal	Total predicted	Observed
$\Delta R_{min}(l_1, j)$	309.23±7.40	36.01±5.38	9.42±0.16	186.12±54.56	540.78±55.33	1.69±0.05	542.47±55.33	0
$M(\ell\ell)$	110.04±4.61	18.73±4.47	2.02±0.04	108.32±31.15	239.11±31.81	1.53±0.05	240.64±31.81	0
$M(l_1jj)$	30.04±2.44	5.89±1.87	0.54±0.02	43.43±12.61	79.91±12.98	1.04±0.04	80.96±12.98	0
$M(all)$	24.23±2.16	4.87±1.67	0.46±0.01	38.64±11.28	68.20±11.61	0.99±0.04	69.19±11.61	0

Table 32: (un)Blinded results of mX=260 GeV search in $e\mu$ channel.

	promptSS	$V+\gamma$	QmisID	Fakes	Total bkg	signal	Total predicted	Observed
$\Delta R_{min}(l_1, j)$	112.20±4.62	33.03±5.51	35.61±0.33	146.32±58.34	327.16±58.78	0.80±0.03	327.97±58.78	0
$M(\ell\ell)$	51.97±3.19	22.72±5.05	22.09±0.21	106.77±42.73	203.54±43.14	0.74±0.03	204.28±43.14	0
$M(l_1jj)$	18.73±1.92	5.31±2.21	7.27±0.08	47.15±19.20	78.47±19.42	0.61±0.03	79.08±19.42	0
$M(all)$	18.39±1.91	5.31±2.21	7.22±0.08	46.70±19.02	77.62±19.24	0.61±0.03	78.23±19.24	0

Table 33: (un)Blinded results of mX=300 GeV search in ee channel.

	promptSS	$V+\gamma$	QmisID	Fakes	Total bkg	signal	Total predicted	Observed
$\Delta R_{min}(l_1, j)$	187.28±6.36	0.01±0.01	0.00±0.00	138.05±46.66	325.34±47.09	1.80±0.06	327.14±47.09	0
$M(\ell\ell)$	103.31±5.04	0.01±0.01	0.00±0.00	116.84±39.60	220.16±39.92	1.66±0.06	221.82±39.92	0
$M(l_1jj)$	52.57±3.36	0.00±0.00	0.00±0.00	76.21±26.08	128.77±26.30	1.47±0.05	130.24±26.30	0
$M(all)$	49.45±3.31	0.00±0.00	0.00±0.00	75.47±25.84	124.92±26.05	1.46±0.05	126.38±26.05	0

Table 34: (un)Blinded results of mX=300 GeV search in $\mu^+\mu^-$ channel.

	promptSS	$V+\gamma$	QmisID	Fakes	Total bkg	signal	Total predicted	Observed
$\Delta R_{min}(l_1, j)$	311.90±7.43	36.28±5.39	9.46±0.16	187.60±55.10	545.24±55.86	2.64±0.07	547.88±55.86	0
$M(\ell\ell)$	193.24±6.06	26.12±4.79	3.99±0.07	153.73±44.51	377.08±45.17	2.57±0.07	379.65±45.17	0
$M(l_1jj)$	71.39±3.66	10.73±2.76	1.41±0.03	71.56±20.67	155.09±21.17	2.05±0.06	157.14±21.17	0
$M(all)$	61.51±3.44	8.94±2.50	1.24±0.03	65.55±19.21	137.25±19.67	1.99±0.06	139.24±19.67	0

Table 35: (un)Blinded results of mX=300 GeV search in $e\mu$ channel.

	promptSS	$V+\gamma$	QmisID	Fakes	Total bkg	signal	Total predicted	Observed
$\Delta R_{min}(l_2, j)$	57.46±3.19	17.85±4.08	17.54±0.26	73.78±22.25	166.63±22.85	1.09±0.05	167.72±22.85	0
$\Delta R_{min}(l_1, j)$	22.81±2.03	3.51±1.10	6.68±0.15	28.44±9.05	61.45±9.34	0.85±0.05	62.30±9.34	0
$M(\ell\ell)$	17.09±1.85	1.25±0.42	4.50±0.12	22.82±7.41	45.66±7.65	0.82±0.04	46.49±7.65	0
$M(l_1jj)$	12.17±1.27	0.83±0.34	3.46±0.10	20.62±6.77	37.08±6.89	0.81±0.04	37.89±6.89	0

Table 36: (un)Blinded results of mX=400 GeV search in ee channel.

	promptSS	$V+\gamma$	QmisID	Fakes	Total bkg	signal	Total predicted	Observed
$\Delta R_{min}(l_2, j)$	64.80±3.13	0.01±0.01	0.00±0.00	47.31±13.67	112.11±14.02	1.72±0.06	113.83±14.02	0
$\Delta R_{min}(l_1, j)$	27.35±1.98	0.00±0.00	0.00±0.00	17.32±5.45	44.67±5.80	1.38±0.05	46.05±5.80	0
$M(\ell\ell)$	19.73±1.77	0.00±0.00	0.00±0.00	15.70±5.00	35.42±5.30	1.34±0.05	36.76±5.30	0
$M(l_1jj)$	14.80±1.43	0.00±0.00	0.00±0.00	13.05±4.27	27.85±4.50	1.30±0.05	29.15±4.50	0

Table 37: (un)Blinded results of mX=400 GeV search in $\mu^+\mu^-$ channel.

	promptSS	$V+\gamma$	QmisID	Fakes	Total bkg	signal	Total predicted	Observed
$\Delta R_{min}(l_2, j)$	156.35±5.23	23.17±4.97	5.06±0.13	77.87±17.23	262.45±18.67	3.33±0.08	265.79±18.67	0
$\Delta R_{min}(l_1, j)$	49.40±2.79	7.96±3.23	1.69±0.07	27.09±7.00	86.14±8.20	2.34±0.07	88.47±8.20	0
$M(\ell\ell)$	35.57±2.40	6.54±3.20	0.86±0.04	21.29±5.73	64.26±6.99	2.27±0.07	66.52±6.99	0
$M(l_1jj)$	24.88±1.99	2.47±1.25	0.60±0.03	19.50±5.51	47.46±5.99	2.16±0.07	49.62±5.99	0

Table 38: (un)Blinded results of mX=400 GeV search in $e\mu$ channel.

	promptSS	$V+\gamma$	QmisID	Fakes	Total bkg	signal	Total predicted	Observed
$\Delta R_{min}(l_2, j)$	39.60±2.73	12.21±3.77	11.32±0.21	52.73±16.13	115.85±16.78	1.40±0.05	117.25±16.79	0
$\Delta R_{min}(l_1, j)$	14.10±1.73	1.89±0.95	4.00±0.12	16.82±5.65	36.80±5.99	1.13±0.04	37.93±5.99	0
$M(\ell\ell)$	5.73±0.81	0.36±0.19	1.59±0.08	3.25±1.57	10.93±1.77	0.90±0.04	11.83±1.77	0
$M(l_1jj)$	4.16±0.71	0.12±0.05	1.24±0.07	1.58±0.98	7.10±1.22	0.85±0.04	7.95±1.22	0

Table 39: (un)Blinded results of mX=500 GeV search in ee channel.

	promptSS	$V+\gamma$	QmisID	Fakes	Total bkg	signal	Total predicted	Observed
$\Delta R_{min}(l_2, j)$	51.91±2.81	0.01±0.01	0.00±0.00	34.85±10.26	86.76±10.64	2.29±0.06	89.05±10.64	0
$\Delta R_{min}(l_1, j)$	10.49±1.23	0.00±0.00	0.00±0.00	5.12±2.03	15.61±2.37	1.50±0.04	17.10±2.37	0
$M(\ell\ell)$	6.85±1.03	0.00±0.00	0.00±0.00	3.68±1.60	10.54±1.91	1.43±0.04	11.97±1.91	0
$M(l_1jj)$	5.05±0.82	0.00±0.00	0.00±0.00	3.30±1.49	8.36±1.69	1.40±0.04	9.76±1.70	0

Table 40: (un)Blinded results of mX=500 GeV search in $\mu^+\mu^-$ channel.

	promptSS	$V+\gamma$	QmisID	Fakes	Total bkg	signal	Total predicted	Observed
$\Delta R_{min}(l_2, j)$	77.17±3.36	12.92±3.94	2.74±0.10	38.41±9.19	131.24±10.55	3.41±0.07	134.65±10.55	0
$\Delta R_{min}(l_1, j)$	16.28±1.65	0.63±0.23	0.53±0.05	6.78±2.59	24.21±3.07	2.19±0.06	26.41±3.08	0
$M(\ell\ell)$	9.47±1.19	0.03±0.03	0.27±0.03	4.27±1.78	14.04±2.14	1.94±0.05	15.98±2.14	0
$M(l_1jj)$	7.52±1.06	0.03±0.03	0.21±0.02	3.91±1.67	11.68±1.98	1.91±0.05	13.58±1.98	0

Table 41: (un)Blinded results of mX=500 GeV search in $e\mu$ channel.

9.3.3 Resonant SS results

Maybe the tables in this section will be re-made, as some tables share the same yields for backgrounds(optmizations done in two mass points).

	promptSS	$V+\gamma$	QmisID	Fakes	Total bkg	signal	Total predicted	Observed
$\Delta R_{min}(l_2, j)$	194.67±6.26	84.84±11.72	81.84±0.54	270.28±107.25	631.62±108.07	3.04±0.21	634.67±108.07	0
$\Delta R_{min}(l_1, j)$	92.43±4.13	29.21±5.40	29.29±0.30	120.27±48.06	271.20±48.53	2.48±0.19	273.68±48.54	0
$M(\ell\ell)$	30.44±2.48	18.51±4.62	12.04±0.15	71.24±28.71	132.22±29.18	2.38±0.18	134.60±29.18	0
$M(l_1jj)$	10.40±1.51	3.34±1.26	3.77±0.06	28.93±12.00	46.44±12.16	1.86±0.16	48.30±12.16	0

Table 42: (un)Blinded results of the search of mX=280 GeV, mS=135 GeV in ee channel.

	promptSS	$V+\gamma$	QmisID	Fakes	Total bkg	signal	Total predicted	Observed
$\Delta R_{min}(l_2, j)$	251.53±7.04	0.01±0.01	0.00±0.00	183.07±61.64	434.61±62.04	6.37±0.27	440.98±62.04	0
$\Delta R_{min}(l_1, j)$	153.09±5.35	0.01±0.01	0.00±0.00	118.29±40.09	271.38±40.44	5.71±0.26	277.10±40.44	0
$M(\ell\ell)$	69.90±3.81	0.00±0.00	0.00±0.00	85.08±29.03	154.97±29.28	5.51±0.26	160.48±29.28	0
$M(l_1jj)$	22.23±2.07	0.00±0.00	0.00±0.00	42.76±14.94	64.99±15.09	4.43±0.24	69.42±15.09	0

Table 43: (un)Blinded results of the search of mX=280 GeV, mS=135 GeV in $\mu\mu$ channel.

	promptSS	$V+\gamma$	QmisID	Fakes	Total bkg	signal	Total predicted	Observed
$\Delta R_{min}(l_2, j)$	328.63±7.74	47.54±6.37	10.98±0.19	201.26±58.42	588.41±59.28	8.34±0.33	596.75±59.28	0
$\Delta R_{min}(l_1, j)$	167.92±5.30	19.51±4.02	5.65±0.13	106.65±30.95	299.74±31.66	6.87±0.29	306.61±31.66	0
$M(\ell\ell)$	73.04±3.58	12.81±3.74	1.40±0.04	73.18±21.28	160.44±21.90	6.52±0.28	166.96±21.90	0
$M(l_1jj)$	27.15±2.30	4.70±1.66	0.49±0.02	39.89±12.11	72.23±12.43	5.15±0.23	77.38±12.44	0

Table 44: (un)Blinded results of the search of mX=280 GeV, mS=135 GeV in $e\mu$ channel.

	promptSS	$V+\gamma$	QmisID	Fakes	Total bkg	signal	Total predicted	Observed
$\Delta R_{min}(l_2, j)$	194.67±6.26	84.84±11.72	81.84±0.54	270.28±107.25	631.62±108.07	3.54±0.19	635.16±108.07	0
$\Delta R_{min}(l_1, j)$	92.43±4.13	29.21±5.40	29.29±0.30	120.27±48.06	271.20±48.53	2.92±0.18	274.12±48.54	0
$M(\ell\ell)$	30.44±2.48	18.51±4.62	12.04±0.15	71.24±28.71	132.22±29.18	2.61±0.17	134.83±29.18	0
$M(l_1jj)$	10.40±1.51	3.34±1.26	3.77±0.06	28.93±12.00	46.44±12.16	2.10±0.15	48.53±12.16	0

Table 45: (un)Blinded results of the search of mX=300 GeV, mS=135 GeV in ee channel.

	promptSS	$V+\gamma$	QmisID	Fakes	Total bkg	signal	Total predicted	Observed
$\Delta R_{min}(l_2, j)$	251.53±7.04	0.01±0.01	0.00±0.00	183.07±61.64	434.61±62.04	7.13±0.29	441.74±62.04	0
$\Delta R_{min}(l_1, j)$	153.09±5.35	0.01±0.01	0.00±0.00	118.29±40.09	271.38±40.44	6.23±0.28	277.62±40.44	0
$M(\ell\ell)$	69.90±3.81	0.00±0.00	0.00±0.00	85.08±29.03	154.97±29.28	5.51±0.26	160.48±29.28	0
$M(l_1jj)$	22.23±2.07	0.00±0.00	0.00±0.00	42.76±14.94	64.99±15.09	4.31±0.22	69.30±15.09	0

Table 46: (un)Blinded results of the search of mX=300 GeV, mS=135 GeV in $\mu\mu$ channel.

	promptSS	$V+\gamma$	QmisID	Fakes	Total bkg	signal	Total predicted	Observed
$\Delta R_{min}(l_2, j)$	328.63±7.74	47.54±6.37	10.98±0.19	201.26±58.42	588.41±59.28	9.25±0.33	597.65±59.28	0
$\Delta R_{min}(l_1, j)$	167.92±5.30	19.51±4.02	5.65±0.13	106.65±30.95	299.74±31.66	7.74±0.31	307.48±31.66	0
$M(\ell\ell)$	73.04±3.58	12.81±3.74	1.40±0.04	73.18±21.28	160.44±21.90	6.87±0.29	167.31±21.90	0
$M(l_1jj)$	27.15±2.30	4.70±1.66	0.49±0.02	39.89±12.11	72.23±12.43	5.46±0.26	77.70±12.44	0

Table 47: (un)Blinded results of the search of mX=300 GeV, mS=135 GeV in $e\mu$ channel.

	promptSS	$V+\gamma$	QmisID	Fakes	Total bkg	signal	Total predicted	Observed
$\Delta R_{min}(l_2, j)$	194.67±6.26	84.84±11.72	81.84±0.54	270.28±107.25	631.62±108.07	4.09±0.22	635.71±108.07	0
$\Delta R_{min}(l_1, j)$	92.43±4.13	29.21±5.40	29.29±0.30	120.27±48.06	271.20±48.53	3.40±0.20	274.60±48.54	0
$M(\ell\ell)$	30.44±2.48	18.51±4.62	12.04±0.15	71.24±28.71	132.22±29.18	2.70±0.18	134.93±29.18	0
$M(l_1jj)$	10.40±1.51	3.34±1.26	3.77±0.06	28.93±12.00	46.44±12.16	2.04±0.16	48.48±12.16	0

Table 48: (un)Blinded results of the search of mX=320 GeV, mS=135 GeV in ee channel.

	promptSS	$V+\gamma$	QmisID	Fakes	Total bkg	signal	Total predicted	Observed
$\Delta R_{min}(l_2, j)$	251.53±7.04	0.01±0.01	0.00±0.00	183.07±61.64	434.61±62.04	7.74±0.31	442.35±62.04	0
$\Delta R_{min}(l_1, j)$	153.09±5.35	0.01±0.01	0.00±0.00	118.29±40.09	271.38±40.44	6.82±0.29	278.21±40.44	0
$M(\ell\ell)$	69.90±3.81	0.00±0.00	0.00±0.00	85.08±29.03	154.97±29.28	5.43±0.26	160.41±29.28	0
$M(l_1jj)$	22.23±2.07	0.00±0.00	0.00±0.00	42.76±14.94	64.99±15.09	3.96±0.23	68.95±15.09	0

Table 49: (un)Blinded results of the search of mX=320 GeV, mS=135 GeV in $\mu\mu$ channel.

	promptSS	$V+\gamma$	QmisID	Fakes	Total bkg	signal	Total predicted	Observed
$\Delta R_{min}(l_2, j)$	328.63±7.74	47.54±6.37	10.98±0.19	201.26±58.42	588.41±59.28	10.86±0.40	599.27±59.28	0
$\Delta R_{min}(l_1, j)$	167.92±5.30	19.51±4.02	5.65±0.13	106.65±30.95	299.74±31.66	8.98±0.37	308.72±31.66	0
$M(\ell\ell)$	73.04±3.58	12.81±3.74	1.40±0.04	73.18±21.28	160.44±21.90	7.18±0.32	167.62±21.90	0
$M(l_1jj)$	27.15±2.30	4.70±1.66	0.49±0.02	39.89±12.11	72.23±12.43	5.37±0.28	77.60±12.44	0

Table 50: (un)Blinded results of the search of mX=320 GeV, mS=135 GeV in $e\mu$ channel.

	promptSS	$V+\gamma$	QmisID	Fakes	Total bkg	signal	Total predicted	Observed
$\Delta R_{min}(l_2, j)$	74.07±3.67	20.22±4.14	23.49±0.31	93.50±27.98	211.27±28.53	3.21±0.22	214.49±28.53	0
$\Delta R_{min}(l_1, j)$	43.94±2.71	10.52±2.58	13.01±0.21	44.19±13.64	111.66±14.15	2.79±0.21	114.45±14.15	0
$M(\ell\ell)$	23.62±2.15	7.57±2.41	8.57±0.15	36.87±11.51	76.64±11.95	2.59±0.20	79.23±11.96	0
$M(l_1jj)$	12.02±1.36	3.51±1.21	4.22±0.08	26.17±8.39	45.91±8.58	2.42±0.20	48.33±8.58	0

Table 51: (un)Blinded results of the search of mX=340 GeV, mS=135 GeV in ee channel.

	promptSS	$V+\gamma$	QmisID	Fakes	Total bkg	signal	Total predicted	Observed
$\Delta R_{min}(l_2, j)$	127.93±4.75	0.01±0.01	0.00±0.00	94.70±26.62	222.63±27.04	6.45±0.29	229.08±27.05	0
$\Delta R_{min}(l_1, j)$	80.44±3.62	0.01±0.01	0.00±0.00	59.98±17.14	140.42±17.51	5.87±0.27	146.29±17.52	0
$M(\ell\ell)$	42.36±2.65	0.01±0.01	0.00±0.00	51.58±14.84	93.95±15.07	5.33±0.26	99.27±15.08	0
$M(l_1jj)$	23.86±1.82	0.00±0.00	0.00±0.00	36.54±10.72	60.39±10.88	4.73±0.25	65.12±10.88	0

Table 52: (un)Blinded results of the search of mX=340 GeV, mS=135 GeV in $\mu\mu$ channel.

	promptSS	$V+\gamma$	QmisID	Fakes	Total bkg	signal	Total predicted	Observed
$\Delta R_{min}(l_2, j)$	169.72±5.40	24.53±4.99	5.42±0.13	82.38±18.06	282.04±19.51	9.25±0.37	291.29±19.51	0
$\Delta R_{min}(l_1, j)$	99.44±4.12	13.51±3.65	3.28±0.10	52.42±12.06	168.65±13.26	8.17±0.34	176.82±13.26	0
$M(\ell\ell)$	67.81±3.50	10.94±3.53	1.47±0.04	43.79±10.16	124.01±11.31	8.07±0.34	132.09±11.32	0
$M(l_1jj)$	23.81±2.02	3.53±1.29	0.52±0.02	22.73±5.93	50.59±6.40	6.08±0.29	56.67±6.40	0

Table 53: (un)Blinded results of the search of mX=340 GeV, mS=135 GeV in $e\mu$ channel.

	promptSS	$V+\gamma$	QmisID	Fakes	Total bkg	signal	Total predicted	Observed
$\Delta R_{min}(l_2, j)$	74.07±3.67	20.22±4.14	23.49±0.31	93.50±27.98	211.27±28.53	8.80±0.50	220.08±28.53	0
$\Delta R_{min}(l_1, j)$	43.94±2.71	10.52±2.58	13.01±0.21	44.19±13.64	111.66±14.15	7.92±0.48	119.58±14.15	0
$M(\ell\ell)$	23.62±2.15	7.57±2.41	8.57±0.15	36.87±11.51	76.64±11.95	7.51±0.47	84.14±11.96	0
$M(l_1jj)$	12.02±1.36	3.51±1.21	4.22±0.08	26.17±8.39	45.91±8.58	6.85±0.46	52.76±8.59	0

Table 54: (un)Blinded results of the search of mX=340 GeV, mS=145 GeV in ee channel.

	promptSS	$V+\gamma$	QmisID	Fakes	Total bkg	signal	Total predicted	Observed
$\Delta R_{min}(l_2, j)$	127.93±4.75	0.01±0.01	0.00±0.00	94.70±26.62	222.63±27.04	18.23±0.80	240.86±27.06	0
$\Delta R_{min}(l_1, j)$	80.44±3.62	0.01±0.01	0.00±0.00	59.98±17.14	140.42±17.51	16.79±0.77	157.22±17.53	0
$M(\ell\ell)$	42.36±2.65	0.01±0.01	0.00±0.00	51.58±14.84	93.95±15.07	15.82±0.76	109.76±15.09	0
$M(l_1jj)$	23.86±1.82	0.00±0.00	0.00±0.00	36.54±10.72	60.39±10.88	14.28±0.72	74.67±10.90	0

Table 55: (un)Blinded results of the search of mX=340 GeV, mS=145 GeV in $\mu\mu$ channel.

	promptSS	$V+\gamma$	QmisID	Fakes	Total bkg	signal	Total predicted	Observed
$\Delta R_{min}(l_2, j)$	169.72±5.40	24.53±4.99	5.42±0.13	82.38±18.06	282.04±19.51	23.71±0.80	305.75±19.52	0
$\Delta R_{min}(l_1, j)$	99.44±4.12	13.51±3.65	3.28±0.10	52.42±12.06	168.65±13.26	20.73±0.75	189.38±13.28	0
$M(\ell\ell)$	67.81±3.50	10.94±3.53	1.47±0.04	43.79±10.16	124.01±11.31	20.63±0.75	144.65±11.34	0
$M(l_1jj)$	23.81±2.02	3.53±1.29	0.52±0.02	22.73±5.93	50.59±6.40	15.95±0.65	66.54±6.43	0

Table 56: (un)Blinded results of the search of mX=340 GeV, mS=145 GeV in $e\mu$ channel.

	promptSS	$V+\gamma$	QmisID	Fakes	Total bkg	signal	Total predicted	Observed
$\Delta R_{min}(l_2, j)$	74.07±3.67	20.22±4.14	23.49±0.31	93.50±27.98	211.27±28.53	16.76±0.90	228.03±28.54	0
$\Delta R_{min}(l_1, j)$	43.94±2.71	10.52±2.58	13.01±0.21	44.19±13.64	111.66±14.15	14.78±0.82	126.44±14.17	0
$M(\ell\ell)$	23.62±2.15	7.57±2.41	8.57±0.15	36.87±11.51	76.64±11.95	14.68±0.82	91.32±11.98	0
$M(l_1jj)$	12.02±1.36	3.51±1.21	4.22±0.08	26.17±8.39	45.91±8.58	13.38±0.79	59.29±8.62	0

Table 57: (un)Blinded results of the search of mX=340 GeV, mS=155 GeV in ee channel.

	promptSS	$V+\gamma$	QmisID	Fakes	Total bkg	signal	Total predicted	Observed
$\Delta R_{min}(l_2, j)$	127.93±4.75	0.01±0.01	0.00±0.00	94.70±26.62	222.63±27.04	37.35±1.44	259.98±27.08	0
$\Delta R_{min}(l_1, j)$	80.44±3.62	0.01±0.01	0.00±0.00	59.98±17.14	140.42±17.51	34.86±1.41	175.29±17.57	0
$M(\ell\ell)$	42.36±2.65	0.01±0.01	0.00±0.00	51.58±14.84	93.95±15.07	33.60±1.38	127.55±15.14	0
$M(l_1jj)$	23.86±1.82	0.00±0.00	0.00±0.00	36.54±10.72	60.39±10.88	30.93±1.33	91.33±10.96	0

Table 58: (un)Blinded results of the search of mX=340 GeV, mS=155 GeV in $\mu\mu$ channel.

	promptSS	$V+\gamma$	QmisID	Fakes	Total bkg	signal	Total predicted	Observed
$\Delta R_{min}(l_2, j)$	169.72±5.40	24.53±4.99	5.42±0.13	82.38±18.06	282.04±19.51	47.30±1.58	329.34±19.57	0
$\Delta R_{min}(l_1, j)$	99.44±4.12	13.51±3.65	3.28±0.10	52.42±12.06	168.65±13.26	41.94±1.48	210.59±13.34	0
$M(\ell\ell)$	67.81±3.50	10.94±3.53	1.47±0.04	43.79±10.16	124.01±11.31	41.78±1.47	165.79±11.41	0
$M(l_1jj)$	23.81±2.02	3.53±1.29	0.52±0.02	22.73±5.93	50.59±6.40	34.23±1.35	84.82±6.54	0

Table 59: (un)Blinded results of the search of mX=340 GeV, mS=155 GeV in $e\mu$ channel.

	promptSS	$V+\gamma$	QmisID	Fakes	Total bkg	signal	Total predicted	Observed
$\Delta R_{min}(l_2, j)$	74.07±3.67	20.22±4.14	23.49±0.31	93.50±27.98	211.27±28.53	28.39±1.51	239.66±28.57	0
$\Delta R_{min}(l_1, j)$	43.94±2.71	10.52±2.58	13.01±0.21	44.19±13.64	111.66±14.15	26.67±1.45	138.32±14.22	0
$M(\ell\ell)$	23.62±2.15	7.57±2.41	8.57±0.15	36.87±11.51	76.64±11.95	26.67±1.45	103.30±12.04	0
$M(l_1jj)$	12.02±1.36	3.51±1.21	4.22±0.08	26.17±8.39	45.91±8.58	24.58±1.38	70.49±8.69	0

Table 60: (un)Blinded results of the search of mX=340 GeV, mS=165 GeV in ee channel.

	promptSS	$V+\gamma$	QmisID	Fakes	Total bkg	signal	Total predicted	Observed
$\Delta R_{min}(l_2, j)$	127.93±4.75	0.01±0.01	0.00±0.00	94.70±26.62	222.63±27.04	61.83±2.09	284.46±27.12	0
$\Delta R_{min}(l_1, j)$	80.44±3.62	0.01±0.01	0.00±0.00	59.98±17.14	140.42±17.51	58.88±2.05	199.30±17.63	0
$M(\ell\ell)$	42.36±2.65	0.01±0.01	0.00±0.00	51.58±14.84	93.95±15.07	58.73±2.05	152.67±15.21	0
$M(l_1jj)$	23.86±1.82	0.00±0.00	0.00±0.00	36.54±10.72	60.39±10.88	54.17±1.98	114.56±11.05	0

Table 61: (un)Blinded results of the search of mX=340 GeV, mS=165 GeV in $\mu\mu$ channel.

	promptSS	$V+\gamma$	QmisID	Fakes	Total bkg	signal	Total predicted	Observed
$\Delta R_{min}(l_2, j)$	169.72±5.40	24.53±4.99	5.42±0.13	82.38±18.06	282.04±19.51	81.71±2.35	363.75±19.65	0
$\Delta R_{min}(l_1, j)$	99.44±4.12	13.51±3.65	3.28±0.10	52.42±12.06	168.65±13.26	76.04±2.27	244.69±13.45	0
$M(\ell\ell)$	67.81±3.50	10.94±3.53	1.47±0.04	43.79±10.16	124.01±11.31	76.04±2.27	200.05±11.54	0
$M(l_1jj)$	23.81±2.02	3.53±1.29	0.52±0.02	22.73±5.93	50.59±6.40	66.49±2.13	117.08±6.74	0

Table 62: (un)Blinded results of the search of mX=340 GeV, mS=165 GeV in $e\mu$ channel.

10 Systematic uncertainties

The systematic uncertainties arise from signal predictions, data-driven methods and experiment.

10.1 Luminosity uncertainties

The uncertainty in the combined 2015+2016 integrated luminosity is 3.2%. It is derived, following a methodology similar to that detailed in Ref [29], from a preliminary calibration of the luminosity scale using x-y beam-separation scans performed in August 2015 and May 2016.

10.2 Theoretical uncertainties on signal

- For the SM non-resonant hh signal, the theoretical uncertainty is taken from di-higgs cross-section working group recommendations in [30] and is determined to be $^{+4.3}_{-6.0}$(scale)$^{+5.0}_{-5.0}$(Th.)$^{+2.1}_{-2.1}$(PDF)$^{+2.3}_{-2.3}(\alpha_S)$%.
- For the resonant hh signal, PDF uncertainties are cosidered. The CT10 (with 26 orthognal parameters) PDF uncertainties are estimated using LHAPDF6. Generated events are reweighted with

$$w_i = \frac{x_1 f_{1i}(x_1;Q) x_2 f_{2i}(x_2;Q)}{x_1 f_{10}(x_1;Q) x_2 f_{20}(x_2;Q} (i = 1, 2..., 52), \tag{7}$$

  where "1" and "2" denote the two incoming partons in the hard process, "0" represents the best fit (nominal) PDF set and i corresponds to the PDF set with variations up or down in the orthognal eigenvector. For each PDF set, the yields after the reweighting is determined and the total PDF uncertainty is taken as the quadrature sum from the variations in the 26 orthognal eigenvectors and symmetrized.
- Parton shower(for resonant hh signal). A truth level analysis is used to find relative differences in acceptance after variations in parton showers.

10.3 Uncertainties on data-driven backgrounds

We have used likelihood method and fake factor method to estimate QmisID and fakes, respectively. As discussed in Sec. 8.2.2, the systematic uncertainty on likelihood method is transferred to that on fake factor. In addition to QmisID component, we have also retrieved components of uncertainties of stat., sample dependence and closure on fake factors. All of them will be considered in limit settings.

10.4 Uncertainties on background cross-sections

The prompt and $V\gamma$ backgrounds are estimated using MC. The major contribution to prompt backgrounds is WZ(70%), and a 11.2% uncertainty is applied to the WZ background estimate as discussed in 3L note. In addition, there is one special background, same-signed WW, which occupies around 10% in prompt backgrounds. And 50% uncertainty is assumed. Then a 50% uncertainty is assumed on the production cross-section of $V\gamma$, tV, $t\bar{t}V$ and $t\bar{t}H$ background simulations. This value is used as a conservative estimate for the small background contributions for which no uncertainties have been derived. To support our claim that this is conservative, in the SM cross section measurments, the uncertainties on tZ and ttW (ttZ) are 15% [31] and 53.3% (33%) [32], respectively.

10.5 Experimental uncertainties

The experimental uncertainties are mostly related with the effect of ATLAS detector, arising from object reconstruction, identification, calibration, etc. The uncertainties from trigger efficiency, pileup-reweighting, energy scale, lepton efficiency, jet energy scale/resolution and b-tagging efficiency are estimated following CP group recommendations (Moriond2017).

- Detector simulation shape systematics affecting the acceptance of the signal region selection
  - Electron energy scale and resolution
  - Reconstruction of $E_{\mathrm{T}}^{\mathrm{miss}}$ due to effects of soft tracks
  - Jet uncertainties (21 nuisance parameters)
- Uncertainties on the corrections to the efficiencies of the reconstruction and selection of final states.
  - Lepton (electron and muon) reconstruction, identification and isolation efficiencies
  - Pile-up reweighting
  - JVT event weight
  - b-tagging efficiency

The experimental uncertainties are considered for signal, prompt and $V\gamma$ backgrounds. An automatic pruning procedure has been adopted: systematics uncertainties giving a normalization effect smaller than 0.5% are neglected. The pruning is applied independently for each systematic uncertainty in each region for each process.

The impact of experimental uncertainties on non-resonant search are shown through Tab. 63 to Tab. 65. The others could be found in App. H. We see most sources of systematics have very small impact on final yields(below 1%), except for `pileupEventWeight` and `JET_Flavor_Composition`, which have impact of several percent. While for $V + \gamma$, there are some quite large numbers(close 100%), that is due to low statistics. Since the contribution from $V + \gamma$ is low in backgrounds, the final effect is small, although with such big variations on yields.

Uncertainty source	Signal	promptSS	Vgam
pileupEventWeight	-1.45/0.73	-3.49/-2.46	-15.35/17.95
MV2c10_70_EventWeight_B0		2.01/-1.92	
MV2c10_70_EventWeight_B1		0.67/-0.66	
MV2c10_70_EventWeight_C0	2.87/-2.87	2.20/-2.20	0.80/-0.80
MV2c10_70_EventWeight_Light0	0.52/-0.52	0.56/-0.56	0.66/-0.65
JVT_EventWeight	0.65/-0.70	0.74/-0.78	0.90/-0.89
lepSFObjTight_EL_SF_ID	1.70/-1.69	1.74/-1.73	1.61/-1.60
lepSFObjTight_EL_SF_Isol	0.53/-0.53	0.59/-0.59	
EG_RESOLUTION_ALL		10.10/0.74	
EG_SCALE_ALL		-0.21/8.16	
JET_EffectiveNP_1	2.04/-2.72	4.33/-0.85	0.78/-8.23
JET_EffectiveNP_2	-0.88/0.55	-0.63/0.18	
JET_EffectiveNP_3	0.19/-0.56		
JET_EffectiveNP_4	-0.53/0.08		
JET_EtaIntercalibration_Modelling	0.63/-0.97	2.32/-0.74	
JET_EtaIntercalibration_TotalStat	0.59/-0.56	0.04/-0.57	
JET_Flavor_Composition	4.70/-6.78	8.80/-1.76	105.24/20.01
JET_Flavor_Response	-1.83/1.36	-0.77/4.21	
JET_Pileup_OffsetMu	-0.51/-0.10		
JET_Pileup_OffsetNPV		0.61/2.05	
JET_Pileup_RhoTopology	3.11/-4.31	6.32/-0.26	105.13/21.67
JET_PunchThrough_MC15			
JET_RelativeNonClosure_AFII	-1.08/0.61		
JET_JER_SINGLE_NP	-0.56/0.56	-4.48/4.48	-7.10/7.10
MET_SoftTrk_ResoPara	-0.92/0.92		
MET_SoftTrk_Scale	0.03/-0.52		

Table 63: The variations of experimental uncertainties on yields of signal, $V + \gamma$ and promptSS, for ee channel. All numbers are in %.

Uncertainty source	Signal	promptSS
pileupEventWeight		2.10/-4.97
MV2c10_70_EventWeight_B0		2.14/-2.07
MV2c10_70_EventWeight_B1		0.77/-0.76
MV2c10_70_EventWeight_C0	2.67/-2.67	1.88/-1.88
JVT_EventWeight	0.57/-0.60	0.59/-0.61
lepSFObjTight_MU_SF_ID_SYST	1.48/-1.46	1.53/-1.51
JET_EffectiveNP_1	1.91/-2.01	-2.47/-2.37
JET_EffectiveNP_2		-3.00/-0.03
JET_EtaIntercalibration_Modelling	0.92/-0.49	0.86/3.17
JET_Flavor_Composition	3.61/-4.41	1.70/0.78
JET_Flavor_Response	-0.83/1.35	-3.29/-1.96
JET_Pileup_OffsetMu		3.34/3.36
JET_Pileup_OffsetNPV	1.32/-0.40	0.09/9.81
JET_Pileup_RhoTopology	2.99/-2.62	-2.20/5.36
JET_PunchThrough_MC15		
JET_RelativeNonClosure_AFII	-0.74/1.02	
MUON_ID		-0.02/0.57
MUON_MS	-0.85/0.96	
JET_JER_SINGLE_NP	-2.10/2.10	9.55/-9.55
MET_SoftTrk_ResoPara	-0.50/0.50	

Table 64: The variations of experimental uncertainties on yields of signal and promptSS, for $\mu\mu$ channel. All numbers are in %.

Uncertainty source	Signal	promptSS	Vgam
pileupEventWeight	-2.12/3.63	-2.24/-0.23	14.83/-20.48
MV2c10_70_EventWeight_B0		2.02/-1.94	
MV2c10_70_EventWeight_B1		0.98/-0.96	
MV2c10_70_EventWeight_C0	2.63/-2.63	1.71/-1.71	
MV2c10_70_EventWeight_Light0		0.50/-0.49	
JVT_EventWeight	0.76/-0.78	0.58/-0.61	0.60/-0.60
lepSFObjTight_EL_SF_ID	0.77/-0.77	0.84/-0.84	0.83/-0.83
lepSFObjTight_MU_SF_ID_SYST	0.75/-0.75	0.84/-0.84	0.64/-0.64
JET_EffectiveNP_1	1.83/-1.28	0.43/-4.68	
JET_EffectiveNP_2	-0.42/0.53		
JET_EtaIntercalibration_Modelling	0.38/-0.54	-0.18/-1.56	
JET_Flavor_Composition	3.36/-3.20	13.69/-9.15	98.34/-0.01
JET_Flavor_Response	-1.19/1.04	-0.58/0.05	
JET_Pileup_OffsetNPV	0.75/-0.29		
JET_Pileup_RhoTopology	2.63/-1.92	4.75/-7.73	98.38/-0.00
JET_PunchThrough_AFII		0.58/0.58	
JET_PunchThrough_MC15		0.58/0.58	
JET_RelativeNonClosure_AFII	-0.60/0.56	0.58/0.58	
MUON_MS	-0.17/0.75		
JET_JER_SINGLE_NP		-2.10/2.10	95.94/-95.94
MET_SoftTrk_ResoPara	-0.53/0.53		
MET_SoftTrk_ResoPerp	-0.59/0.59		
MET_SoftTrk_Scale		0.06/-1.24	

Table 65: The variations of experimental uncertainties on yields of signal, $V + \gamma$ and promptSS, for $e\mu$ channel. All numbers are in %.

11 Statistical interpretation

We start statistical interpretations for the event yields after optimization cuts list in Sec. 9.

A likelihood ratio based test statistic is used, which is defined as follows:

$$\tilde{q}_\mu = \begin{cases} -2\ln \frac{\mathcal{L}(\mu,\hat{\hat{\theta}}(\mu))}{\mathcal{L}(0,\hat{\hat{\theta}}(0))} & \text{if } \hat{\mu} < 0 \\ -2\ln \frac{\mathcal{L}(\mu,\hat{\hat{\theta}}(\mu))}{\mathcal{L}(\hat{\mu},\hat{\theta})} & \text{if } 0 \leq \hat{\mu} \leq \mu \\ 0 & \text{if } \hat{\mu} > \mu \end{cases}$$

where $\hat{\theta}$ indicates an unconditional fit and $\hat{\hat{\theta}}$ indicates a conditional fit (i.e., μ is fixed to a certain value). With this test statistic, one can derive the upper limits of the cross section production times the branching ratio for each scanned mass point by using the CL$_s$ method [33] under the asymptotic approximation [34].

11.1 Search for non-resonant Higgs boson pair production

Assuming SM prediction for $\sigma(pp \to hh)$ production(33.41 fb), the expected 95% CL_s upper limit on the non-resonant Higgs pair production process $pp \to hh$ is 151.45 pb.

11.2 Search for resonant Higgs boson pair production

The expected 95% CL$_s$ upper limits on the cross section $X \to hh$ as a function of m_X is shown in Figure 9.

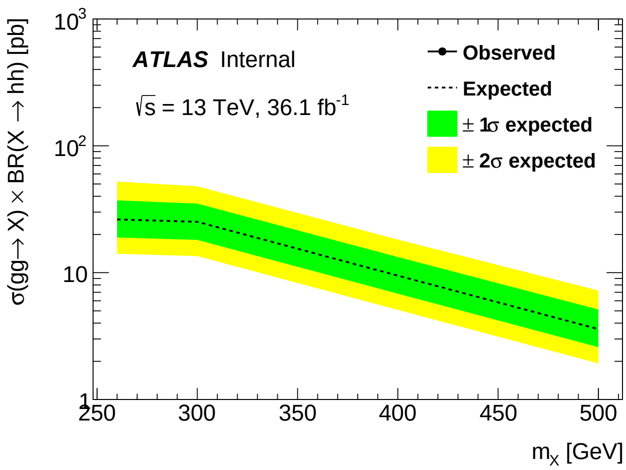

Figure 9: The expected limits for $pp \to X \to hh$, as a function of mX.

The upper limits for non-res as well as resonance are shown in Tab. 66.

	SM Higgs pair	260 GeV	300 GeV	400 GeV	500 GeV
Median	165.02	26.27	25.15	9.47	3.59
Observed	blinded	blinded	blinded	blinded	blinded
$+2\sigma$	330.34	52.24	47.93	18.22	7.23
$+1\sigma$	234.96	37.15	35.01	13.28	5.12
-1σ	118.90	18.93	18.12	6.83	2.59
-2σ	88.57	14.10	13.50	5.08	1.93

Table 66: The combined exclusion limits at the 95% CL for the production cross section of a gluon fusion produced X boson times its branching ratio to hh.

11.3 Search for resonant SS production

The expected 95% CL$_s$ upper limits on the cross section $X \to SS$ as a function of m_S or m_X is shown in Fig. 10. The detailed limits are shown in Tab. 67.

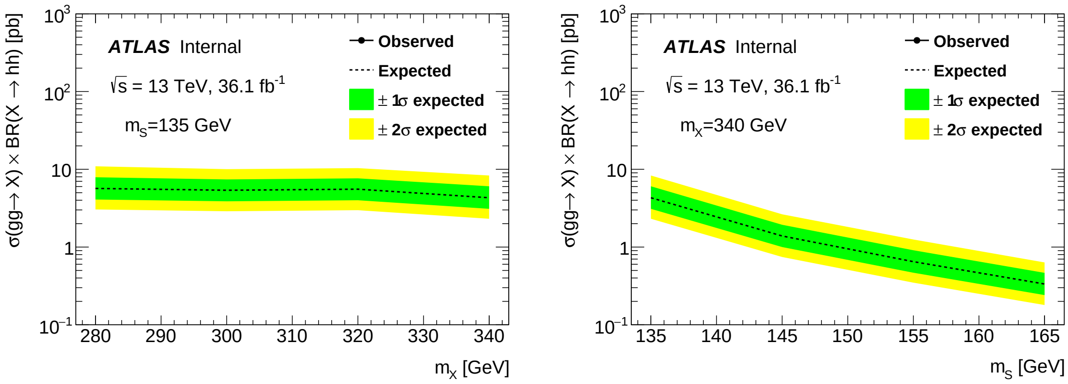

Figure 10: The expected limits for $pp \to X \to SS$ production. Left: fixing m_S=135 GeV; right: fixing m_X=340 GeV.

	X280, S135	X300, S135	X320, S135	X340, S135	X340, S145	X340, S155	X340, S165
Median	5.67	5.38	5.55	4.30	1.39	0.65	0.33
Observed	blinded	blinded	blinded	blinded	blinded	blinded	blinded
$+2\sigma$	10.93	10.04	10.35	8.32	2.64	1.25	0.63
$+1\sigma$	7.90	7.41	7.65	6.05	1.93	0.91	0.47
-1σ	4.09	3.87	4.00	3.10	1.00	0.47	0.24
-2σ	3.04	2.89	2.98	2.31	0.74	0.35	0.18

Table 67: The combined exclusion limits at the 95% CL for the production cross section of a gluon fusion produced X boson times its branching ratio to SS.

11.4 Checks on nuisance parameters

In order to understand the impact of nuisance parameters(NPs), the rankings of NPs are made based on the uncertainty from the fit, $\Delta\hat{\mu}$(here μ is cross-section of $pp \to hh/SS$). For instance, the plot of NP ranking for non-resonant search is shown in Fig. 11. In the figure, one can see `JETFlavor_Composition` has largest impact on final limits, which is consistent with the biggest variations shown from Tab. 63 to

Tab. 63.
Apart from NP ranking, to inspect the behavior of nuisance parameters in limit setting workspace, checks on the pull of nuisance parameters ($\theta_{fit} - \theta_0/\Delta\theta$) are performed with an unconditional fit to the amount of expected backgrounds, as shown in Fig. 12. The values of the pull of nuisance parameters are always close to 0, which suggests a correct implementation of the statistical model. The checks on the correlations between all parameters in the statistical model are also performed. Then checks on the pull of nuisance parameters with a conditional fit to the amount of expected signal plus backgrounds are performed, as well as done for corresponding correlations(Fig. 13). Similar checks are done with the observed data in order to check the data constraints on nuisance parameters, as shown in Fig. 14.
The checks for the searches of remaining mass points are done, whose plots can be found in App. I.

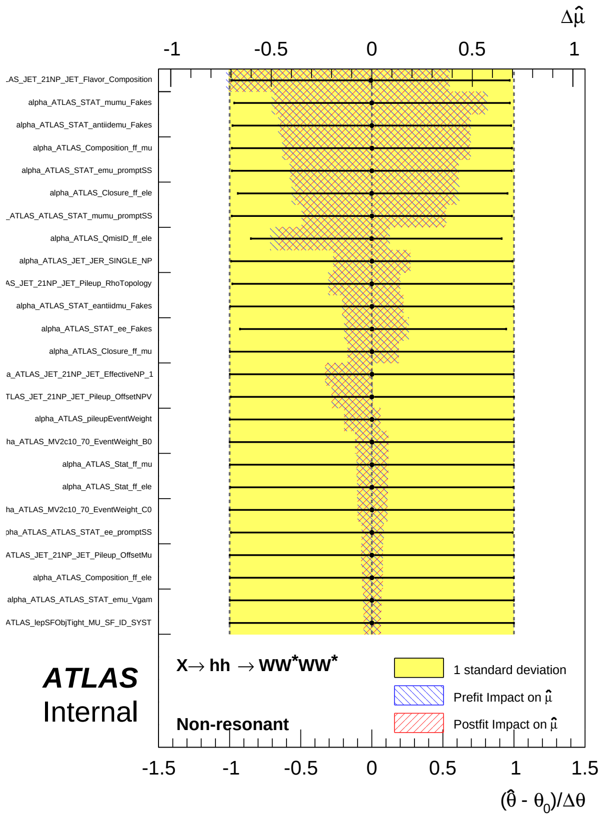

Figure 11: The ranking of NP impact on μ for non-resonant search.

12 Conclusions

A search for the production of SM Higgs boson pairs, hh, is performed using 36.1 fb^{-1} of pp data at a center-of-mass of $\sqrt(s)$ = 13 TeV collected at the ATLAS experiment in 2015 and 2016. This search uses the decay channel in which each Higgs boson decays into a pair of W-bosons with a final state consisting of two same-signed leptons, at least two(three) hadronic jets, and missing transverse energy. Standard Model background processes that result in two same-signed prompt leptons as well as $V\gamma$ production are modeled using MC. Other background processes containing of fake leptons and charge-mis-identified electrons are

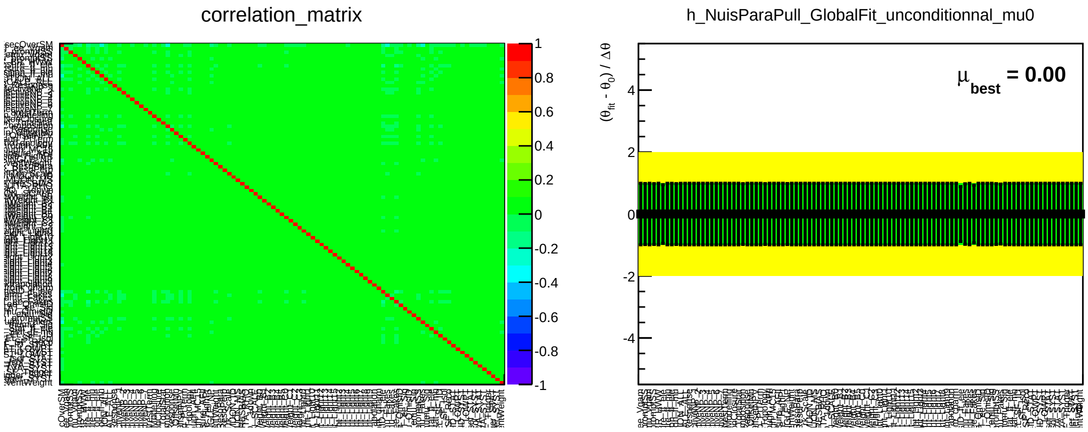

Figure 12: The correlations of NPs and pull checks for non-resonant search with a fit to expected backgrounds only.

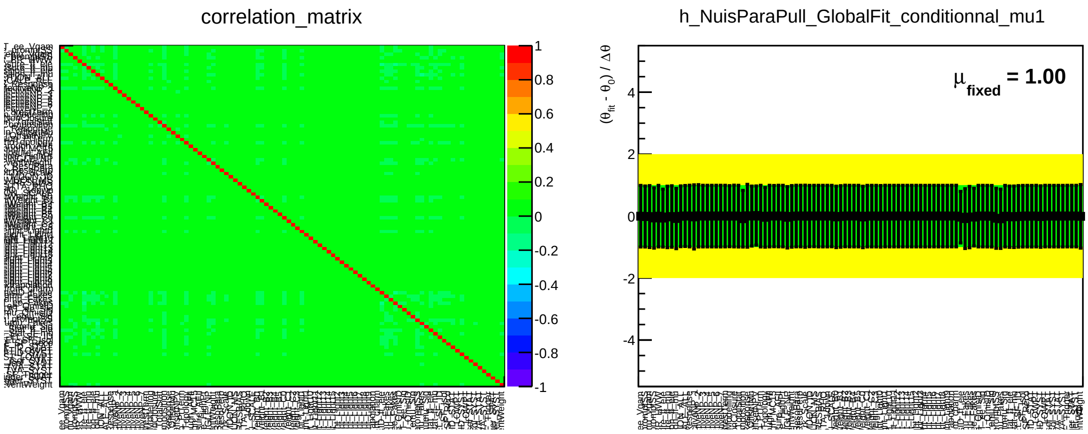

Figure 13: The correlations of NPs and pull checks for non-resonant search with a fit to expected signal plus backgrounds.

estimated by using data-driven methods. Events are classified into three categories based on the flavor of the leptons in order to exploit the different background compositions. Cross-section times branching ratio limits are set on non-resonant hh production as well as resonant hh production from a heavy Higgs boson, X. For non-resonant hh production, the expected limit is 151.45 *pb*. For resonant hh production, the limits range from 3.88 *pb* to 24.74 *pb* as a function of resonant mass in the range 260 GeV < m_X <500 GeV, assuming that the narrow-width approximation holds. For resonant SS searches, the expected limits range from 0.29 *pb* to 5.25 *pb*, as a function of m_X and m_S in the ranges 280 GeV ≤ m_X ≤ 340 GeV and 135 GeV ≤ m_S ≤ 165 GeV. The narrow-width approximation is assumed for all heavy-Higgs models used in this analysis.

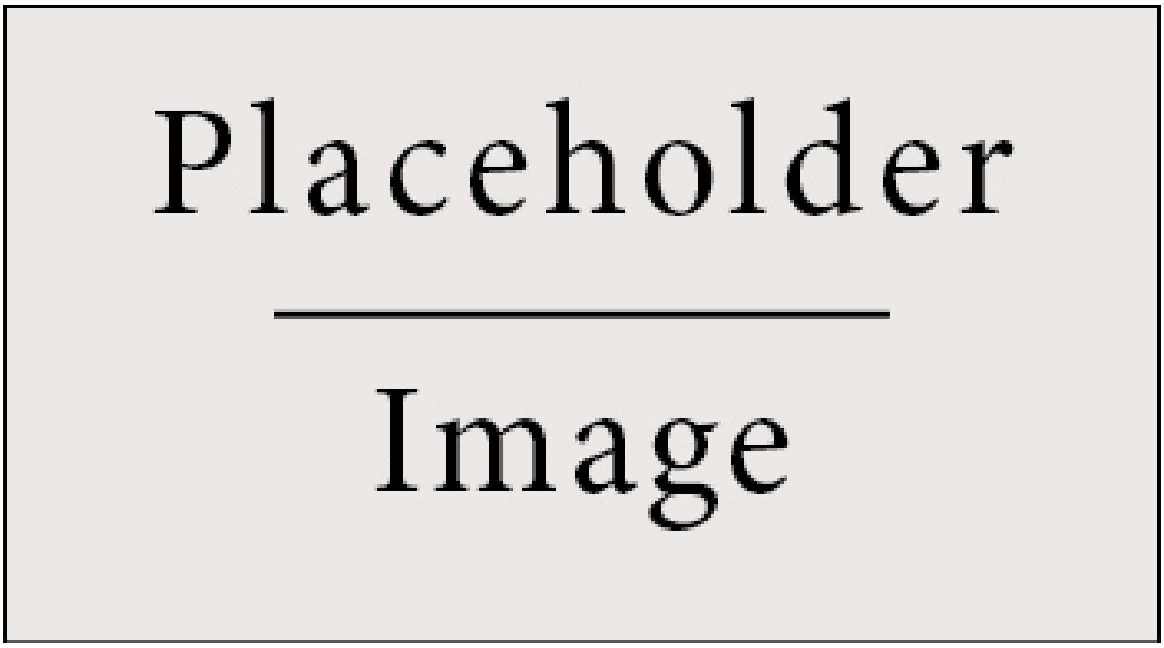

Figure 14: The correlations of NPs and pull checks for non-resonant search with a fit to observed data.

References

[1] ATLAS Collaboration, *Observation of a new particle in the search for the Standard Model Higgs boson with the ATLAS detector at the LHC*, Phys. Lett. B **716** (2012) 1, URL: {http://www.sciencedirect.com/science/article/pii/S037026931200857X}.

[2] CMS Collaboration, *Observation of a new boson at a mass of 125 GeV with the CMS experiment at the LHC*, Phys. Lett. B **716** (2012) 30, URL: {http://www.sciencedirect.com/science/article/pii/S0370269312008581}.

[3] G. Aad et al., *Search For Higgs Boson Pair Production in the $\gamma\gamma b\bar{b}$ Final State using pp Collision Data at $\sqrt{s}$ = 8 TeV from the ATLAS Detector*, Phys. Rev. Lett. **114** (2015) 081802, arXiv: 1406.5053 [hep-ex].

[4] G. Aad et al., *Search for Higgs boson pair production in the $b\bar{b}b\bar{b}$ final state from pp collisions at $\sqrt{s}$ = 8 TeVwith the ATLAS detector*, Eur. Phys. J. **C75** (2015) 412, arXiv: 1506.00285 [hep-ex].

[5] G. Aad et al., *Searches for Higgs boson pair production in the $hh \to bb\tau\tau, \gamma\gamma WW^*, \gamma\gamma bb, bbbb$ channels with the ATLAS detector*, Phys. Rev. **D92** (2015) 092004, arXiv: 1509.04670 [hep-ex].

[6] U. Baur, T. Plehn and D. Rainwater, *Measuring the Higgs Boson Self-Coupling at the Large Hadron Collider*, Phys. Rev. Lett. **89** (2002) 151801.

[7] L. Qiang and L. Zhao and Q. Yan, and X. Zhao, *Probe Higgs boson pair production via the $3\ell 2j$ + missing E_T mode*, Phys. Rev. D **92** (2015) 014015.

[8] ().

[9] ATLAS Collaboration, *Search for the Associated Production of a Higgs Boson and a Top Quark Pair in Multilepton Final States with the ATLAS Detector*, ATLAS-CONF-2016-058, 2016, URL: https://cds.cern.ch/record/2206153.

[10] ATLAS Collaboration, *Evidence of the electroweak production of $W^{\pm}W^{\pm}jj$ in pp collisions at $\sqrt{s}$ = 8 TeV with the ATLAS detector*, ATLAS-CONF-2014-013, 2014, URL: https://cds.cern.ch/record/1690282.

[11] ATLAS Collaboration, *The ATLAS Experiment at the CERN Large Hadron Collider*, JINST **3** (2008) S08003.

[12] web pages, F. Maltoni, Higgs pair production. https://cp3.irmp.ucl.ac.be/projects/madgraph/wiki/HiggsPairProduction, Dec 2013.

[13] S. Borowka et al., *Higgs Boson Pair Production in Gluon Fusion at Next-to-Leading Order with Full Top-Quark Mass Dependence*, Phys. Rev. Lett. **117** (2016) 012001, [Erratum: Phys. Rev. Lett.117,no.7,079901(2016)], arXiv: 1604.06447 [hep-ph].

[14] T. Sjostrand, S. Mrenna and P. Z. Skands, *A Brief Introduction to PYTHIA 8.1*, Comput.Phys.Commun. **178** (2008) 852, arXiv: 0710.3820 [hep-ph].

[15] R. D. Ball et al., *Parton distributions with LHC data*, Nucl. Phys. **B867** (2013) 244, arXiv: 1207.1303 [hep-ph].

[16] A. Denner et al., *Standard Model Higgs-boson branching ratios with uncertainties*, Eur. Phys. J. **C71** (2011) 1753, arXiv: 1107.5909 [hep-ph].

[17] P. Nason, *A New method for combining NLO QCD with shower Monte Carlo algorithms*, JHEP **11** (2004) 040.

[18] *ATLAS simulation infrastructure*, Eur. Phys. J. **C70** (2010) 823.

[19] GEANT4 Collaboration, S. Agostinelli et al., *GEANT4: A simulation toolkit*, Nucl. Instrum. Meth. **A506** (2003) 250.

[20] A. Martin et al., *Parton distributions for the LHC*, Eur. Phys. J. **C63** (2009) 189, arXiv: 0901.0002 [hep-ph].

[21] D Adams et al., 'Recommendations of the Physics Objects and Analysis Harmonisation Study Groups 2014', tech. rep. ATL-PHYS-INT-2014-018, CERN, 2014, URL: https://cds.cern.ch/record/1743654.

[22] ATLAS Collaboration, *Vertex Reconstruction Performance of the ATLAS Detector at $\sqrt{s}$=13 TeV*, ATL-PHYS-PUB-2015-026 (2015).

[23] The ATLAS Collaboration, *Search for heavy neutrino, W_R and Z_R gauge bosons in events with two high-P_T leptons and jets with the ATLAS detector in pp collisions at $\sqrt{s}$ = 8 TeV*, ATL-COM-PHYS-2013-810 (2013).

[24] A. Alonso and B. Meirose, *New data-driven methods for lepton charge mis-identification*, ATL-COM-PHYS-2012-164 (2012).

[25] B. Ali et al., ‘Search for the associated production of a Higgs Boson with a top quark pair in multilepton final states with the ATLAS detector (ICHEP 2016)’, tech. rep. ATL-COM-PHYS-2016-419, Supporting note to ttH to multilepton ICHEP 2016 CONF note: ATLAS-CONF-2016-058 Because supporting notes should be approved as INT after the CONF note has been approved according to paragraph A.3.2.j of this documentation: https://twiki.cern.ch/twiki/bin/view/AtlasProtected/PubComConfCheckList: CERN, 2016, URL: https://cds.cern.ch/record/2150024.

[26] S Biondi et al., ‘Search for ttH in the multilepton final 1 state: backgrounds and their estimation’, tech. rep. ATL-COM-PHYS-2014-222, Version 1 of note, to be completed with other channels as agreed: CERN, 2014, URL: https://cds.cern.ch/record/1670273.

[27] J. Alison, ‘The Fake Factor Method’, *The Road to Discovery: Detector Alignment, Electron Identification, Particle Misidentification, WW Physics, and the Discovery of the Higgs Boson*, Springer International Publishing, 2015 151, ISBN: 978-3-319-10344-0, URL: http://dx.doi.org/10.1007/978-3-319-10344-0_9.

[28] A. Hoecker et al., *TMVA: Toolkit for Multivariate Data Analysis*, PoS **ACAT** (2007) 040, arXiv: physics/0703039.

[29] ATLAS Collaboration, *Luminosity determination in pp collisions at $\sqrt{s}$ = 8 TeV using the ATLAS detector at the LHC*, (2016), arXiv: 1608.03953 [hep-ex].

[30] ATLAS Collaboration, *Analytical parametrization and shape classification of anomalous HH production in EFT approach*, LHCHXSWG-INT-2016-001 (2016).

[31] ATLAS Collaboration, *Measurement of the $W^{\pm}Z$ boson pair-production cross-section in pp collisions at $\sqrt{s}$ = 13 TeV with the ATLAS detector*, Phys. Lett. **B762** (2016) 1.

[32] ATLAS Collaboration, *Measurement of the $t\bar{t}Z$ and $t\bar{t}W$ production cross sections in multilepton final states using 3.2 fb^{-1} of pp collisions at $\sqrt{s}$ = 13 TeV with the ATLAS detector*, Eur. Phys. J. **C77** (2017) 40.

[33] A. L. Read, *Presentation of search results: The CL(s) technique*, J.Phys. **G28** (2002) 2693.

[34] G. Cowan et al., *Asymptotic formulae for likelihood-based tests of new physics*, Eur. Phys. J. **C71** (2011) 1554, arXiv: 1007.1727 [physics.data-an].

Appendix

A MadGraph5 card used for resonance signal

The run card used for generating heavy resonant scalar at the mass point of 300 GeV is attached.

```
#************************************************************************
#                        MadGraph5_aMC@NLO                              *
#                                                                       *
#                      run_card.dat aMC@NLO                             *
#                                                                       *
#  This file is used to set the parameters of the run.                  *
#                                                                       *
#  Some notation/conventions:                                           *
#                                                                       *
#   Lines starting with a hash (#) are info or comments                 *
#                                                                       *
#   mind the format:   value    = variable     ! comment                *
#************************************************************************
#
#*******************
# Running parameters
#*******************
#
#************************************************************************
# Tag name for the run (one word)                                       *
#************************************************************************
  tag_1     = run_tag ! name of the run
#************************************************************************
# Number of LHE events (and their normalization) and the required       *
# (relative) accuracy on the Xsec.                                      *
# These values are ignored for fixed order runs                         *
#************************************************************************
  10000       = nevents ! Number of unweighted events requested
    -1 = req_acc ! Required accuracy (-1=auto determined from nevents)
    -1 = nevt_job! Max number of events per job in event generation.
                 !  (-1= no split).
#************************************************************************
# Normalize the weights of LHE events such that they sum or average to *
# the total cross section                                               *
#************************************************************************
 average = event_norm      ! average or sum
#************************************************************************
```

```
# Number of points per itegration channel (ignored for aMC@NLO runs)   *
#************************************************************************
 0.01   = req_acc_FO       ! Required accuracy (-1=ignored, and use the
                     ! number of points and iter. below)
# These numbers are ignored except if req_acc_FO is equal to -1
 5000   = npoints_FO_grid  ! number of points to setup grids
 4      = niters_FO_grid   ! number of iter. to setup grids
 10000  = npoints_FO       ! number of points to compute Xsec
 6      = niters_FO        ! number of iter. to compute Xsec
#************************************************************************
# Random number seed                                                   *
#************************************************************************
   2016      = iseed   ! rnd seed (0=assigned automatically=default))
#************************************************************************
# Collider type and energy                                             *
#************************************************************************
    1   = lpp1    ! beam 1 type (0 = no PDF)
    1   = lpp2    ! beam 2 type (0 = no PDF)
   6500      = ebeam1  ! beam 1 energy in GeV
   6500      = ebeam2  ! beam 2 energy in GeV
#************************************************************************
# PDF choice: this automatically fixes also alpha_s(MZ) and its evol.  *
#************************************************************************
 lhapdf    = pdlabel   ! PDF set
 11000    = lhaid     ! if pdlabel=lhapdf, this is the lhapdf number
#************************************************************************
# Include the NLO Monte Carlo subtr. terms for the following parton    *
# shower (HERWIG6 | HERWIGPP | PYTHIA6Q | PYTHIA6PT | PYTHIA8)         *
# WARNING: PYTHIA6PT works only for processes without FSR!!!!          *
#************************************************************************
 HERWIGPP    = parton_shower
#************************************************************************
# Renormalization and factorization scales                             *
# (Default functional form for the non-fixed scales is the sum of      *
# the transverse masses of all final state particles and partons. This *
# can be changed in SubProcesses/set_scales.f)                         *
#************************************************************************
 .true.   = fixed_ren_scale  ! if .true. use fixed ren scale
 .true.   = fixed_fac_scale  ! if .true. use fixed fac scale
 130.0    = muR_ref_fixed    ! fixed ren reference scale
 130.0    = muF1_ref_fixed   ! fixed fact reference scale for pdf1
 130.0    = muF2_ref_fixed   ! fixed fact reference scale for pdf2
#************************************************************************
# Renormalization and factorization scales (advanced and NLO options)  *
#************************************************************************
 .true.   = fixed_QES_scale  ! if .true. use fixed Ellis-Sexton scale
 130.0    = QES_ref_fixed    ! fixed Ellis-Sexton reference scale
```

```
 1        = muR_over_ref     ! ratio of current muR over reference muR
 1        = muF1_over_ref    ! ratio of current muF1 over reference muF1
 1        = muF2_over_ref    ! ratio of current muF2 over reference muF2
 1        = QES_over_ref     ! ratio of current QES over reference QES
#***********************************************************************
# Reweight flags to get scale dependence and PDF uncertainty           *
# For scale dependence: factor rw_scale_up/down around central scale   *
# For PDF uncertainty: use LHAPDF with supported set                   *
#***********************************************************************
 .true.   = reweight_scale   ! reweight to get scale dependence
  0.5     = rw_Rscale_down   ! lower bound for ren scale variations
  2.0     = rw_Rscale_up     ! upper bound for ren scale variations
  0.5     = rw_Fscale_down   ! lower bound for fact scale variations
  2.0     = rw_Fscale_up     ! upper bound for fact scale variations
 .false.  = reweight_PDF     ! reweight to get PDF uncertainty
 11001    = PDF_set_min      ! First of the error PDF sets
 11052    = PDF_set_max      ! Last of the error PDF sets
#***********************************************************************
# Merging - WARNING! Applies merging only at the hard-event level.     *
# After showering an MLM-type merging should be applied as well.       *
# See http://amcatnlo.cern.ch/FxFx_merging.htm for more details.       *
#***********************************************************************
 0        = ickkw            ! 0 no merging, 3 FxFx merging, 4 UNLOPS
#***********************************************************************
#
#***********************************************************************
# BW cutoff (M+/-bwcutoff*Gamma)                                       *
#***********************************************************************
 15  = bwcutoff
#***********************************************************************
# Cuts on the jets                                                     *
# Jet clustering is performed by FastJet.
# When matching to a parton shower, these generation cuts should be    *
# considerably softer than the analysis cuts.                          *
# (more specific cuts can be specified in SubProcesses/cuts.f)         *
#***********************************************************************
  -1  = jetalgo   ! FastJet jet algorithm (1=kT, 0=C/A, -1=anti-kT)
 0.4  = jetradius ! The radius parameter for the jet algorithm
  10  = ptj       ! Min jet transverse momentum
  -1  = etaj      ! Max jet abs(pseudo-rap) (a value .lt.0 means no cut)
#***********************************************************************
# Cuts on the charged leptons (e+, e-, mu+, mu-, tau+ and tau-)        *
# (more specific gen cuts can be specified in SubProcesses/cuts.f)     *
#***********************************************************************
   0  = ptl     ! Min lepton transverse momentum
  -1  = etal    ! Max lepton abs(pseudo-rap) (a value .lt.0 means no cut)
   0  = drll    ! Min distance between opposite sign lepton pairs
```

```
  0  = drll_sf ! Min distance between opp. sign same-flavor lepton pairs
  0  = mll     ! Min inv. mass of all opposite sign lepton pairs
 30  = mll_sf  ! Min inv. mass of all opp. sign same-flavor lepton pairs
#***********************************************************************
# Photon-isolation cuts, according to hep-ph/9801442                   *
# When ptgmin=0, all the other parameters are ignored                  *
#***********************************************************************
 20  = ptgmin    ! Min photon transverse momentum
 -1  = etagamma  ! Max photon abs(pseudo-rap)
0.4  = R0gamma   ! Radius of isolation code
1.0  = xn        ! n parameter of eq.(3.4) in hep-ph/9801442
1.0  = epsgamma  ! epsilon_gamma parameter of eq.(3.4) in hep-ph/9801442
.true.  = isoEM  ! isolate photons from EM energy (photons and leptons)
#***********************************************************************
# Maximal PDG code for quark to be considered a jet when applying cuts.*
# At least all massless quarks of the model should be included here.   *
#***********************************************************************
 4 = maxjetflavor
#***********************************************************************
# For aMCfast+APPLGRID use in PDF fitting (http://amcfast.hepforge.org)*
#***********************************************************************
 0 = iappl   ! aMCfast switch (0=OFF, 1=prepare APPLgrids, 2=fill grids)
#***********************************************************************
```

B The cutflow for signal and prompt backgrounds

This section documents the cut flow of resonant hh and SS signal samples and prompt backgrounds, through Tab. 78 to Tab. 82.

B.1 The cutflow of resonant hh

Cut flow	Event yield			Eff.		
Evgen	-			100%		
HIGG8D1	72.22			49.40%		
Event cleaning	72.22			49.40%		
Trigger	45.13			30.83%		
Channel	ee	$\mu\mu$	$e\mu$	ee	$\mu\mu$	$e\mu$
OB, OLR	6.34	7.08	13.19	4.30%	4.98%	9.16%
Tight leptons, trigger match	2.80	4.94	7.28	1.92%	3.47%	5.05%
$p_T(\ell)$	1.73	2.75	4.16	1.14%	1.88%	2.80%
b veto	1.64	2.66	4.02	1.08%	1.82%	2.70%
MET	1.58	2.58	3.89	1.04%	1.76%	2.61%
Drell-Yan cut	1.54	2.52	3.81	1.01%	1.71%	2.55%
Z veto	1.34	2.52	3.81	0.88%	1.71%	2.55%
$N_{\text{jet}} \geq 2$	0.75	1.41	2.17	0.50%	0.99%	1.48%

Table 68: Cutflow of pre-selection for mX=260 GeV.

Cut flow	Event yield			Eff.		
Evgen	-			100%		
HIGG8D1	76.99			51.40%		
Event cleaning	76.99			51.40%		
Trigger	50.91			34.03%		
Channel	ee	$\mu\mu$	$e\mu$	ee	$\mu\mu$	$e\mu$
OB, OLR	6.91	7.84	14.32	4.71%	5.29%	9.82%
Tight leptons, trigger match	3.10	5.58	8.25	2.12%	3.75%	5.65%
$p_T(\ell)$	2.11	3.39	5.27	1.39%	2.22%	3.48%
b veto	2.00	3.25	5.04	1.33%	2.13%	3.32%
MET	1.91	3.13	4.89	1.28%	2.06%	3.22%
Drell-Yan cut	1.89	3.12	4.83	1.26%	2.04%	3.18%
Z veto	1.48	3.12	4.83	0.99%	2.04%	3.18%
$N_{\text{jet}} \geq 2$	1.06	2.23	3.27	0.70%	1.46%	2.21%

Table 69: Cutflow of pre-selection for mX=300 GeV.

Cut flow	Event yield			Eff.		
Evgen	-			100%		
HIGG8D1	121.57			54.94%		
Event cleaning	121.57			54.94%		
Trigger	89.20			40.26%		
Channel	ee	$\mu\mu$	$e\mu$	ee	$\mu\mu$	$e\mu$
OB, OLR	12.35	11.85	25.50	5.71%	5.72%	11.23%
Tight leptons, trigger match	6.00	8.62	15.00	2.73%	4.16%	6.68%
$p_T(\ell)$	4.47	6.04	10.89	2.00%	2.91%	4.79%
b veto	4.24	5.75	10.35	1.88%	2.75%	4.55%
MET	4.11	5.58	10.04	1.83%	2.67%	4.41%
Drell-Yan cut	4.10	5.57	10.03	1.83%	2.67%	4.40%
Z veto	3.33	5.57	10.03	1.48%	2.67%	4.40%
$N_{\text{jet}} \geq 3$	1.85	3.37	5.53	0.81%	1.61%	2.58%

Table 70: Cutflow of pre-selection for mX=400 GeV.

Cut flow	Event yield			Eff.		
Evgen	-			100%		
HIGG8D1	83.86			56.91%		
Event cleaning	83.86			56.91%		
Trigger	64.82			43.73%		
Channel	ee	$\mu\mu$	$e\mu$	ee	$\mu\mu$	$e\mu$
OB, OLR	9.07	8.65	17.60	6.06%	6.05%	12.00%
Tight leptons, trigger match	4.33	6.06	10.17	2.84%	4.25%	6.93%
$p_T(\ell)$	3.53	4.59	7.95	2.25%	3.18%	5.32%
b veto	3.30	4.31	7.43	2.10%	2.99%	4.96%
MET	3.21	4.22	7.23	2.06%	2.93%	4.83%
Drell-Yan cut	3.21	4.22	7.23	2.06%	2.93%	4.83%
Z veto	2.78	4.22	7.23	1.77%	2.93%	4.83%
$N_{\text{jet}} \geq 3$	1.76	3.03	4.85	1.11%	2.15%	3.31%

Table 71: Cutflow of pre-selection for mX=500 GeV.

Cut flow	Event yield			Eff.		
Evgen	-			100%		
HIGG8D1	239.63			53.05%		
Event cleaning	239.63			53.05%		
Trigger	157.39			34.82%		
Channel	ee	$\mu\mu$	$e\mu$	ee	$\mu\mu$	$e\mu$
OB, OLR	21.52	23.57	44.06	4.72%	5.37%	10.04%
Tight leptons, trigger match	8.51	16.72	24.52	1.89%	3.83%	5.53%
$p_T(\ell)$	5.78	10.45	15.57	1.25%	2.39%	3.43%
b veto	5.44	9.97	14.65	1.18%	2.27%	3.24%
MET	5.29	9.62	14.23	1.15%	2.19%	3.14%
Drell-Yan cut	5.14	9.40	13.93	1.12%	2.14%	3.07%
Z veto	4.41	9.40	13.93	0.99%	2.14%	3.07%
$N_{\rm jet} \geq 2$	3.19	6.95	10.44	0.71%	1.60%	2.29%

Table 72: Cutflow of pre-selection for mX=280 GeV, mS=135 GeV.

Cut flow	Event yield			Eff.		
Evgen	-			100%		
HIGG8D1	243.72			53.88%		
Event cleaning	243.72			53.88%		
Trigger	164.56			36.31%		
Channel	ee	$\mu\mu$	$e\mu$	ee	$\mu\mu$	$e\mu$
OB, OLR	22.69	24.49	45.08	4.94%	5.59%	10.17%
Tight leptons, trigger match	10.14	17.22	24.76	2.19%	3.93%	5.58%
$p_T(\ell)$	6.99	10.89	16.21	1.48%	2.43%	3.57%
b veto	6.52	10.23	15.39	1.38%	2.28%	3.38%
MET	6.26	9.92	14.81	1.33%	2.21%	3.24%
Drell-Yan cut	6.16	9.79	14.57	1.31%	2.18%	3.19%
Z veto	5.00	9.79	14.57	1.07%	2.18%	3.19%
$N_{\rm jet} \geq 2$	3.66	7.66	11.56	0.82%	1.73%	2.57%

Table 73: Cutflow of pre-selection for mX=300 GeV, mS=135 GeV.

B.2 The cutflow of resonant SS

Cut flow	Event yield			Eff.		
Evgen	-			100%		
HIGG8D1	249.12			54.77%		
Event cleaning	249.12			54.77%		
Trigger	172.38			37.89%		
Channel	ee	$\mu\mu$	$e\mu$	ee	$\mu\mu$	$e\mu$
OB, OLR	23.18	24.87	47.39	5.16%	5.67%	10.61%
Tight leptons, trigger match	10.66	17.65	26.64	2.34%	3.98%	5.87%
$p_T(\ell)$	7.53	11.51	17.73	1.62%	2.55%	3.81%
b veto	7.08	10.84	16.71	1.52%	2.40%	3.60%
MET	6.91	10.57	16.18	1.48%	2.34%	3.46%
Drell-Yan cut	6.76	10.47	16.07	1.45%	2.31%	3.43%
Z veto	5.36	10.47	16.07	1.14%	2.31%	3.43%
$N_{\text{jet}} \geq 2$	4.28	8.64	12.94	0.91%	1.91%	2.80%

Table 74: Cutflow of pre-selection for mX=320 GeV, mS=135 GeV.

Cut flow	Event yield			Eff.		
Evgen	-			100%		
HIGG8D1	250.76			55.17%		
Event cleaning	250.76			55.17%		
Trigger	175.55			38.62%		
Channel	ee	$\mu\mu$	$e\mu$	ee	$\mu\mu$	$e\mu$
OB, OLR	24.63	25.01	48.55	5.41%	5.69%	10.94%
Tight leptons, trigger match	10.90	18.00	28.26	2.35%	4.06%	6.27%
$p_T(\ell)$	8.05	12.12	19.16	1.69%	2.65%	4.17%
b veto	7.55	11.33	17.92	1.58%	2.48%	3.90%
MET	7.37	10.86	17.40	1.54%	2.39%	3.80%
Drell-Yan cut	7.25	10.77	17.25	1.51%	2.37%	3.76%
Z veto	5.71	10.77	17.25	1.21%	2.37%	3.76%
$N_{\text{jet}} \geq 3$	3.14	6.18	9.71	0.68%	1.39%	2.13%

Table 75: Cutflow of pre-selection for mX=340 GeV, mS=135 GeV.

Cut flow	Event yield			Eff.		
Evgen	-			100%		
HIGG8D1	664.46			57.34%		
Event cleaning	664.46			57.34%		
Trigger	477.45			41.18%		
Channel	ee	$\mu\mu$	$e\mu$	ee	$\mu\mu$	$e\mu$
OB, OLR	69.39	68.75	130.30	5.87%	6.11%	11.47%
Tight leptons, trigger match	31.76	49.92	73.88	2.74%	4.38%	6.52%
$p_T(\ell)$	23.91	34.06	54.22	2.02%	2.94%	4.68%
b veto	22.11	32.04	50.67	1.87%	2.74%	4.36%
MET	21.58	31.25	49.33	1.82%	2.67%	4.24%
Drell-Yan cut	21.13	31.04	48.39	1.79%	2.65%	4.16%
Z veto	16.61	31.04	48.39	1.41%	2.65%	4.16%
$N_{\text{jet}} \geq 3$	9.74	19.98	29.44	0.86%	1.71%	2.61%

Table 76: Cutflow of pre-selection for mX=340 GeV, mS=145 GeV.

Cut flow	Event yield			Eff.		
Evgen	-			100%		
HIGG8D1	1204.54			59.23%		
Event cleaning	1204.54			59.23%		
Trigger	875.37			43.07%		
Channel	ee	$\mu\mu$	$e\mu$	ee	$\mu\mu$	$e\mu$
OB, OLR	125.89	132.22	236.53	6.17%	6.64%	11.92%
Tight leptons, trigger match	55.96	93.36	131.90	2.74%	4.69%	6.68%
$p_T(\ell)$	41.92	67.48	97.25	2.00%	3.35%	4.88%
b veto	39.48	63.13	91.36	1.88%	3.12%	4.58%
MET	38.24	61.35	89.13	1.83%	3.04%	4.45%
Drell-Yan cut	37.56	59.96	87.83	1.80%	2.96%	4.39%
Z veto	30.21	59.96	87.83	1.45%	2.96%	4.39%
$N_{\text{jet}} \geq 3$	19.27	40.95	56.92	0.96%	2.02%	2.87%

Table 77: Cutflow of pre-selection for mX=340 GeV, mS=155 GeV.

Cut flow	Event yield			Eff.		
Evgen	-			100%		
HIGG8D1	1798.34			60.66%		
Event cleaning	1798.34			60.66%		
Trigger	1345.04			45.44%		
Channel	ee	$\mu\mu$	$e\mu$	ee	$\mu\mu$	$e\mu$
OB, OLR	190.13	194.17	372.33	6.34%	6.80%	12.85%
Tight leptons, trigger match	80.80	138.33	204.99	2.73%	4.86%	7.12%
$p_T(\ell)$	64.03	107.01	159.99	2.13%	3.74%	5.47%
b veto	59.71	99.17	146.36	1.98%	3.46%	5.00%
MET	57.67	96.10	141.48	1.91%	3.36%	4.85%
Drell-Yan cut	56.11	94.68	138.01	1.87%	3.31%	4.74%
Z veto	46.85	94.68	138.01	1.55%	3.31%	4.74%
$N_{\text{jet}} \geq 3$	31.24	66.07	95.90	1.04%	2.36%	3.35%

Table 78: Cutflow of pre-selection for mX=340 GeV, mS=165 GeV.

Cut flow	Event yield			Eff.		
Evgen	-			100%		
HIGG8D1	995594.85			21.49%		
Event cleaning	995594.85			21.49%		
Trigger	624003.23			13.80%		
Channel	ee	$\mu\mu$	$e\mu$	ee	$\mu\mu$	$e\mu$
OB, OLR	3984.73	1646.65	5582.67	0.11%	0.05%	0.15%
Tight leptons, trigger match	184.60	229.09	391.64	0.01%	0.01%	0.02%
$p_T(\ell)$	50.08	38.99	89.60	0.01%	0.01%	0.01%
b veto	22.14	22.88	49.73	0.00%	0.00%	0.00%
MET	22.03	22.19	48.62	0.00%	0.00%	0.00%
Drell-Yan cut	22.02	22.15	48.27	0.00%	0.00%	0.00%
Z veto	18.29	22.15	48.27	0.00%	0.00%	0.00%
$N_{\text{jet}} \geq 3$	3.26	3.40	10.56	0.00%	0.00%	0.00%

Table 79: Cutflow of pre-selection for tV process.

Cut flow	Event yield			Eff.		
Evgen	-			100%		
HIGG8D1	18004.39			44.92%		
Event cleaning	18004.39			44.92%		
Trigger	12255.24			33.67%		
Channel	ee	$\mu\mu$	$e\mu$	ee	$\mu\mu$	$e\mu$
OB, OLR	230.03	181.05	401.39	0.72%	0.56%	1.23%
Tight leptons, trigger match	90.61	126.42	214.72	0.30%	0.40%	0.69%
$p_T(\ell)$	76.06	101.93	176.13	0.25%	0.32%	0.56%
b veto	15.33	20.64	36.35	0.05%	0.06%	0.11%
MET	15.21	20.41	35.92	0.05%	0.06%	0.11%
Drell-Yan cut	15.14	20.31	35.76	0.05%	0.06%	0.11%
Z veto	13.18	20.31	35.76	0.04%	0.06%	0.11%
$N_{\text{jet}} \geq 3$	9.21	14.14	25.06	0.03%	0.05%	0.09%

Table 80: Cutflow of pre-selection for $t\bar{t}V$ process.

945
B.3 The cutflow of prompt backgrounds

Cut flow	Event yield			Eff.		
Evgen	-			100%		
HIGG8D1	6644.15			50.21%		
Event cleaning	6644.15			50.21%		
Trigger	4173.82			35.76%		
Channel	ee	$\mu\mu$	$e\mu$	ee	$\mu\mu$	$e\mu$
OB, OLR	72.70	49.64	122.03	0.55%	0.36%	0.91%
Tight leptons, trigger match	22.34	29.28	51.38	0.16%	0.21%	0.37%
$p_T(\ell)$	17.16	21.34	38.23	0.12%	0.15%	0.27%
b veto	3.15	3.97	6.99	0.02%	0.03%	0.05%
MET	3.11	3.91	6.98	0.02%	0.03%	0.05%
Drell-Yan cut	3.11	3.90	6.94	0.02%	0.03%	0.05%
Z veto	2.60	3.90	6.94	0.02%	0.03%	0.05%
$N_{\text{jet}} \geq 3$	2.29	3.45	6.04	0.02%	0.02%	0.04%

Table 81: Cutflow of pre-selection for $t\bar{t}H$ process.

Cut flow	Event yield			Eff.		
Evgen	-			100%		
HIGG8D1	258257.86			38.34%		
Event cleaning	258257.86			38.34%		
Trigger	155669.52			25.82%		
Channel	ee	$\mu\mu$	$e\mu$	ee	$\mu\mu$	$e\mu$
OB, OLR	3743.74	4100.06	6769.52	0.70%	0.64%	1.23%
Tight leptons, trigger match	1260.01	1976.38	2921.45	0.25%	0.34%	0.57%
$p_T(\ell)$	752.47	958.24	1637.09	0.17%	0.18%	0.35%
b veto	735.21	936.82	1602.76	0.16%	0.18%	0.34%
MET	700.85	895.05	1536.14	0.15%	0.17%	0.33%
Drell-Yan cut	680.96	881.19	1511.15	0.15%	0.17%	0.32%
Z veto	575.00	881.19	1511.15	0.13%	0.17%	0.32%
$N_{\text{jet}} \geq 3$	83.34	121.69	216.17	0.04%	0.05%	0.09%

Table 82: Cutflow of pre-selection for Di-boson(VV) process.

$t\bar{t}$	Two tight leptons with opposite sign leptons $(M(\ell\ell) - M(Z)) > 20$ GeV At least two b-jets
Zjets	Two tight leptons with opposite sign and same flavor $(M(\ell\ell) - M(Z)) < 45$ GeV b veto, at least one jet

Table 83: Definitions of $t\bar{t}$ and Z+jets control regions.

C Validation regions

At pre-selection level, two validation regions are defined in Tab. 83, for $t\bar{t}$ and Zjets[8]. Both $t\bar{t}$ and Zjets can contribute charge-mis-identification backgrounds in signal region. In addition, $t\bar{t}$ can be one source of jet fakes. Although charge-mis-identification and jet fakes backgrounds are not going to be estimated using MC directly, both MC samples serve data-driven estimations, which is described in Sec. 8.2.1. The kinematic distributions of $t\bar{t}$ and Zjets in each individual control region are shown in Fig. 15 and Fig. 16, respectively. They are dominant in each individual control region as expected, which confirms well modeling of $t\bar{t}$ and Zjets samples.

[8] If the cuts conflicts with pre-selection, the cuts defined for validation region are used, while the remaining keep the same as pre-selection.

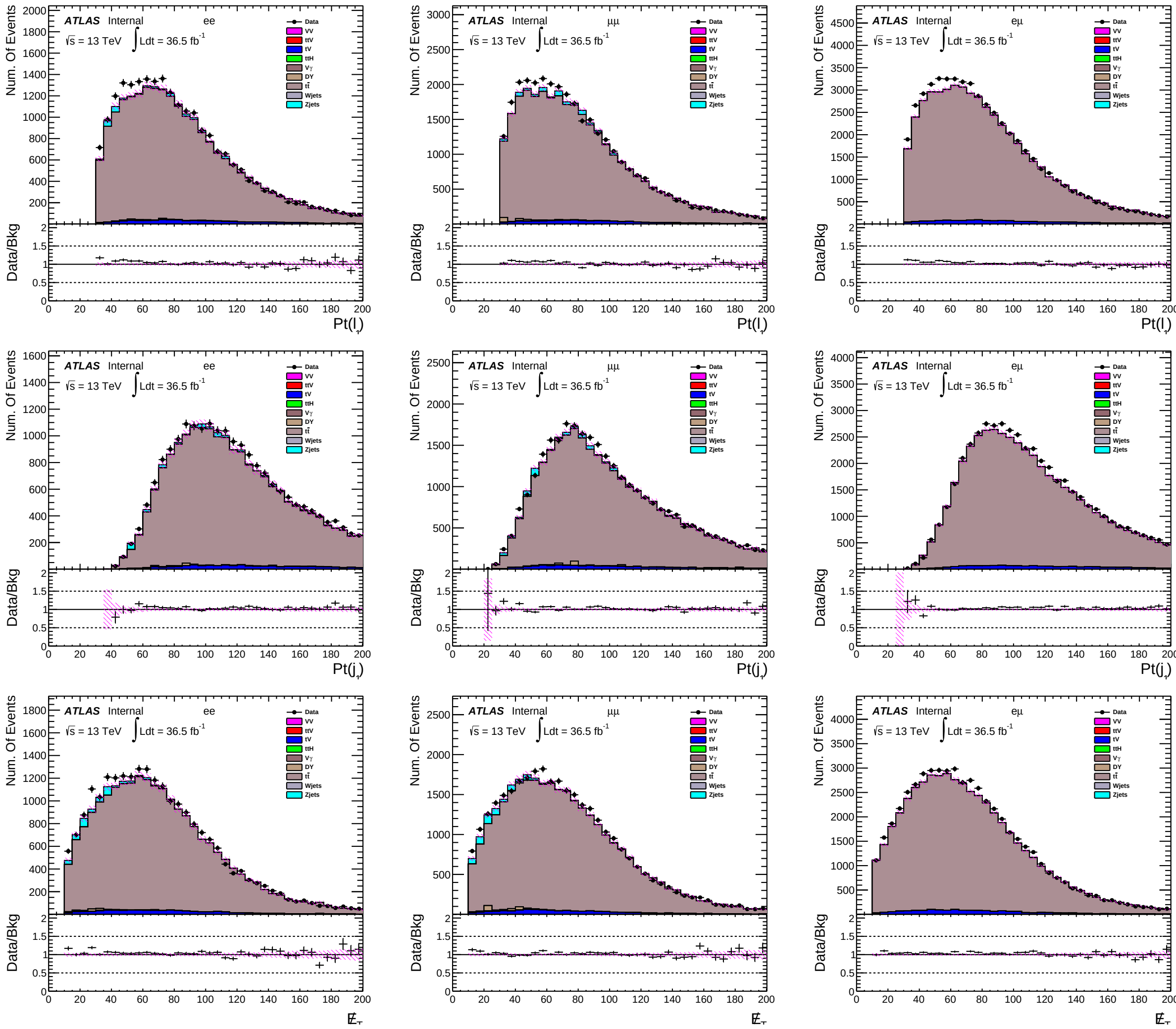

Figure 15: Validation region of $t\bar{t}$ sample. Left: ee, middle: $\mu\mu$, right: $e\mu$.

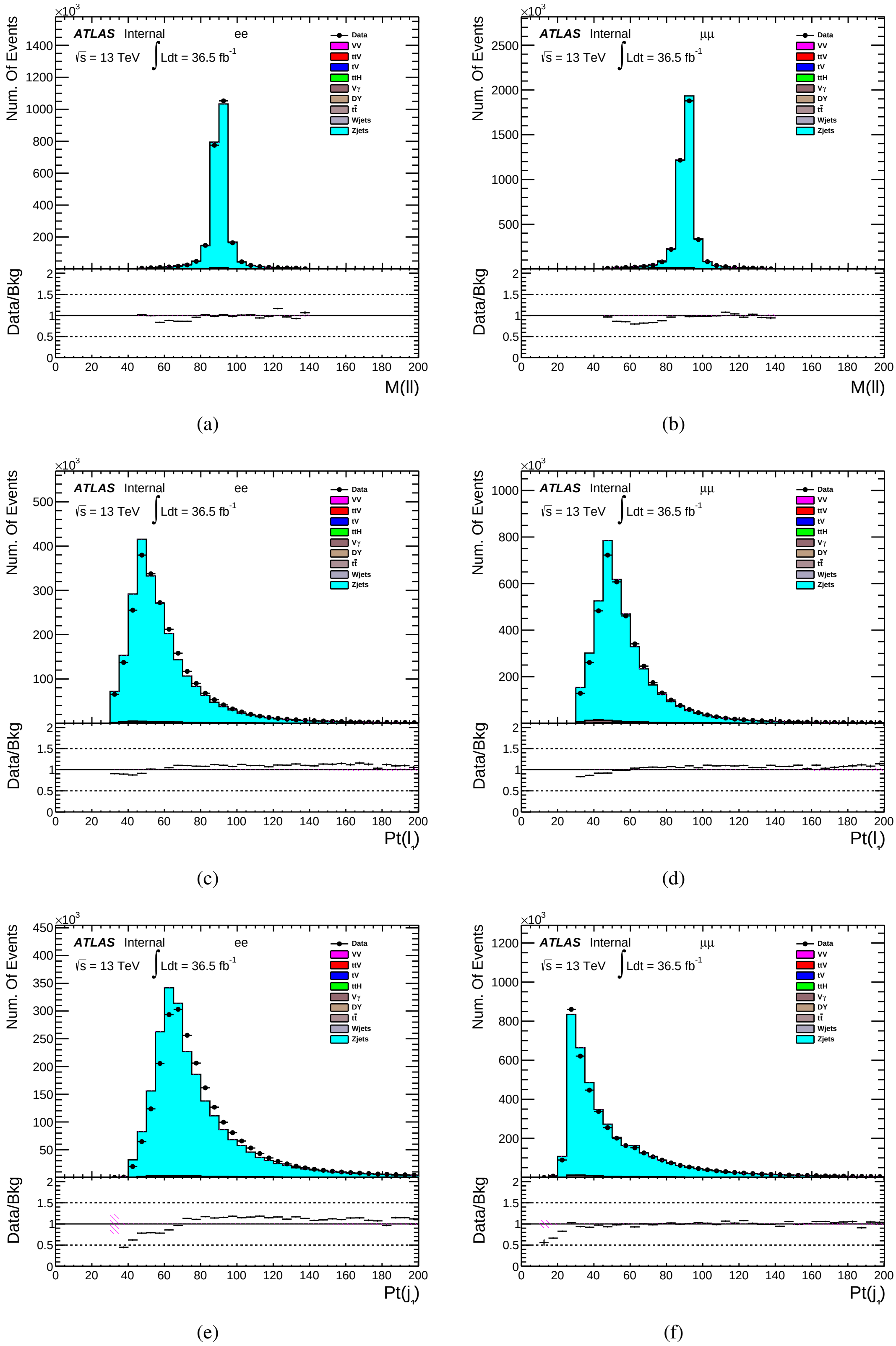

Figure 16: Validation region of Zjets sample. Left: ee, right: $\mu\mu$.

D N_{jet} division

Since we have different number of jets requirements for low and high masspoints, we were asked to check signal contamination. This sections contains two parts: significance validations and signal contamination in each mass point search. The cross-section of $pp \to X \to hh$ is assumed to be 1 pb for all mass points, with SM branching ratios.

D.1 Significance validations

The motivation of requiring different number of jets is to get high significance as we can as possible. Here, we check if we could reverse the Njet requirements for low and high mass points. It is found that, $N_{\text{jet}} \geq 2$ for mX=260, 300 GeV and $N_{\text{jet}} \geq 3$ for mX=400, 500 GeV and non-res, is our optimal choice. For instance, $e\mu$ channel at mX=300 GeV, applying $N_{\text{jet}} \geq 3$ results in 16% sensitivity loss. It is noted that, we have done this check at pre-selection level, where statistical fluctuations are small.

	mX260	mX300	mX400	mX500	Non-res
	$N_{jet} \geq 2$		$N_{jet} \geq 3$		
ee	0.0271	0.0381	0.0730	0.1002	0.0830
$\mu\mu$	0.0569	0.0899	0.1363	0.1781	0.1627
$e\mu$	0.0653	0.0984	0.1720	0.2181	0.1860
	$N_{jet} \geq 3$		$N_{jet} \geq 2$		
ee	0.0211	0.0316	0.0699	0.0867	0.0764
$\mu\mu$	0.0391	0.0742	0.1324	0.1557	0.1483
$e\mu$	0.0468	0.0825	0.1689	0.1970	0.1726

Table 84: The signal significance($S/\sqrt{B}$) changes as N_{jet} varies for different mass points. Here we assume cross-section of $pp \to hh$ equals 1 pb.

D.2 Signal contamination

We require at least 2 jets for mX=260, 300 GeV and at least 3 jets for remaining mass points. Below tables show the contamination for each mass point after optimization cuts. It is seen that the contamination from high mass points is quite large, while not vice-verse. We think it is OK, as long as we don't excess when after unblinding. But if there is some excess, we should re-consider the contamination carefully.

	X260	X300	X400	X500	Non-resonant
Applying mX260 selections	0.255±0.018	0.339±0.021	0.312±0.025	0.275±0.029	0.284±0.020
Applying mX300 selections	0.263±0.018	0.364±0.022	0.361±0.027	0.355±0.031	0.327±0.021
Applying mX400 selections	0.065±0.010	0.160±0.014	0.668±0.041	0.990±0.041	0.708±0.029
Applying mX500 selections	0.000±0.000	0.020±0.005	0.281±0.026	0.664±0.034	0.440±0.019
Applying non-resonant selections	0.060±0.011	0.150±0.015	0.662±0.039	1.108±0.043	0.834±0.033

Table 85: The signal contamination for each mass point in ee channel.

	X260	X300	X400	X500	Non-resonant
Applying mX260 selections	0.551±0.028	0.563±0.032	0.327±0.023	0.214±0.016	0.286±0.022
Applying mX300 selections	0.735±0.031	1.263±0.050	1.146±0.044	0.888±0.036	0.984±0.037
Applying mX400 selections	0.142±0.015	0.418±0.032	1.387±0.052	2.144±0.057	1.652±0.048
Applying mX500 selections	0.007±0.003	0.079±0.012	0.809±0.039	1.762±0.052	1.226±0.041
Applying non-resonant selections	0.005±0.002	0.058±0.011	0.668±0.034	1.622±0.050	1.201±0.040
Applying non-resonant selections	0.046±0.008	0.140±0.017	0.663±0.034	1.402±0.043	1.009±0.036

Table 86: The signal contamination for each mass point in $\mu\mu$ channel.

	X260	X300	X400	X500	Non-resonant
Applying mX260 selections	0.765±0.031	0.827±0.035	0.560±0.032	0.352±0.021	0.443±0.023
Applying mX300 selections	0.964±0.034	1.463±0.048	1.436±0.049	1.167±0.039	1.258±0.043
Applying mX400 selections	0.250±0.020	0.627±0.033	2.030±0.063	2.658±0.062	2.066±0.066
Applying mX500 selections	0.015±0.005	0.118±0.012	1.150±0.047	2.347±0.059	1.588±0.061
Applying non-resonant selections	0.007±0.003	0.063±0.009	0.808±0.040	1.938±0.052	1.420±0.057

Table 87: The signal contamination for each mass point in $e\mu$ channel.

E Plots at pre-selection level

The comparisons between data and MC plus data-driven backgrounds are shown in Fig 17 and Fig 18.

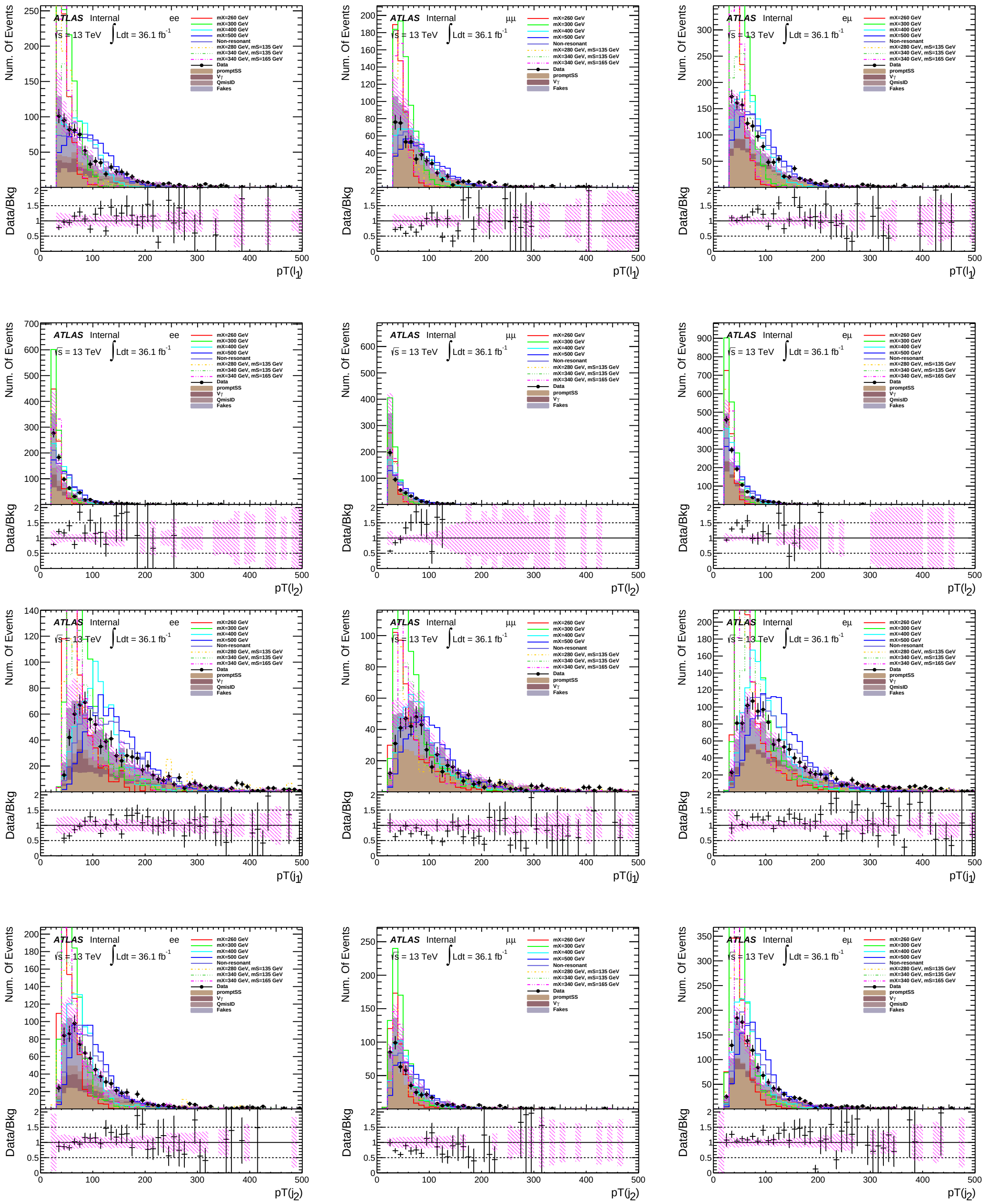
ATLAS Internal
ee
μμ
eμ
√s = 13 TeV
∫Ldt = 36.1 fb⁻¹
Num. Of Events
Data/Bkg
pT(l1)
pT(l2)
pT(j1)
pT(j2)

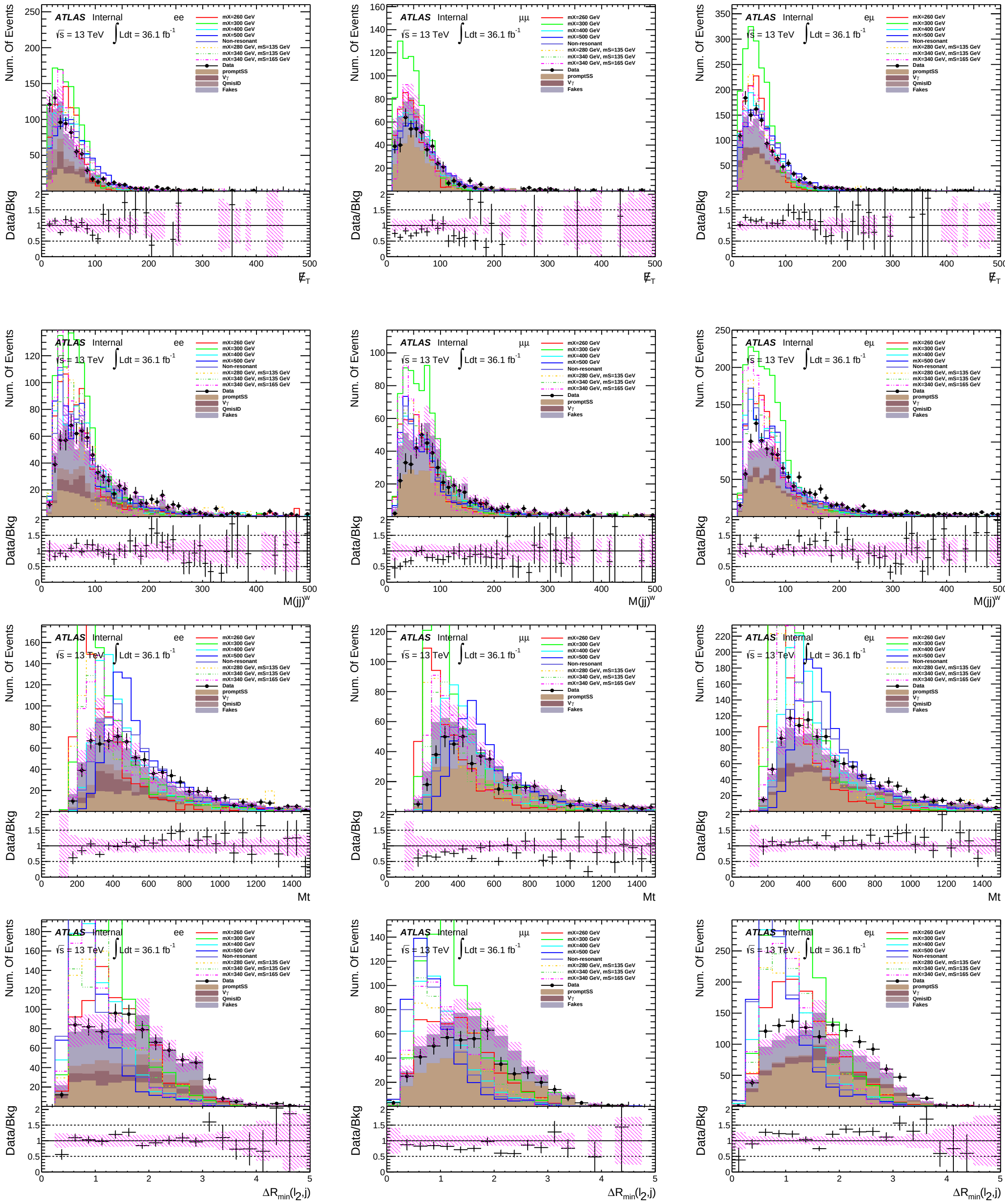

Figure 17: The comparisons between data set and backgrounds at pre-selection level, corresponding to $N_{\text{jet}} \geq 2$. Left: ee, middle: $e\mu$, right: $e\mu$. The backgrounds consist of promptSS(which contribute two prompt same-sign leptons), QmisID and fakes(jet faking lepton).

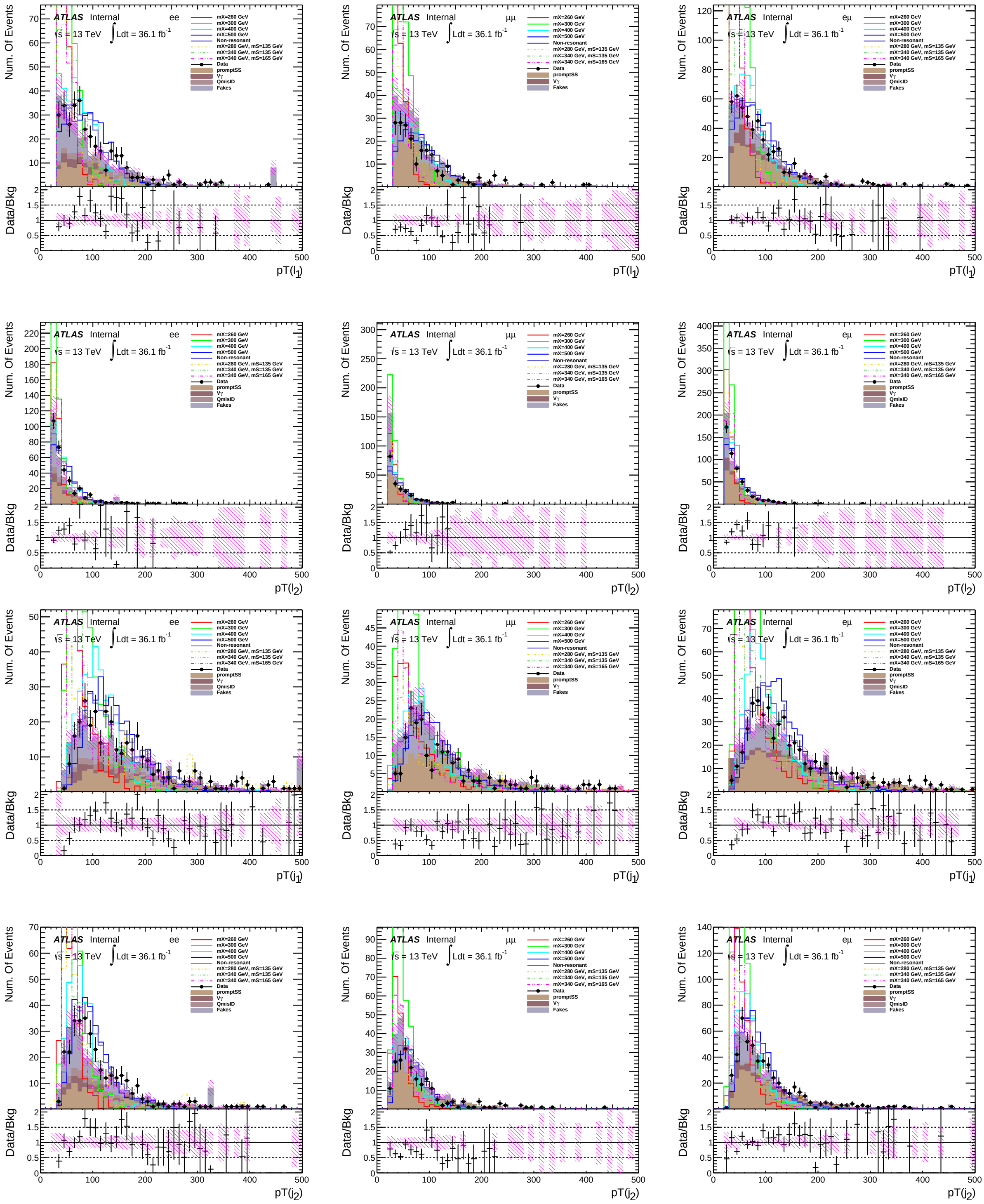
ATLAS Internal
ee
μμ
eμ
√s = 13 TeV
∫Ldt = 36.1 fb⁻¹
mX=260 GeV
mX=300 GeV
mX=400 GeV
mX=500 GeV
Non-resonant
mX=280 GeV, mS=135 GeV
mX=340 GeV, mS=135 GeV
mX=340 GeV, mS=165 GeV
Data
promptSS
Vγ
QmisID
Fakes
Num. Of Events
Data/Bkg
pT(l1)
pT(l2)
pT(j1)
pT(j2)

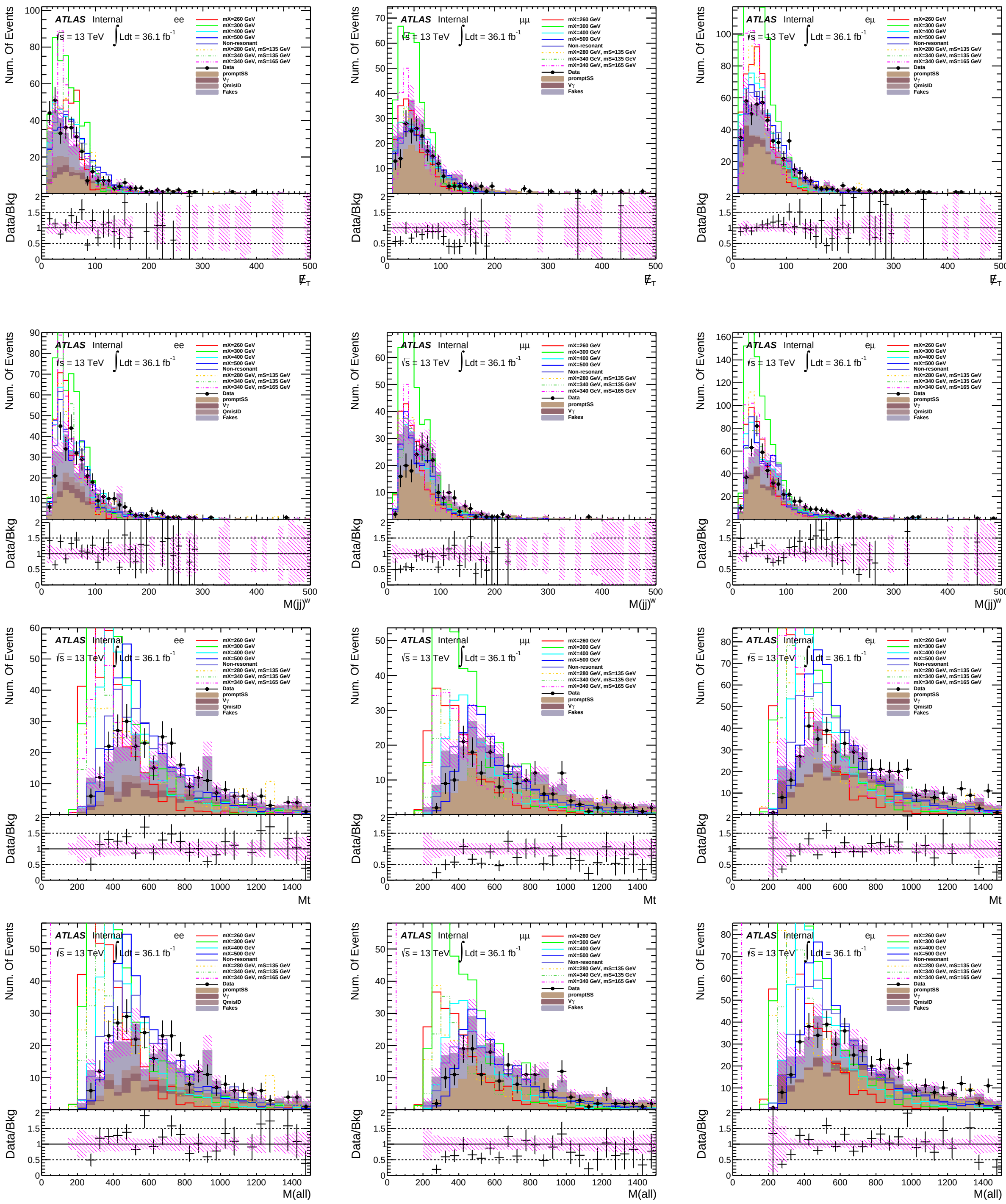

Figure 18: The comparisons between data set and backgrounds at pre-selection level, corresponding to $N_{\text{jet}} \geq 3$. Left: ee, middle: $e\mu$, right: $e\mu$. The backgrounds consist of promptSS(which contribute two prompt same-sign leptons), QmisID and fakes(jet faking lepton).

F The new BDT variables

In v26 NTuples, two new variables are introduced: `PromptLeptonIso_TagWeight` and `ChargeIDBDTTight`, which are used to suppress fakes and QmisID, respectively. Both vaiables are BDT responses.

F.1 `PromptLeptonIso_TagWeight`

The vairable,`PromptLeptonIso_TagWeight` is based on impact parameter, isolation and PID. The distributions of `PromptLeptonIso_TagWeight` are shown in Fig. 19 at pre-selection level, corresponding to Tab. 23 in Sec. 8. The agreement between data and total backgrounds is within $\pm 1\sigma$. -1 denotes that one lepton is prompt, while 1 means not prompt. We find that selected data events are dominant in prompt leptons, which indicates tight requirements on leptons are useful. While for background fakes, which is estimated by fake factor method, we see a bump at 1, especially for Fig. 19(e). This is just due to the fact that we select one tight and one anti-tight lepton to compute the fakes in signal region. The anti-tight lepton is expected to be non-prompt. Since our selected data does not suffer from non-prompt leptons seriously, plus `PromptLeptonIso_TagWeight` is not calibrated, it is not implemented in this analysis.

F.2 `ChargeIDBDTTight`

We turn to `ChargeIDBDTTight` investigation. Without the cut on `ChargeIDBDTTight`, we find their distributions in Fig. 20, corresponding to Tab. 88. We know that -1 means electron is charge-mis-identified, 1 is correctly charge identified. Clearly, we see the selected data events contain a lot of charge-mis-identified electrons. While for background QmisID, which is estimated by re-scaling events that contain two opposite-signed electrons with QmisID rates, the electrons in background QmisID are expected to be correctly charge identified essentially. In conclusion, this variable is used when selecting tight electrons, the WP. is `ChargeIDBDTTight` $>$ 0.0670415. With the cut on `ChargeIDBDTTight`, we find the distributions in Fig. 21. And the corresponding event yields are shown in Tab. 88, which is extracted from Tab. 23 in Sec. 8. In general, the QmisID is killed by a factor of 10 with the cut on `ChargeIDBDTTight`.

G Di-lepton triggers effect

The biggest change in v27.01 samples is including Di-lepton triggers. It is worthwhile to check the signal acceptance, fakes and systematics variations.

G.1 Signal acceptance

The comparison is made at pre-selection level, to avoid statistical fluctuations, especially of fakes. Note that N_{jet} $\geq$2 for mX260 and mX300, while N_{jet} $\geq$3 for the rest mass points. Clearly, we see $2\tilde{5}$% improvement on signal acceptance.

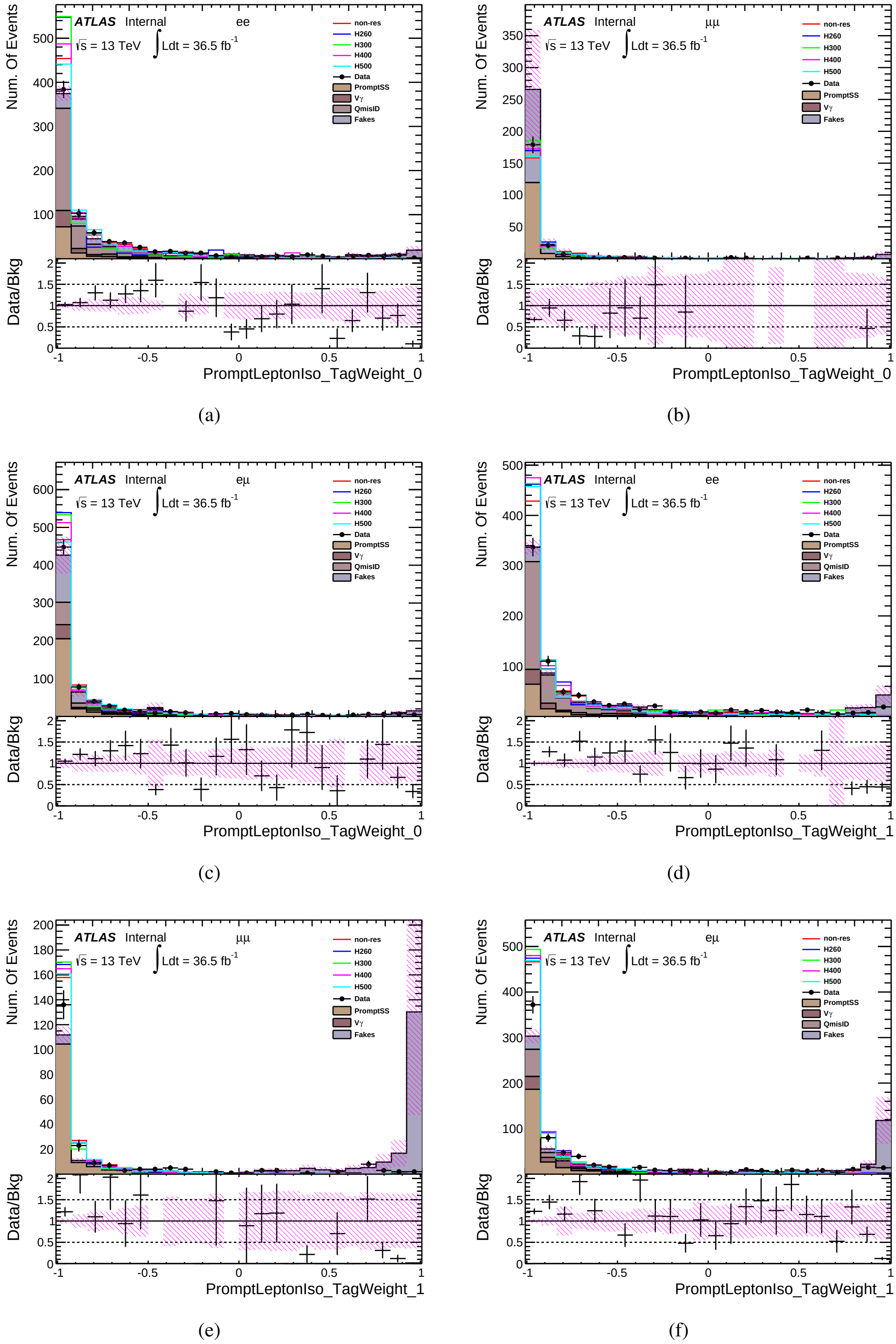

Figure 19: Distributions of `PromptLeptonIso_TagWeight` at pre-selection level, corresponding to $N_{\text{jet}} \geq 3$.

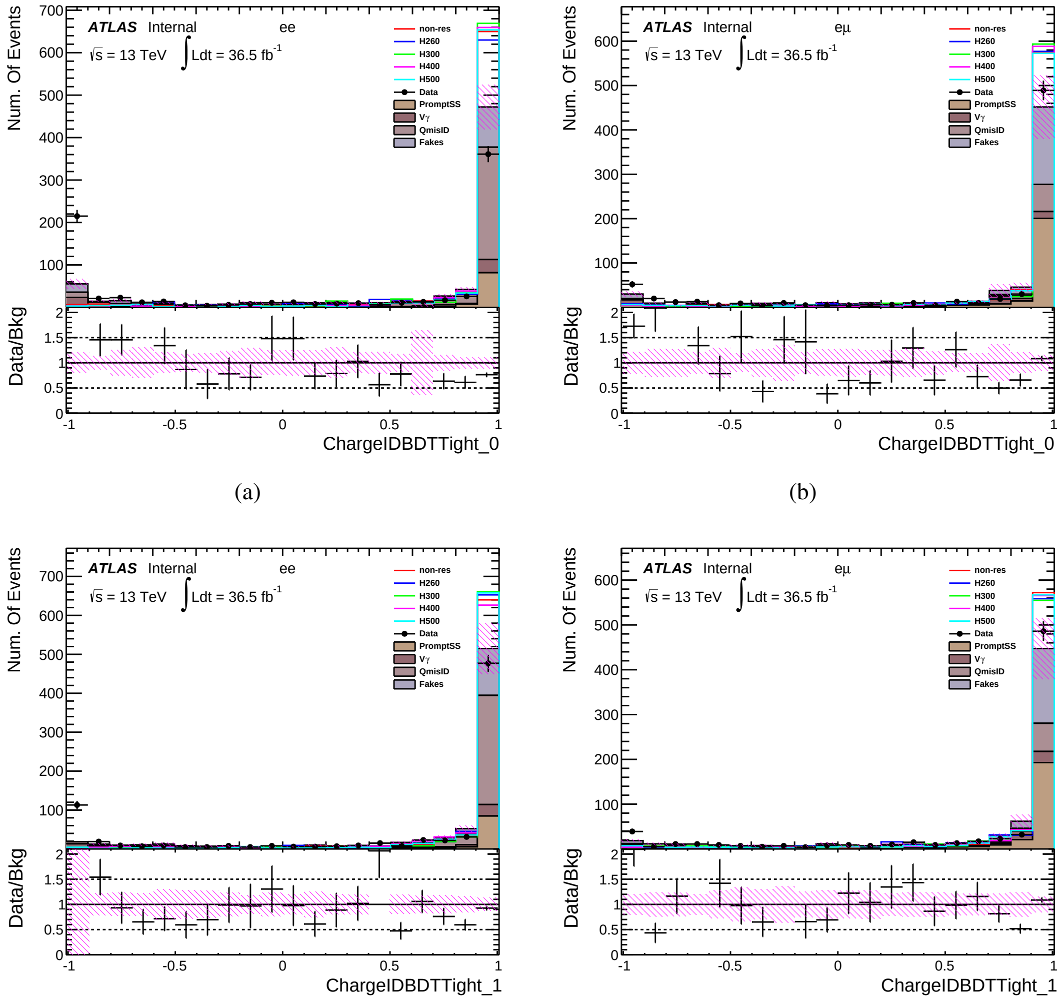

(a) (b)

(c) (d)

Figure 20: Distributions of `ChargeIDBDTTight` at pre-selection level without `ChargeIDBDTTight` > 0.0670415 cut, corresponding to $N_{\text{jet}} \geq 3$. Left: ee, right: $e\mu$.

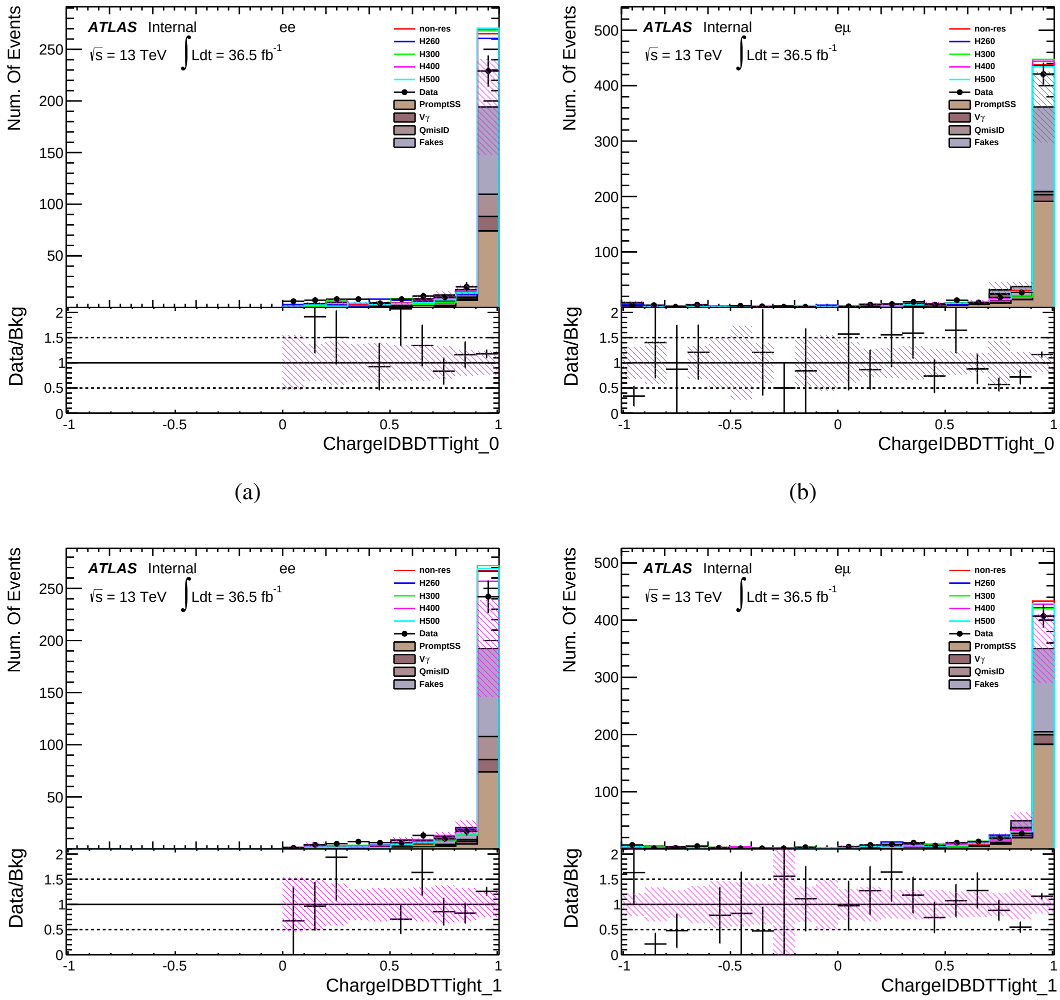

(a) (b) (c) (d)

Figure 21: Distributions of `ChargeIDBDTTight` at pre-selection level with `ChargeIDBDTTight` > 0.0670415 cut, corresponding to N_{jet} ≥3. Left: ee, right: $e\mu$.

Without `ChargeIDBDTTight` > 0.0670415	ee	$e\mu$
Jet fakes	165.83±90.42	251.20±102.45
PromptSS	111.43±4.78	269.66±7.43
$V+\gamma$	77.70±6.23	83.03±14.82
QmisID	396.92±3.86	89.81±1.52
Total backgrounds	751.87±90.84	693.71±103.80
Observed	792	727
With `ChargeIDBDTTight` > 0.0670415	ee	$e\mu$
Jet fakes	115.01±50.43	199.12±76.93
PromptSS	88.48±4.01	243.27±6.77
$V+\gamma$	22.62±3.36	50.06±14.06
QmisID	27.41±0.32	7.04±0.14
Total backgrounds	253.52±50.70	499.50±78.50
Observed	311	536

Table 88: The comparison between with and without `ChargeIDBDTTight` > 0.0670415 cut on tight electrons. The event yields are at pre-selection level, corresponding to $N_{\text{jet}} \geq 3$. We see the QmisID is suppress by a factor of more than 10 with `ChargeIDBDTTight` > 0.0670415 cut. It is worthwhile to note that the agreements between data and total backgrounds are within $\pm 1\sigma$, otherwise, the comparison is meaningless.

Pre-selection	ee	mX260	mX300	mX400	mX500	Non-res
Without di-lepton triggers	S	0.70±0.03	1.00±0.04	1.23±0.05	1.71±0.06	1.41±0.04
	$S/\sqrt{B}$	0.0262	0.0371	0.0695	0.0969	0.0800
With di-lepton triggers	S	0.75±0.03	1.05±0.04	1.26±0.05	1.73±0.06	1.43±0.04
	$S/\sqrt{B}$	0.0272	0.0381	0.0730	0.100	0.0830

Table 89: The event yields of signal ee channel at pre-selection level for w/o di-lepton triggers. Please note that for mX=260 and 300 GeV, we require $N_{\text{jet}} \geq 2$; while for the rest, $N_{\text{jet}} \geq 3$.

G.2 Variations on fakes

We have re-done fakes estimations using v27.01 samples with single lepton triggers only. Comparing to Tab. 13, the fake factors(Tab. 92) are slightly bigger.

Similarily, as described in Sec. 8.2.2, all systematics on fake factors on retrieved, which are summarized in Tab. 93 and Tab. 94. Comparing to Tab. 20 and Tab. 21, we see the biggest change is on sample dependence. For electron, the systematics on sample dependence becomes bigger if including di-lepton triggers. For muon case, the systematics si smaller when including di-lepton triggers, which results in smaller total systematic variations.

G.3 Event yields with single lepton triggers at pre-selection level

Finally, we compare the event yields w/o di-lepton triggers at pre-selectioin level. Below talbes present event yields of using single lepton triggers. We compare Tab. 95 and Tab. 95 with Tab. **??** and Tab. **??**:

Pre-selection	$\mu\mu$	mX260	mX300	mX400	mX500	Non-res
Without di-lepton triggers	S	1.35±0.04	2.12±0.06	2.23±0.06	2.92±0.06	2.66±0.06
	$S/\sqrt{B}$	0.0561	0.0885	0.1364	0.1787	0.1628
With di-lepton triggers	S	1.41±0.05	2.22±0.07	2.29±0.06	2.99±0.06	2.73±0.06
	$S/\sqrt{B}$	0.0569	0.0899	0.1363	0.1781	0.1627

Table 90: The event yields of signal $\mu\mu$ channel at pre-selection level for w/o di-lepton triggers. Please note that for mX=260 and 300 GeV, we require N_{jet} ≥2; while for the rest, N_{jet} ≥3.

Pre-selection	$e\mu$	mX260	mX300	mX400	mX500	Non-res
Without di-lepton triggers	S	2.09±0.05	3.17±0.07	3.72±0.09	4.73±0.09	4.03±0.09
	$S/\sqrt{B}$	0.0638	0.0967	0.1660	0.2111	0.1799
With di-lepton triggers	S	2.16±0.06	3.25±0.07	3.78±0.09	4.79±0.09	4.08±0.09
	$S/\sqrt{B}$	0.0653	0.0984	0.1720	0.2181	0.1860

Table 91: The event yields of signal $e\mu$ channel at pre-selection level for w/o di-lepton triggers. Please note that for mX=260 and 300 GeV, we require N_{jet} ≥2; while for the rest, N_{jet} ≥3.

Only single lepton triggers	Fake factor	Value
N_{jet} ==1	θ_e	0.5324±0.0322
	θ_μ	0.5279±0.0563
$1 \leq N_{\text{jet}} \leq 2$	θ_e	0.5492±0.0281
	θ_μ	0.4556±0.0382

Table 92: Summary of fake factors of electron and muon with different N_{jet} requirements. Uncertainties are statistical.

	N_{jet} ==1	$1 \leq N_{\text{jet}} \leq 2$
Statistics	6.05	5.12
QmisID	25.0	23.0
θ_ℓ syst.	12.86	12.86
Sample dependence	15.97	5.01
Total	32.89	27.31

Table 93: Summary of systematic uncertainty on θ_e with different N_{jet} selections(in %).

for $N_{\text{jet}} \geq 2$, there are more number of fakes for di-lepton triggers included, but the sysematics becomes smaller; for $N_{\text{jet}} \geq 3$ case, we have both smaller numbers of fakes and systematics.

	N_{jet} ==1	$1 \leq N_{\text{jet}} \leq 2$
Statistics	10.66	8.38
θ_ℓ syst.	11.17	11.17
Sample dependence	38.72	34.20
Total	41.49	36.95

Table 94: Summary of systematic uncertainty on θ_μ with different N_{jet} selections(in %).

Without di-lepton triggers	ee	$\mu\mu$	$e\mu$
Jet fakes	297.93±98.80	223.88±93.52	358.12±94.35
PromptSS	224.61±6.79	350.82±8.80	595.18±10.87
$V+\gamma$	103.38±12.39	0.01±0.01	104.86±15.11
QmisID	100.13±0.60	0.00±0.00	18.08±0.23
Total backgrounds	726.05±99.80	574.72±93.94	1076.24±96.16
Observed	759	467	1232

Table 95: Event yields at pre-selection level, corresponding to $N_{\text{jet}} \geq 2$. Uncertainties include all systematics.

Without di-lepton triggers	ee	$\mu\mu$	$e\mu$
Jet fakes	146.05±40.88	102.83±38.61	162.34±36.82
PromptSS	102.82±4.42	163.78±5.76	280.89±7.24
$V+\gamma$	27.61±4.51	0.01±0.01	50.21±13.72
QmisID	35.24±0.38	0.00±0.00	8.32±0.16
Total backgrounds	311.71±41.36	266.62±39.04	501.77±39.95
Observed	322	208	500

Table 96: Event yields at pre-selection level, corresponding to $N_{\text{jet}} \geq 3$. Uncertainties include all systematics.

H Impact of experimental uncertainties on event yields

The variations of experimental uncertainties on yields are summarized from Tab. 97 to Tab. 129, for each channel of each mass point. All numbers are in %.

H.1 The hh searches

Uncertainty source	Signal	promptSS	Vgam
pileupEventWeight	2.05/-1.40	7.12/-2.29	-1.97/-3.28
MV2c10_70_EventWeight_B0		0.96/-0.91	
MV2c10_70_EventWeight_C0	1.58/-1.58	1.42/-1.42	
MV2c10_70_EventWeight_Light0		0.52/-0.52	0.74/-0.73
JVT_EventWeight	1.17/-1.20	0.95/-1.02	0.71/-0.81
lepSFObjTight_EL_SF_Reco			0.50/-0.50
lepSFObjTight_EL_SF_ID	2.14/-2.12	2.41/-2.39	2.20/-2.18
lepSFObjTight_EL_SF_Isol	0.54/-0.54		
EG_RESOLUTION_ALL	-0.60/-0.26	0.59/0.14	
EG_SCALE_ALL		0.85/1.62	
JET_BJES_Response			0.00/7.49
JET_EffectiveNP_1	3.62/-4.15	6.61/-0.28	1.14/15.38
JET_EffectiveNP_2	-0.53/0.20	1.68/1.18	
JET_EtaIntercalibration_Modelling	0.86/0.50	1.19/0.43	
JET_EtaIntercalibration_NonClosure	-0.25/0.52	0.63/1.04	
JET_EtaIntercalibration_TotalStat		1.14/1.75	
JET_Flavor_Composition	7.89/-11.31	5.24/-8.23	22.80/8.27
JET_Flavor_Response	-1.88/1.97	-0.47/5.53	8.23/0.01
JET_Pileup_OffsetMu	0.71/0.28	1.64/0.08	
JET_Pileup_OffsetNPV	0.64/-1.75	0.98/-1.86	0.00/7.49
JET_Pileup_PtTerm		-0.05/1.63	
JET_Pileup_RhoTopology	6.22/-8.16	5.48/-3.91	33.46/15.75
JET_RelativeNonClosure_AFII	-1.13/0.97		
JET_JER_SINGLE_NP	2.05/-2.05	-4.17/4.17	12.46/-12.46
MET_SoftTrk_ResoPara			9.57/-9.57
MET_SoftTrk_ResoPerp			9.57/-9.57
MET_SoftTrk_Scale			0.00/9.57

Table 97: The variations of experimental uncertainties on yields of m_X=260 GeV, $V + \gamma$ and promptSS, for ee channel.

Uncertainty source	Signal	promptSS
pileupEventWeight	-1.69/1.57	17.97/-9.39
MV2c10_70_EventWeight_B0		0.67/-0.63
MV2c10_70_EventWeight_C0	1.73/-1.73	0.89/-0.89
MV2c10_70_EventWeight_C1	-0.53/0.53	
JVT_EventWeight	0.69/-0.74	0.68/-0.71
lepSFObjTight_MU_SF_ID_SYST	1.27/-1.26	1.23/-1.22
JET_EffectiveNP_1	3.86/-4.89	8.68/1.47
JET_EffectiveNP_2	-1.08/1.62	2.07/1.83
JET_EffectiveNP_3	0.44/-0.82	
JET_EffectiveNP_7	-0.56/0.44	
JET_EtaIntercalibration_Modelling	1.25/-1.27	2.29/1.08
JET_EtaIntercalibration_NonClosure		2.24/5.39
JET_EtaIntercalibration_TotalStat	1.38/-0.83	-0.04/2.17
JET_Flavor_Composition	4.65/-9.31	15.35/-17.69
JET_Flavor_Response	-2.42/1.86	1.66/5.03
JET_Pileup_OffsetMu	-0.40/1.07	-0.07/-3.23
JET_Pileup_OffsetNPV	-1.65/0.86	5.74/0.22
JET_Pileup_PtTerm		1.93/0.11
JET_Pileup_RhoTopology	3.08/-5.77	15.53/-16.09
JET_RelativeNonClosure_AFII	-2.62/3.20	
MUON_ID		-1.35/-1.36
MUON_MS		-0.13/-1.01
MUON_SCALE	-0.20/0.60	
JET_JER_SINGLE_NP	-3.08/3.08	16.41/-16.41

Table 98: The variations of experimental uncertainties on yields of m_X=260 GeV, $V + \gamma$ and promptSS, for $\mu\mu$ channel.

Uncertainty source	Signal	promptSS	Vgam
pileupEventWeight	-1.52/0.84	-8.00/2.83	32.40/-4.63
MV2c10_70_EventWeight_B0		1.22/-1.18	
MV2c10_70_EventWeight_C0	1.66/-1.66	0.86/-0.86	
MV2c10_70_EventWeight_C1	-0.50/0.50		
JVT_EventWeight	0.76/-0.81	0.77/-0.80	1.06/-1.05
lepSFObjTight_EL_SF_ID	1.06/-1.06	1.03/-1.03	0.73/-0.73
lepSFObjTight_MU_SF_ID_SYST	0.60/-0.60	0.65/-0.65	0.56/-0.55
EG_RESOLUTION_ALL		-1.91/0.00	0.00/1.34
EG_SCALE_ALL		-0.88/-0.06	0.04/1.30
JET_EffectiveNP_1	3.71/-3.57	10.50/-5.99	13.43/0.00
JET_EffectiveNP_2	-1.94/1.08	-5.32/4.03	
JET_EffectiveNP_3		0.79/-1.15	0.00/inf
JET_EffectiveNP_4		-1.15/0.04	
JET_EffectiveNP_5		0.03/-0.76	
JET_EffectiveNP_7		-0.68/1.29	
JET_EffectiveNP_8restTerm		-0.45/-0.66	
JET_EtaIntercalibration_Modelling	0.73/-0.83	4.37/-3.58	13.08/0.00
JET_EtaIntercalibration_NonClosure	-1.07/0.19	1.63/-2.84	
JET_EtaIntercalibration_TotalStat	0.73/-1.09	2.46/-4.33	
JET_Flavor_Composition	5.79/-7.73	12.34/-10.83	4.60/-15.76
JET_Flavor_Response	-2.53/2.71	-2.46/6.66	0.00/13.08
JET_Pileup_OffsetMu	-0.88/0.21	-1.35/-0.71	
JET_Pileup_OffsetNPV		3.65/-1.07	
JET_Pileup_PtTerm		-1.44/1.25	
JET_Pileup_RhoTopology	4.09/-4.65	12.19/-10.42	13.43/-15.76
JET_RelativeNonClosure_AFII	-1.56/1.88		
MUON_ID		-1.82/0.17	1.30/0.00
MUON_MS		-0.46/-0.87	1.30/0.00
MUON_SCALE			1.30/0.00
JET_JER_SINGLE_NP	-0.73/0.73	10.02/-10.02	-25.03/25.03
MET_SoftTrk_ResoPerp		0.57/-0.57	

Table 99: The variations of experimental uncertainties on yields of m_X=260 GeV, $V + \gamma$ and promptSS, for $e\mu$ channel.

Uncertainty source	Signal	promptSS	Vgam
pileupEventWeight	-3.84/4.31	5.12/-1.47	-8.16/0.24
MV2c10_70_EventWeight_B0		1.17/-1.13	
MV2c10_70_EventWeight_C0	1.85/-1.85	1.37/-1.37	1.68/-1.68
MV2c10_70_EventWeight_Light0		0.52/-0.51	0.57/-0.57
JVT_EventWeight	0.91/-0.97	0.91/-0.96	0.78/-0.84
lepSFObjTight_EL_SF_ID	2.12/-2.10	2.13/-2.11	1.67/-1.66
lepSFObjTight_EL_SF_Isol	0.55/-0.55		
EG_RESOLUTION_ALL		0.38/0.75	
JET_BJES_Response		-0.04/-1.29	0.00/4.74
JET_EffectiveNP_1	1.08/-2.78	5.03/-4.27	43.47/4.55
JET_EffectiveNP_2		-1.83/0.81	
JET_EffectiveNP_3		-0.01/-0.53	
JET_EffectiveNP_6		0.08/-0.59	
JET_EtaIntercalibration_Modelling	0.25/-0.86	2.37/-1.80	
JET_EtaIntercalibration_NonClosure	-0.33/0.56	-1.83/0.66	
JET_EtaIntercalibration_TotalStat		0.79/-0.51	
JET_Flavor_Composition	4.53/-6.95	8.19/-12.03	67.99/6.70
JET_Flavor_Response	-1.52/0.51	-3.14/4.55	
JET_Pileup_OffsetMu	0.15/0.72		
JET_Pileup_OffsetNPV	0.15/-0.86	-1.46/-2.40	0.02/4.74
JET_Pileup_RhoTopology	3.32/-5.12	6.79/-7.70	63.93/4.80
JET_PunchThrough_MC15			
JET_RelativeNonClosure_AFII	-0.88/1.34		
JET_JER_SINGLE_NP	1.63/-1.63	-6.91/6.91	2.32/-2.32
MET_SoftTrk_ResoPara	-0.61/0.61		6.07/-6.07
MET_SoftTrk_ResoPerp			6.07/-6.07
MET_SoftTrk_Scale			0.00/6.07

Table 100: The variations of experimental uncertainties on yields of m_X=300 GeV, $V+\gamma$ and promptSS, for ee channel.

Uncertainty source	Signal	promptSS
pileupEventWeight	3.40/-1.24	2.87/-1.00
MV2c10_70_EventWeight_B0		0.99/-0.96
MV2c10_70_EventWeight_C0	1.71/-1.71	1.21/-1.21
JVT_EventWeight	0.54/-0.59	0.47/-0.51
lepSFObjTight_MU_SF_ID_SYST	1.28/-1.27	1.32/-1.31
JET_EffectiveNP_1	2.68/-2.86	6.88/-7.07
JET_EffectiveNP_2	-0.73/-0.26	-1.70/3.11
JET_EffectiveNP_3		0.55/-0.64
JET_EffectiveNP_4		-0.23/0.54
JET_EffectiveNP_5		-0.24/0.55
JET_EffectiveNP_6		0.56/-0.67
JET_EffectiveNP_7		-0.69/0.58
JET_EffectiveNP_8restTerm		0.57/-0.24
JET_EtaIntercalibration_Modelling	0.32/-1.22	2.89/-3.98
JET_EtaIntercalibration_NonClosure	-0.95/-0.64	1.03/2.37
JET_EtaIntercalibration_TotalStat	-0.13/-1.25	2.02/-1.26
JET_Flavor_Composition	3.83/-5.85	10.78/-10.22
JET_Flavor_Response	-1.86/0.71	-3.76/4.84
JET_Pileup_OffsetMu	-1.03/-0.55	0.12/0.78
JET_Pileup_OffsetNPV	-0.07/-0.69	0.96/-1.53
JET_Pileup_PtTerm	-0.21/-0.68	0.34/-0.59
JET_Pileup_RhoTopology	3.04/-3.99	8.51/-8.14
JET_PunchThrough_MC15		
JET_RelativeNonClosure_AFII	-2.07/0.48	
MUON_ID	-0.32/0.55	-1.04/-1.44
JET_JER_SINGLE_NP	-1.71/1.71	
MET_SoftTrk_ResoPerp	-0.56/0.56	1.06/-1.06
MET_SoftTrk_Scale		0.54/0.89

Table 101: The variations of experimental uncertainties on yields of m_X=300 GeV, $V + \gamma$ and promptSS, for $\mu\mu$ channel.

Uncertainty source	Signal	promptSS	Vgam
pileupEventWeight	0.13/0.71	-3.84/0.78	12.08/-1.83
MV2c10_70_EventWeight_B0		1.42/-1.37	
MV2c10_70_EventWeight_C0	1.69/-1.69	1.11/-1.11	
MV2c10_70_EventWeight_Light0			0.51/-0.51
JVT_EventWeight	0.65/-0.71	0.68/-0.71	1.18/-1.17
lepSFObjTight_EL_SF_ID	0.92/-0.92	0.93/-0.93	1.01/-1.01
lepSFObjTight_MU_SF_ID_SYST	0.61/-0.61	0.67/-0.67	0.52/-0.52
EG_SCALE_ALL		-0.65/0.25	
JET_EffectiveNP_1	1.88/-2.86	10.35/-3.88	19.28/-0.75
JET_EffectiveNP_2	-0.83/0.16	-1.95/1.58	
JET_EffectiveNP_3		0.86/0.02	0.00/inf
JET_EffectiveNP_4		0.04/0.56	
JET_EtaIntercalibration_Modelling	0.37/-0.60	5.08/-1.97	9.35/0.03
JET_EtaIntercalibration_NonClosure	-0.57/0.20	0.60/1.16	
JET_EtaIntercalibration_TotalStat		1.03/-1.05	
JET_Flavor_Composition	3.87/-6.14	15.50/-8.85	18.35/-12.54
JET_Flavor_Response	-1.71/1.04	-1.93/9.31	-0.00/9.38
JET_Pileup_OffsetMu		-1.02/0.55	
JET_Pileup_OffsetNPV	0.18/-0.66	3.52/0.39	
JET_Pileup_PtTerm		-0.71/0.94	
JET_Pileup_RhoTopology	2.71/-3.52	12.15/-6.91	19.28/-12.04
JET_PunchThrough_MC15			
JET_RelativeNonClosure_AFII	-1.34/0.64		
MUON_ID		0.06/-0.66	
JET_JER_SINGLE_NP	-2.48/2.48	2.39/-2.39	-5.38/5.38
MET_SoftTrk_ResoPerp		0.75/-0.75	

Table 102: The variations of experimental uncertainties on yields of m_X=300 GeV, $V + \gamma$ and promptSS, for $e\mu$ channel.

Uncertainty source	Signal	promptSS	Vgam
pileupEventWeight	3.77/-3.40	-0.14/-4.35	-13.37/13.41
MV2c10_70_EventWeight_B0		1.88/-1.81	
MV2c10_70_EventWeight_B1		0.74/-0.73	
MV2c10_70_EventWeight_C0	2.21/-2.21	1.84/-1.84	
MV2c10_70_EventWeight_Light0	0.56/-0.55	0.56/-0.56	0.62/-0.62
JVT_EventWeight	0.94/-0.97	0.81/-0.85	
lepSFObjTight_EL_SF_ID	1.72/-1.71	1.76/-1.75	1.51/-1.50
lepSFObjTight_EL_SF_Isol		0.54/-0.54	
EG_RESOLUTION_ALL		5.80/0.74	
EG_SCALE_ALL	0.12/-0.93	-0.07/5.82	
JET_EffectiveNP_1	2.21/-4.38	6.05/-1.62	0.63/-6.64
JET_EffectiveNP_2	-1.05/0.45	-1.26/0.00	
JET_EtaIntercalibration_Modelling		2.40/-0.54	
JET_EtaIntercalibration_NonClosure	-1.07/0.19		
JET_EtaIntercalibration_TotalStat	0.32/-0.71	-0.15/-1.25	
JET_Flavor_Composition	3.46/-9.71	9.61/-6.17	67.89/12.39
JET_Flavor_Response	-2.53/1.00	-1.51/5.97	
JET_Pileup_OffsetMu	-0.87/-0.02		
JET_Pileup_OffsetNPV	-0.04/-1.64	-0.63/1.53	
JET_Pileup_RhoTopology	2.82/-6.68	6.47/-1.85	67.82/12.61
JET_PunchThrough_MC15			
JET_RelativeNonClosure_AFII	-1.46/0.94		
JET_JER_SINGLE_NP		-2.51/2.51	-18.84/18.84

Table 103: The variations of experimental uncertainties on yields of m_X=400 GeV, $V + \gamma$ and promptSS, for ee channel.

Uncertainty source	Signal	promptSS
pileupEventWeight	3.05/-1.82	0.29/-0.64
MV2c10_70_EventWeight_B0		2.05/-1.97
MV2c10_70_EventWeight_B1		0.69/-0.68
MV2c10_70_EventWeight_C0	2.11/-2.11	1.53/-1.53
JVT_EventWeight	0.59/-0.63	0.60/-0.62
lepSFObjTight_MU_SF_ID_SYST	1.33/-1.31	1.45/-1.44
JET_EffectiveNP_1	2.08/-1.43	9.75/-5.81
JET_EffectiveNP_2	-0.52/1.08	-1.97/1.62
JET_EtaIntercalibration_NonClosure	-0.06/0.56	0.05/2.66
JET_EtaIntercalibration_TotalStat	0.89/-0.28	1.76/-1.13
JET_Flavor_Composition	4.56/-4.15	11.61/-15.40
JET_Flavor_Response	-1.09/1.82	-1.56/5.62
JET_Pileup_OffsetMu	0.32/0.69	
JET_Pileup_OffsetNPV	0.51/0.18	2.89/-1.65
JET_Pileup_RhoTopology	3.38/-2.11	9.01/-7.26
JET_PunchThrough_MC15		
JET_RelativeNonClosure_AFII	-0.30/0.62	
MUON_ID		-0.58/0.19
MUON_MS	-0.30/1.32	
JET_JER_SINGLE_NP	-2.02/2.02	9.48/-9.48
MET_SoftTrk_Scale	-0.66/-0.10	

Table 104: The variations of experimental uncertainties on yields of m_X=400 GeV, $V+\gamma$ and promptSS, for $\mu\mu$ channel.

Uncertainty source	Signal	promptSS	Vgam
pileupEventWeight	-0.13/0.84		-7.74/1.73
MV2c10_70_EventWeight_B0		1.91/-1.84	
MV2c10_70_EventWeight_B1		0.69/-0.68	
MV2c10_70_EventWeight_C0	2.29/-2.29	1.62/-1.62	
MV2c10_70_EventWeight_Light0		0.51/-0.50	
JVT_EventWeight	0.84/-0.87	0.65/-0.68	0.94/-0.94
lepSFObjTight_EL_SF_ID	0.83/-0.83	0.89/-0.89	0.51/-0.51
lepSFObjTight_MU_SF_ID_SYST	0.70/-0.70	0.75/-0.75	0.68/-0.68
EG_RESOLUTION_ALL		1.02/0.32	
EG_SCALE_ALL		-0.10/1.09	
JET_EffectiveNP_1	2.11/-2.17	5.69/-4.42	0.19/-1.94
JET_EffectiveNP_2		-0.79/1.11	
JET_EffectiveNP_3		0.42/0.64	
JET_EffectiveNP_4		0.66/0.44	
JET_EffectiveNP_8restTerm		0.65/0.01	
JET_EtaIntercalibration_Modelling	0.27/-0.72	1.57/-2.16	
JET_EtaIntercalibration_NonClosure		-0.10/-1.00	
JET_EtaIntercalibration_TotalStat		1.26/-1.13	
JET_Flavor_Composition	4.39/-5.61	13.45/-10.45	2.82/-5.50
JET_Flavor_Response	-1.39/1.06	-2.12/2.21	
JET_Pileup_OffsetMu		-0.50/-0.23	
JET_Pileup_OffsetNPV	0.04/-0.54	0.90/-0.38	
JET_Pileup_PtTerm		1.06/0.03	
JET_Pileup_RhoTopology	3.52/-3.54	9.96/-6.65	1.33/-4.15
JET_PunchThrough_MC15			
JET_RelativeNonClosure_AFII	-1.00/0.89		
MUON_ID	0.36/-0.65		
MUON_MS		0.00/0.54	
JET_JER_SINGLE_NP	0.66/-0.66	2.96/-2.96	25.61/-25.61
MET_SoftTrk_ResoPara		0.59/-0.59	
MET_SoftTrk_ResoPerp		0.63/-0.63	
MET_SoftTrk_Scale		0.65/-0.02	

Table 105: The variations of experimental uncertainties on yields of m_X=400 GeV, $V+\gamma$ and promptSS, for $e\mu$ channel.

Uncertainty source	Signal	promptSS	Vgam
pileupEventWeight	0.08/1.94	-3.01/-3.73	-26.98/42.53
MV2c10_70_EventWeight_B0		2.48/-2.37	
MV2c10_70_EventWeight_B1		0.76/-0.74	
MV2c10_70_EventWeight_C0	2.78/-2.78	2.38/-2.38	
MV2c10_70_EventWeight_Light0	0.51/-0.51	0.52/-0.52	0.72/-0.71
JVT_EventWeight	0.64/-0.69	0.78/-0.80	0.75/-0.76
lepSFObjTight_EL_SF_ID	1.59/-1.57	1.88/-1.86	2.08/-2.07
lepSFObjTight_EL_SF_Isol		0.75/-0.74	0.99/-0.99
EG_RESOLUTION_ALL		18.86/-0.30	
EG_SCALE_ALL		0.00/18.68	-0.79/0.00
JET_EffectiveNP_1	1.45/-1.36	4.90/-0.65	3.67/-0.09
JET_EffectiveNP_2	-0.56/0.71	-0.60/0.18	
JET_EtaIntercalibration_Modelling		5.06/-0.56	-0.88/-0.09
JET_Flavor_Composition	4.20/-4.76	11.77/0.93	4.16/-7.56
JET_Flavor_Response	-1.43/0.64	-0.56/4.80	-0.09/-0.88
JET_Pileup_OffsetNPV	0.07/-0.57	0.31/5.01	-0.98/0.01
JET_Pileup_RhoTopology	2.41/-2.53	6.18/1.21	3.68/-0.09
JET_PunchThrough_MC15			
JET_RelativeNonClosure_AFII	-0.83/0.81		
MUON_ID	0.00/690.28		
JET_JER_SINGLE_NP	-1.60/1.60	1.62/-1.62	5.08/-5.08

Table 106: The variations of experimental uncertainties on yields of m_X=500 GeV, $V + \gamma$ and promptSS, for ee channel.

Uncertainty source	Signal	promptSS
pileupEventWeight	-4.30/4.09	2.10/-4.97
MV2c10_70_EventWeight_B0		2.14/-2.07
MV2c10_70_EventWeight_B1		0.77/-0.76
MV2c10_70_EventWeight_C0	2.68/-2.68	1.88/-1.88
JVT_EventWeight		0.59/-0.61
lepSFObjTight_MU_SF_ID_SYST	1.50/-1.49	1.53/-1.51
JET_EffectiveNP_1	0.65/-1.73	-2.47/-2.37
JET_EffectiveNP_2	-0.31/0.67	-3.00/-0.03
JET_EtaIntercalibration_Modelling		0.86/3.17
JET_EtaIntercalibration_TotalStat	0.66/-0.31	
JET_Flavor_Composition	1.96/-4.23	1.70/0.78
JET_Flavor_Response	-1.22/0.49	-3.29/-1.96
JET_Pileup_OffsetMu		3.34/3.36
JET_Pileup_OffsetNPV		0.09/9.81
JET_Pileup_RhoTopology	1.17/-3.08	-2.20/5.36
JET_PunchThrough_MC15		
MUON_ID	-0.05/678.83	-0.02/0.57
JET_JER_SINGLE_NP	-1.03/1.03	9.55/-9.55

Table 107: The variations of experimental uncertainties on yields of m_X=500 GeV, $V + \gamma$ and promptSS, for $\mu\mu$ channel.

Uncertainty source	Signal	promptSS	Vgam
pileupEventWeight	-4.01/3.18	-4.16/1.52	-16.34/-4.95
MV2c10_70_EventWeight_B0		2.08/-1.99	
MV2c10_70_EventWeight_B1		0.98/-0.96	
MV2c10_70_EventWeight_C0	2.72/-2.72	1.88/-1.88	
JVT_EventWeight	0.62/-0.65	0.52/-0.55	0.72/-0.72
lepSFObjTight_EL_SF_ID	0.79/-0.79	0.87/-0.87	1.04/-1.04
lepSFObjTight_MU_SF_ID_SYST	0.76/-0.76	0.90/-0.90	0.85/-0.84
JET_EffectiveNP_1	1.09/-1.10	0.36/-5.92	
JET_EffectiveNP_2	-0.64/0.39		
JET_Flavor_Composition	3.85/-2.90	6.13/-10.09	
JET_Flavor_Response	-0.47/0.52		
JET_Pileup_OffsetNPV	0.92/-0.28		
JET_Pileup_RhoTopology	2.96/-1.99	4.54/-9.94	
JET_PunchThrough_AFII		0.77/0.77	
JET_PunchThrough_MC15		0.77/0.77	
JET_RelativeNonClosure_AFII		0.77/0.77	
MUON_ID	0.16/710.76		
MUON_MS	-0.21/0.56		
JET_JER_SINGLE_NP	1.57/-1.57	-1.33/1.33	-2.16/2.16

Table 108: The variations of experimental uncertainties on yields of m_X=500 GeV, $V + \gamma$ and promptSS, for $e\mu$ channel.

1022 H.2 The SS searches

Uncertainty source	Signal	promptSS	Vgam
pileupEventWeight	-0.31/3.26	4.82/-3.32	-1.97/-3.28
MV2c10_70_EventWeight_B0		1.26/-1.20	
MV2c10_70_EventWeight_C0	2.15/-2.15	1.57/-1.57	
MV2c10_70_EventWeight_Light0		0.54/-0.54	0.74/-0.73
JVT_EventWeight	1.09/-1.12	0.98/-1.03	0.71/-0.81
lepSFObjTight_EL_SF_Reco			0.50/-0.50
lepSFObjTight_EL_SF_ID	1.99/-1.97	2.29/-2.27	2.20/-2.18
lepSFObjTight_EL_SF_Isol	0.54/-0.53		
EG_RESOLUTION_ALL		-1.13/0.31	
EG_SCALE_ALL	-1.26/-0.41	0.94/0.00	
JET_EffectiveNP_1	1.73/-2.85	4.03/-2.52	1.14/-0.34
JET_EffectiveNP_2	-1.20/0.32	-1.42/1.43	
JET_EffectiveNP_3		-0.03/-1.56	
JET_EtaIntercalibration_Modelling	-0.46/-0.83	0.76/-1.21	
JET_EtaIntercalibration_NonClosure	-0.59/0.35	-1.16/-0.25	
JET_EtaIntercalibration_TotalStat	0.35/-1.21	1.32/0.14	
JET_Flavor_Composition	4.36/-6.40	6.96/-14.12	33.81/0.03
JET_Flavor_Response	-2.73/0.33	-1.22/2.80	
JET_Pileup_OffsetNPV	0.42/-0.60	-2.48/-1.77	
JET_Pileup_PtTerm		-1.62/0.04	
JET_Pileup_RhoTopology	2.89/-6.11	5.04/-6.62	33.46/0.02
JET_RelativeNonClosure_AFII	-0.81/0.56		
JET_JER_SINGLE_NP		2.90/-2.90	21.77/-21.77
MET_SoftTrk_ResoPara			9.57/-9.57
MET_SoftTrk_ResoPerp			9.57/-9.57
MET_SoftTrk_Scale			0.00/9.57

Table 109: The variations of experimental uncertainties on yields of m_X=280 GeV, m_S=135 GeV signal, $V + \gamma$ and promptSS, for ee channel.

Uncertainty source	Signal	promptSS
pileupEventWeight	-3.66/1.24	-2.77/0.81
MV2c10_70_EventWeight_B0		1.13/-1.08
MV2c10_70_EventWeight_C0	2.05/-2.05	1.25/-1.25
JVT_EventWeight	0.65/-0.69	0.57/-0.61
lepSFObjTight_MU_SF_ID_SYST	1.28/-1.27	1.35/-1.34
JET_EffectiveNP_1	1.84/-2.82	5.51/-0.43
JET_EffectiveNP_2	-0.51/0.74	-0.80/1.34
JET_EffectiveNP_3		0.59/-0.90
JET_EffectiveNP_4		0.53/0.56
JET_EffectiveNP_6		0.50/-1.07
JET_EffectiveNP_7		-1.12/0.03
JET_EffectiveNP_8restTerm		0.54/-0.00
JET_EtaIntercalibration_Modelling	0.36/-0.80	
JET_EtaIntercalibration_NonClosure	-0.24/0.71	0.79/1.98
JET_EtaIntercalibration_TotalStat		-0.55/0.45
JET_Flavor_Composition	3.65/-6.64	15.20/-5.60
JET_Flavor_Response	-1.29/0.60	0.51/2.44
JET_Pileup_OffsetMu		1.35/-2.53
JET_Pileup_OffsetNPV	-0.12/-0.76	2.87/-1.44
JET_Pileup_PtTerm		0.76/0.79
JET_Pileup_RhoTopology	2.42/-4.42	10.25/-3.04
JET_RelativeNonClosure_AFII	-1.37/1.70	
MUON_ID		-0.55/-0.99
MUON_SCALE		-0.01/0.50
JET_JER_SINGLE_NP	-4.27/4.27	25.77/-25.77
MET_SoftTrk_Scale		0.01/2.09

Table 110: The variations of experimental uncertainties on yields of m_X=280 GeV, m_S=135 GeV signal, $V+\gamma$ and promptSS, for $\mu\mu$ channel.

Uncertainty source	Signal	promptSS	Vgam
pileupEventWeight	-4.18/1.54	-2.14/0.01	32.93/-5.55
MV2c10_70_EventWeight_B0		1.63/-1.54	
MV2c10_70_EventWeight_C0	1.82/-1.82	1.04/-1.04	
MV2c10_70_EventWeight_Light0			0.51/-0.50
JVT_EventWeight	0.79/-0.83	0.85/-0.88	1.16/-1.15
lepSFObjTight_EL_SF_ID	0.90/-0.90	1.03/-1.03	0.64/-0.64
lepSFObjTight_MU_SF_ID_SYST	0.65/-0.64	0.67/-0.67	0.56/-0.56
EG_RESOLUTION_ALL		-0.88/0.28	
EG_SCALE_ALL		1.24/0.60	
JET_EffectiveNP_1	4.15/-5.15	5.00/-5.24	14.95/0.00
JET_EffectiveNP_2	-1.41/1.09	-2.58/3.53	
JET_EffectiveNP_3		0.73/0.03	0.00/inf
JET_EffectiveNP_4		0.88/0.02	
JET_EffectiveNP_6		1.33/0.03	
JET_EffectiveNP_7		-0.59/0.70	
JET_EffectiveNP_8restTerm		1.86/-0.61	
JET_EtaIntercalibration_Modelling	1.08/-0.98	2.13/-2.49	
JET_EtaIntercalibration_NonClosure	-0.89/0.25	0.74/-4.06	
JET_EtaIntercalibration_TotalStat	0.99/-1.35	3.16/-2.81	
JET_Flavor_Composition	8.26/-7.71	3.99/-9.87	-1.93/-8.64
JET_Flavor_Response	-3.65/1.36	-2.96/3.36	
JET_Pileup_OffsetMu		-1.77/0.77	
JET_Pileup_OffsetNPV	2.15/-2.83	2.01/-0.99	
JET_Pileup_RhoTopology	5.68/-6.67	5.25/-8.30	14.95/-7.86
JET_RelativeNonClosure_AFII	-2.09/1.05		
JET_JER_SINGLE_NP	-3.39/3.39	3.93/-3.93	-13.22/13.22
MET_SoftTrk_ResoPerp		1.18/-1.18	
MET_SoftTrk_Scale		0.61/0.02	

Table 111: The variations of experimental uncertainties on yields of m_X=280 GeV, m_S=135 GeV signal, $V + \gamma$ and promptSS, for $e\mu$ channel.

Uncertainty source	Signal	promptSS	Vgam
pileupEventWeight	-3.82/-0.32	4.82/-3.32	-1.97/-3.28
MV2c10_70_EventWeight_B0		1.26/-1.20	
MV2c10_70_EventWeight_C0	2.33/-2.33	1.57/-1.57	
MV2c10_70_EventWeight_Light0	0.55/-0.55	0.54/-0.54	0.74/-0.73
JVT_EventWeight	0.98/-1.03	0.98/-1.03	0.71/-0.81
lepSFObjTight_EL_SF_Reco			0.50/-0.50
lepSFObjTight_EL_SF_ID	2.07/-2.06	2.29/-2.27	2.20/-2.18
lepSFObjTight_EL_SF_Isol	0.54/-0.54		
EG_RESOLUTION_ALL	-0.68/-0.60	-1.13/0.31	
EG_SCALE_ALL	-0.72/-0.01	0.94/0.00	
JET_EffectiveNP_1	2.77/-5.70	4.03/-2.52	1.14/-0.34
JET_EffectiveNP_2	-0.88/0.47	-1.42/1.43	
JET_EffectiveNP_3		-0.03/-1.56	
JET_EtaIntercalibration_Modelling	1.32/-0.27	0.76/-1.21	
JET_EtaIntercalibration_NonClosure	0.60/-0.06	-1.16/-0.25	
JET_EtaIntercalibration_TotalStat	0.48/-0.84	1.32/0.14	
JET_Flavor_Composition	3.70/-6.46	6.96/-14.12	33.81/0.03
JET_Flavor_Response	-2.72/1.66	-1.22/2.80	
JET_Pileup_OffsetNPV	0.73/-1.65	-2.48/-1.77	
JET_Pileup_PtTerm	-0.04/0.54	-1.62/0.04	
JET_Pileup_RhoTopology	4.20/-5.81	5.04/-6.62	33.46/0.02
JET_PunchThrough_MC15	-100.00/-100.00		
JET_RelativeNonClosure_AFII	-1.46/1.14		
JET_JER_SINGLE_NP	2.84/-2.84	2.90/-2.90	21.77/-21.77
MET_SoftTrk_ResoPara			9.57/-9.57
MET_SoftTrk_ResoPerp			9.57/-9.57
MET_SoftTrk_Scale			0.00/9.57

Table 112: The variations of experimental uncertainties on yields of m_X=300 GeV, m_S=135 GeV signal, $V + \gamma$ and promptSS, for ee channel.

Uncertainty source	Signal	promptSS
pileupEventWeight	-3.88/1.77	-2.77/0.81
MV2c10_70_EventWeight_B0		1.13/-1.08
MV2c10_70_EventWeight_C0	1.99/-1.99	1.25/-1.25
JVT_EventWeight		0.57/-0.61
lepSFObjTight_MU_SF_ID_SYST	1.25/-1.24	1.35/-1.34
JET_EffectiveNP_1	1.99/-2.24	5.51/-0.43
JET_EffectiveNP_2	-0.57/0.31	-0.80/1.34
JET_EffectiveNP_3		0.59/-0.90
JET_EffectiveNP_4		0.53/0.56
JET_EffectiveNP_6		0.50/-1.07
JET_EffectiveNP_7		-1.12/0.03
JET_EffectiveNP_8restTerm		0.54/-0.00
JET_EtaIntercalibration_Modelling	0.05/-1.30	
JET_EtaIntercalibration_NonClosure	-0.57/-0.18	0.79/1.98
JET_EtaIntercalibration_TotalStat	-0.28/-0.79	-0.55/0.45
JET_Flavor_Composition	3.86/-2.97	15.20/-5.60
JET_Flavor_Response	-0.62/1.09	0.51/2.44
JET_Pileup_OffsetMu	-0.58/-0.29	1.35/-2.53
JET_Pileup_OffsetNPV		2.87/-1.44
JET_Pileup_PtTerm	-0.31/-0.56	0.76/0.79
JET_Pileup_RhoTopology	2.04/-3.30	10.25/-3.04
JET_PunchThrough_MC15	-100.00/-100.00	
JET_RelativeNonClosure_AFII	-1.03/0.52	
MUON_ID		-0.55/-0.99
MUON_SCALE		-0.01/0.50
JET_JER_SINGLE_NP	-2.90/2.90	25.77/-25.77
MET_SoftTrk_Scale		0.01/2.09

Table 113: The variations of experimental uncertainties on yields of m_X=300 GeV, m_S=135 GeV signal, $V + \gamma$ and promptSS, for $\mu\mu$ channel.

Uncertainty source	Signal	promptSS	Vgam
pileupEventWeight	-1.16/1.22	-2.14/0.01	32.93/-5.55
MV2c10_70_EventWeight_B0		1.63/-1.54	
MV2c10_70_EventWeight_C0	2.05/-2.05	1.04/-1.04	
MV2c10_70_EventWeight_Light0			0.51/-0.50
JVT_EventWeight	0.73/-0.79	0.85/-0.88	1.16/-1.15
lepSFObjTight_EL_SF_ID	0.94/-0.94	1.03/-1.03	0.64/-0.64
lepSFObjTight_MU_SF_ID_SYST	0.64/-0.64	0.67/-0.67	0.56/-0.56
EG_RESOLUTION_ALL		-0.88/0.28	
EG_SCALE_ALL		1.24/0.60	
JET_EffectiveNP_1	2.06/-3.31	5.00/-5.24	14.95/0.00
JET_EffectiveNP_2	-0.21/0.55	-2.58/3.53	
JET_EffectiveNP_3	-0.75/-0.11	0.73/0.03	0.00/inf
JET_EffectiveNP_4	-0.11/-0.58	0.88/0.02	
JET_EffectiveNP_6		1.33/0.03	
JET_EffectiveNP_7		-0.59/0.70	
JET_EffectiveNP_8restTerm		1.86/-0.61	
JET_EtaIntercalibration_Modelling	0.87/-0.35	2.13/-2.49	
JET_EtaIntercalibration_NonClosure		0.74/-4.06	
JET_EtaIntercalibration_TotalStat		3.16/-2.81	
JET_Flavor_Composition	4.99/-6.21	3.99/-9.87	-1.93/-8.64
JET_Flavor_Response	-1.85/0.93	-2.96/3.36	
JET_Pileup_OffsetMu	-0.19/0.70	-1.77/0.77	
JET_Pileup_OffsetNPV	-0.11/-1.21	2.01/-0.99	
JET_Pileup_PtTerm	-0.38/-0.89		
JET_Pileup_RhoTopology	4.32/-4.76	5.25/-8.30	14.95/-7.86
JET_PunchThrough_MC15	-100.00/-100.00		
JET_RelativeNonClosure_AFII	-1.40/0.83		
JET_JER_SINGLE_NP	-1.94/1.94	3.93/-3.93	-13.22/13.22
MET_SoftTrk_ResoPerp		1.18/-1.18	
MET_SoftTrk_Scale		0.61/0.02	

Table 114: The variations of experimental uncertainties on yields of m_X=300 GeV, m_S=135 GeV signal, $V + \gamma$ and promptSS, for $e\mu$ channel.

Uncertainty source	Signal	promptSS	Vgam
pileupEventWeight	-1.30/1.07	4.82/-3.32	-1.97/-3.28
MV2c10_70_EventWeight_B0		1.26/-1.20	
MV2c10_70_EventWeight_C0	1.97/-1.97	1.57/-1.57	
MV2c10_70_EventWeight_Light0	0.57/-0.57	0.54/-0.54	0.74/-0.73
JVT_EventWeight	0.74/-0.81	0.98/-1.03	0.71/-0.81
lepSFObjTight_EL_SF_Reco			0.50/-0.50
lepSFObjTight_EL_SF_ID	2.01/-2.00	2.29/-2.27	2.20/-2.18
lepSFObjTight_EL_SF_Isol	0.52/-0.52		
EG_RESOLUTION_ALL		-1.13/0.31	
EG_SCALE_ALL	0.00/-1.02	0.94/0.00	
JET_EffectiveNP_1	0.11/-1.90	4.03/-2.52	1.14/-0.34
JET_EffectiveNP_2	-0.65/0.98	-1.42/1.43	
JET_EffectiveNP_3	-0.00/-0.62	-0.03/-1.56	
JET_EffectiveNP_6	-0.00/-0.65		
JET_EffectiveNP_7	-0.63/-0.00		
JET_EtaIntercalibration_Modelling	-0.88/-1.11	0.76/-1.21	
JET_EtaIntercalibration_NonClosure	-0.22/-1.17	-1.16/-0.25	
JET_EtaIntercalibration_TotalStat	-0.57/0.23	1.32/0.14	
JET_Flavor_Composition	0.46/-4.70	6.96/-14.12	33.81/0.03
JET_Flavor_Response		-1.22/2.80	
JET_Pileup_OffsetMu	-1.24/-0.01		
JET_Pileup_OffsetNPV	-0.83/-0.64	-2.48/-1.77	
JET_Pileup_PtTerm	-1.21/0.86	-1.62/0.04	
JET_Pileup_RhoTopology	1.32/-3.56	5.04/-6.62	33.46/0.02
JET_RelativeNonClosure_AFII	-1.01/1.21		
JET_JER_SINGLE_NP	-2.84/2.84	2.90/-2.90	21.77/-21.77
MET_SoftTrk_ResoPara	0.76/-0.76		9.57/-9.57
MET_SoftTrk_ResoPerp			9.57/-9.57
MET_SoftTrk_Scale			0.00/9.57

Table 115: The variations of experimental uncertainties on yields of m_X=320 GeV, m_S=135 GeV signal, $V + \gamma$ and promptSS, for ee channel.

Uncertainty source	Signal	promptSS
pileupEventWeight	-1.08/1.87	-2.77/0.81
MV2c10_70_EventWeight_B0		1.13/-1.08
MV2c10_70_EventWeight_C0	1.98/-1.98	1.25/-1.25
JVT_EventWeight	0.59/-0.64	0.57/-0.61
lepSFObjTight_MU_SF_ID_SYST	1.35/-1.33	1.35/-1.34
JET_EffectiveNP_1	2.76/-3.20	5.51/-0.43
JET_EffectiveNP_2	-0.48/0.87	-0.80/1.34
JET_EffectiveNP_3		0.59/-0.90
JET_EffectiveNP_4		0.53/0.56
JET_EffectiveNP_6		0.50/-1.07
JET_EffectiveNP_7		-1.12/0.03
JET_EffectiveNP_8restTerm		0.54/-0.00
JET_EtaIntercalibration_Modelling	0.63/-0.70	
JET_EtaIntercalibration_NonClosure	0.15/0.67	0.79/1.98
JET_EtaIntercalibration_TotalStat	0.90/-0.55	-0.55/0.45
JET_Flavor_Composition	3.38/-5.35	15.20/-5.60
JET_Flavor_Response	-2.22/0.81	0.51/2.44
JET_Pileup_OffsetMu	-0.70/0.83	1.35/-2.53
JET_Pileup_OffsetNPV	0.16/1.05	2.87/-1.44
JET_Pileup_PtTerm		0.76/0.79
JET_Pileup_RhoTopology	2.36/-4.19	10.25/-3.04
JET_RelativeNonClosure_AFII	-0.42/1.73	
MUON_ID	-1.58/-0.16	-0.55/-0.99
MUON_MS	0.74/-0.35	
MUON_SCALE		-0.01/0.50
JET_JER_SINGLE_NP	1.15/-1.15	25.77/-25.77
MET_SoftTrk_ResoPara	-1.20/1.20	
MET_SoftTrk_Scale		0.01/2.09

Table 116: The variations of experimental uncertainties on yields of m_X=320 GeV, m_S=135 GeV signal, $V + \gamma$ and promptSS, for $\mu\mu$ channel.

Uncertainty source	Signal	promptSS	Vgam
pileupEventWeight	1.88/-1.29	-2.14/0.01	32.93/-5.55
MV2c10_70_EventWeight_B0		1.63/-1.54	
MV2c10_70_EventWeight_C0	2.21/-2.21	1.04/-1.04	
MV2c10_70_EventWeight_Light0			0.51/-0.50
JVT_EventWeight	0.70/-0.75	0.85/-0.88	1.16/-1.15
lepSFObjTight_EL_SF_ID	0.86/-0.86	1.03/-1.03	0.64/-0.64
lepSFObjTight_MU_SF_ID_SYST	0.63/-0.63	0.67/-0.67	0.56/-0.56
EG_RESOLUTION_ALL		-0.88/0.28	
EG_SCALE_ALL		1.24/0.60	
JET_EffectiveNP_1	2.11/-1.94	5.00/-5.24	14.95/0.00
JET_EffectiveNP_2	-0.35/1.28	-2.58/3.53	
JET_EffectiveNP_3		0.73/0.03	0.00/inf
JET_EffectiveNP_4		0.88/0.02	
JET_EffectiveNP_6		1.33/0.03	
JET_EffectiveNP_7		-0.59/0.70	
JET_EffectiveNP_8restTerm		1.86/-0.61	
JET_EtaIntercalibration_Modelling	0.81/-0.87	2.13/-2.49	
JET_EtaIntercalibration_NonClosure		0.74/-4.06	
JET_EtaIntercalibration_TotalStat	1.00/0.07	3.16/-2.81	
JET_Flavor_Composition	4.12/-4.15	3.99/-9.87	-1.93/-8.64
JET_Flavor_Response	-1.71/0.78	-2.96/3.36	
JET_Pileup_OffsetMu	0.52/0.39	-1.77/0.77	
JET_Pileup_OffsetNPV		2.01/-0.99	
JET_Pileup_RhoTopology	2.78/-2.39	5.25/-8.30	14.95/-7.86
JET_RelativeNonClosure_AFII	-1.73/1.47		
JET_JER_SINGLE_NP	-2.25/2.25	3.93/-3.93	-13.22/13.22
MET_SoftTrk_ResoPara	-0.55/0.55		
MET_SoftTrk_ResoPerp	-0.53/0.53	1.18/-1.18	
MET_SoftTrk_Scale	-0.52/0.00	0.61/0.02	

Table 117: The variations of experimental uncertainties on yields of m_X=320 GeV, m_S=135 GeV signal, $V + \gamma$ and promptSS, for $e\mu$ channel.

Uncertainty source	Signal	promptSS	Vgam
pileupEventWeight	1.92/-0.56	5.21/-2.07	-8.69/-1.60
MV2c10_70_EventWeight_B0		1.73/-1.66	
MV2c10_70_EventWeight_B1		0.65/-0.64	
MV2c10_70_EventWeight_C0	2.37/-2.37	1.69/-1.69	
MV2c10_70_EventWeight_Light0	0.58/-0.58	0.60/-0.60	0.74/-0.73
JVT_EventWeight	1.23/-1.25	0.88/-0.93	
lepSFObjTight_EL_SF_ID	1.85/-1.83	1.72/-1.71	2.12/-2.10
lepSFObjTight_EL_SF_Isol	0.50/-0.50		
EG_RESOLUTION_ALL	-0.04/0.81	-0.08/3.65	
EG_SCALE_ALL	0.01/-0.53	0.84/-0.11	
JET_EffectiveNP_1	0.97/-1.98	6.12/0.87	97.30/-0.50
JET_EffectiveNP_2	0.51/0.83	-0.05/1.03	
JET_EffectiveNP_3		0.68/-0.03	
JET_EffectiveNP_6		0.73/-0.04	
JET_EffectiveNP_7		0.01/0.62	
JET_EtaIntercalibration_Modelling	0.18/0.75	4.11/2.91	
JET_EtaIntercalibration_NonClosure	0.01/0.62	-1.00/0.75	
JET_EtaIntercalibration_TotalStat	0.83/0.49	0.92/0.05	
JET_Flavor_Composition	5.92/-5.73	9.60/0.25	104.60/-11.43
JET_Flavor_Response		1.87/4.99	6.01/0.32
JET_Pileup_OffsetMu		-0.10/0.98	
JET_Pileup_OffsetNPV		0.91/3.07	0.00/6.01
JET_Pileup_PtTerm	-0.62/0.42	-0.04/1.84	0.00/6.04
JET_Pileup_RhoTopology	1.69/-3.60	6.19/0.79	118.95/-5.26
JET_RelativeNonClosure_AFII	-1.05/0.83		
JET_JER_SINGLE_NP	-3.97/3.97	-2.18/2.18	-12.97/12.97

Table 118: The variations of experimental uncertainties on yields of m_X=340 GeV, m_S=135 GeV signal, $V + \gamma$ and promptSS, for ee channel.

Uncertainty source	Signal	promptSS
pileupEventWeight	-2.42/1.44	-2.74/0.16
MV2c10_70_EventWeight_B0		1.67/-1.61
MV2c10_70_EventWeight_B1		0.50/-0.50
MV2c10_70_EventWeight_C0	2.36/-2.36	1.75/-1.75
JVT_EventWeight	0.71/-0.75	0.57/-0.60
lepSFObjTight_MU_SF_ID_SYST	1.34/-1.32	1.38/-1.37
JET_BJES_Response		1.53/0.08
JET_EffectiveNP_1	1.47/-2.45	4.68/-4.86
JET_EffectiveNP_2	-0.63/0.79	-2.67/1.46
JET_EtaIntercalibration_Modelling	-0.30/-0.58	1.88/-2.29
JET_EtaIntercalibration_NonClosure		0.73/1.76
JET_EtaIntercalibration_TotalStat		0.48/-2.09
JET_Flavor_Composition	6.27/-5.31	6.79/-11.63
JET_Flavor_Response	-1.17/1.11	-2.87/3.77
JET_Pileup_OffsetMu		-0.82/0.74
JET_Pileup_OffsetNPV	-0.58/-0.09	0.89/-1.45
JET_Pileup_PtTerm		0.37/-0.54
JET_Pileup_RhoTopology	2.98/-3.33	5.31/-5.54
JET_RelativeNonClosure_AFII	-1.14/0.91	
MUON_ID		-1.30/-0.64
MUON_MS	-0.08/-0.72	-0.69/0.48
MUON_SCALE		-0.72/0.48
JET_JER_SINGLE_NP	-4.84/4.84	2.21/-2.21
MET_SoftTrk_ResoPerp		1.10/-1.10

Table 119: The variations of experimental uncertainties on yields of m_X=340 GeV, m_S=135 GeV signal, $V + \gamma$ and promptSS, for $\mu\mu$ channel.

Uncertainty source	Signal	promptSS	Vgam
pileupEventWeight	-1.82/0.84	-1.87/-0.46	39.89/-2.98
MV2c10_70_EventWeight_B0		2.06/-1.98	
MV2c10_70_EventWeight_C0	2.13/-2.13	1.31/-1.31	0.57/-0.57
MV2c10_70_EventWeight_C1	-0.51/0.52		
MV2c10_70_EventWeight_Light0		0.53/-0.53	0.54/-0.54
JVT_EventWeight	0.99/-1.02	0.92/-0.94	1.22/-1.21
lepSFObjTight_EL_SF_ID	0.86/-0.86	0.93/-0.93	0.56/-0.56
lepSFObjTight_MU_SF_ID_SYST	0.66/-0.66	0.71/-0.71	0.65/-0.65
EG_SCALE_ALL		1.27/0.59	
JET_EffectiveNP_1	1.48/-2.59	6.51/-7.63	0.50/0.01
JET_EffectiveNP_2	-0.81/0.27	-3.11/1.51	
JET_EffectiveNP_4		1.01/0.01	
JET_EffectiveNP_6		0.67/0.10	
JET_EffectiveNP_7		-0.57/-0.02	
JET_EffectiveNP_8restTerm		2.02/-0.60	
JET_EtaIntercalibration_Modelling	0.24/-0.50	1.41/-4.17	
JET_EtaIntercalibration_NonClosure	-1.18/-0.08	-0.45/-2.45	
JET_EtaIntercalibration_TotalStat		1.68/-3.77	
JET_Flavor_Composition	4.73/-5.38	10.94/-12.31	1.76/-11.37
JET_Flavor_Response	-1.36/0.04	-4.70/2.93	
JET_Pileup_OffsetMu	-0.51/-0.19	0.25/-0.85	
JET_Pileup_OffsetNPV		-0.26/-1.83	
JET_Pileup_PtTerm		-0.20/-0.57	
JET_Pileup_RhoTopology	2.66/-4.05	11.66/-10.99	1.37/-10.34
JET_RelativeNonClosure_AFII	-1.12/0.93		
JET_JER_SINGLE_NP		4.86/-4.86	4.99/-4.99
MET_SoftTrk_ResoPara	-0.96/0.96	0.63/-0.63	
MET_SoftTrk_ResoPerp		0.59/-0.59	
MET_SoftTrk_Scale	-0.13/-0.61	0.68/-0.04	

Table 120: The variations of experimental uncertainties on yields of m_X=340 GeV, m_S=135 GeV signal, $V + \gamma$ and promptSS, for $e\mu$ channel.

Uncertainty source	Signal	promptSS	Vgam
pileupEventWeight	0.17/-0.88	5.21/-2.07	-8.69/-1.60
MV2c10_70_EventWeight_B0		1.73/-1.66	
MV2c10_70_EventWeight_B1		0.65/-0.64	
MV2c10_70_EventWeight_C0	2.70/-2.70	1.69/-1.69	
MV2c10_70_EventWeight_Light0		0.60/-0.60	0.74/-0.73
JVT_EventWeight	1.12/-1.16	0.88/-0.93	
lepSFObjTight_EL_SF_ID	1.77/-1.76	1.72/-1.71	2.12/-2.10
EG_RESOLUTION_ALL	-0.95/0.20	-0.08/3.65	
EG_SCALE_ALL		0.84/-0.11	
JET_EffectiveNP_1	2.77/-2.04	6.12/0.87	97.30/-0.50
JET_EffectiveNP_2	-1.21/0.84	-0.05/1.03	
JET_EffectiveNP_3		0.68/-0.03	
JET_EffectiveNP_6		0.73/-0.04	
JET_EffectiveNP_7		0.01/0.62	
JET_EtaIntercalibration_Modelling	1.76/-0.87	4.11/2.91	
JET_EtaIntercalibration_NonClosure	-0.71/1.33	-1.00/0.75	
JET_EtaIntercalibration_TotalStat	0.83/-0.31	0.92/0.05	
JET_Flavor_Composition	3.96/-4.34	9.60/0.25	104.60/-11.43
JET_Flavor_Response	-1.74/2.72	1.87/4.99	6.01/0.32
JET_Pileup_OffsetMu	-0.17/1.22	-0.10/0.98	
JET_Pileup_OffsetNPV	0.55/0.55	0.91/3.07	0.00/6.01
JET_Pileup_PtTerm	0.62/-0.03	-0.04/1.84	0.00/6.04
JET_Pileup_RhoTopology	3.04/-2.39	6.19/0.79	118.95/-5.26
JET_RelativeNonClosure_AFII	-1.14/2.38		
JET_JER_SINGLE_NP	3.23/-3.23	-2.18/2.18	-12.97/12.97
MET_SoftTrk_Scale	0.64/-0.28		

Table 121: The variations of experimental uncertainties on yields of m_X=340 GeV, m_S=145 GeV signal, $V + \gamma$ and promptSS, for ee channel.

Uncertainty source	Signal	promptSS
pileupEventWeight	5.58/-2.15	-2.74/0.16
MV2c10_70_EventWeight_B0		1.67/-1.61
MV2c10_70_EventWeight_B1		0.50/-0.50
MV2c10_70_EventWeight_C0	2.32/-2.32	1.75/-1.75
JVT_EventWeight	0.58/-0.63	0.57/-0.60
lepSFObjTight_MU_SF_ID_SYST	1.31/-1.30	1.38/-1.37
JET_BJES_Response		1.53/0.08
JET_EffectiveNP_1	1.21/-2.20	4.68/-4.86
JET_EffectiveNP_2	-0.57/0.04	-2.67/1.46
JET_EtaIntercalibration_Modelling	-0.29/-0.55	1.88/-2.29
JET_EtaIntercalibration_NonClosure		0.73/1.76
JET_EtaIntercalibration_TotalStat	0.25/-0.58	0.48/-2.09
JET_Flavor_Composition	4.30/-5.03	6.79/-11.63
JET_Flavor_Response	-1.86/0.13	-2.87/3.77
JET_Pileup_OffsetMu	-0.80/-0.24	-0.82/0.74
JET_Pileup_OffsetNPV	1.13/-1.69	0.89/-1.45
JET_Pileup_PtTerm		0.37/-0.54
JET_Pileup_RhoTopology	2.78/-3.21	5.31/-5.54
JET_RelativeNonClosure_AFII	-1.62/-0.53	
MUON_ID	-0.56/-0.15	-1.30/-0.64
MUON_MS		-0.69/0.48
MUON_SCALE		-0.72/0.48
JET_JER_SINGLE_NP	-4.97/4.97	2.21/-2.21
MET_SoftTrk_ResoPerp		1.10/-1.10

Table 122: The variations of experimental uncertainties on yields of m_X=340 GeV, m_S=145 GeV signal, $V + \gamma$ and promptSS, for $\mu\mu$ channel.

Uncertainty source	Signal	promptSS	Vgam
pileupEventWeight	-4.83/3.20	-1.87/-0.46	39.89/-2.98
MV2c10_70_EventWeight_B0		2.06/-1.98	
MV2c10_70_EventWeight_C0	2.59/-2.59	1.31/-1.31	0.57/-0.57
MV2c10_70_EventWeight_Light0	0.50/-0.50	0.53/-0.53	0.54/-0.54
JVT_EventWeight	0.82/-0.88	0.92/-0.94	1.22/-1.21
lepSFObjTight_EL_SF_ID	0.85/-0.85	0.93/-0.93	0.56/-0.56
lepSFObjTight_MU_SF_ID_SYST	0.65/-0.64	0.71/-0.71	0.65/-0.65
EG_SCALE_ALL		1.27/0.59	
JET_EffectiveNP_1	3.50/-2.88	6.51/-7.63	0.50/0.01
JET_EffectiveNP_2	-0.79/1.13	-3.11/1.51	
JET_EffectiveNP_4		1.01/0.01	
JET_EffectiveNP_6		0.67/0.10	
JET_EffectiveNP_7		-0.57/-0.02	
JET_EffectiveNP_8restTerm		2.02/-0.60	
JET_EtaIntercalibration_Modelling	1.45/-1.24	1.41/-4.17	
JET_EtaIntercalibration_NonClosure	0.33/0.67	-0.45/-2.45	
JET_EtaIntercalibration_TotalStat	0.95/-0.29	1.68/-3.77	
JET_Flavor_Composition	4.77/-4.29	10.94/-12.31	1.76/-11.37
JET_Flavor_Response	-1.84/3.55	-4.70/2.93	
JET_Pileup_OffsetMu		0.25/-0.85	
JET_Pileup_OffsetNPV	1.96/-0.75	-0.26/-1.83	
JET_Pileup_PtTerm		-0.20/-0.57	
JET_Pileup_RhoTopology	4.98/-3.19	11.66/-10.99	1.37/-10.34
JET_RelativeNonClosure_AFII	-1.66/1.91		
JET_JER_SINGLE_NP	1.17/-1.17	4.86/-4.86	4.99/-4.99
MET_SoftTrk_ResoPara		0.63/-0.63	
MET_SoftTrk_ResoPerp		0.59/-0.59	
MET_SoftTrk_Scale		0.68/-0.04	

Table 123: The variations of experimental uncertainties on yields of m_X=340 GeV, m_S=145 GeV signal, $V + \gamma$ and promptSS, for $e\mu$ channel.

Uncertainty source	Signal	promptSS	Vgam
pileupEventWeight	-7.15/5.57	5.21/-2.07	-8.69/-1.60
MV2c10_70_EventWeight_B0		1.73/-1.66	
MV2c10_70_EventWeight_B1		0.65/-0.64	
MV2c10_70_EventWeight_C0	2.32/-2.32	1.69/-1.69	
MV2c10_70_EventWeight_C1	-0.62/0.62		
MV2c10_70_EventWeight_Light0	0.59/-0.58	0.60/-0.60	0.74/-0.73
JVT_EventWeight	0.91/-0.97	0.88/-0.93	
lepSFObjTight_EL_SF_ID	1.84/-1.82	1.72/-1.71	2.12/-2.10
lepSFObjTight_EL_SF_Isol	0.50/-0.50		
EG_RESOLUTION_ALL	0.02/0.50	-0.08/3.65	
EG_SCALE_ALL	0.60/-0.20	0.84/-0.11	
JET_EffectiveNP_1	1.96/-2.44	6.12/0.87	97.30/-0.50
JET_EffectiveNP_2	-1.09/-0.55	-0.05/1.03	
JET_EffectiveNP_3		0.68/-0.03	
JET_EffectiveNP_6		0.73/-0.04	
JET_EffectiveNP_7		0.01/0.62	
JET_EtaIntercalibration_Modelling	0.49/-0.87	4.11/2.91	
JET_EtaIntercalibration_NonClosure	-1.22/0.54	-1.00/0.75	
JET_EtaIntercalibration_TotalStat	-0.48/-1.11	0.92/0.05	
JET_Flavor_Composition	4.98/-5.25	9.60/0.25	104.60/-11.43
JET_Flavor_Response	-2.08/1.32	1.87/4.99	6.01/0.32
JET_Pileup_OffsetMu	-0.87/-0.53	-0.10/0.98	
JET_Pileup_OffsetNPV		0.91/3.07	0.00/6.01
JET_Pileup_PtTerm		-0.04/1.84	0.00/6.04
JET_Pileup_RhoTopology	3.89/-3.61	6.19/0.79	118.95/-5.26
JET_RelativeNonClosure_AFII	-1.93/1.40		
JET_JER_SINGLE_NP	1.07/-1.07	-2.18/2.18	-12.97/12.97
MET_SoftTrk_ResoPerp	1.26/-1.26		

Table 124: The variations of experimental uncertainties on yields of m_X=340 GeV, m_S=155 GeV signal, $V + \gamma$ and promptSS, for ee channel.

Uncertainty source	Signal	promptSS
pileupEventWeight	1.97/-1.70	-2.74/0.16
MV2c10_70_EventWeight_B0		1.67/-1.61
MV2c10_70_EventWeight_B1		0.50/-0.50
MV2c10_70_EventWeight_C0	2.37/-2.37	1.75/-1.75
JVT_EventWeight	0.60/-0.66	0.57/-0.60
lepSFObjTight_MU_SF_ID_SYST	1.31/-1.29	1.38/-1.37
JET_BJES_Response		1.53/0.08
JET_EffectiveNP_1	0.77/-2.77	4.68/-4.86
JET_EffectiveNP_2	-0.51/0.52	-2.67/1.46
JET_EtaIntercalibration_Modelling		1.88/-2.29
JET_EtaIntercalibration_NonClosure		0.73/1.76
JET_EtaIntercalibration_TotalStat	0.44/-0.53	0.48/-2.09
JET_Flavor_Composition	1.43/-4.52	6.79/-11.63
JET_Flavor_Response	-1.48/0.88	-2.87/3.77
JET_Pileup_OffsetMu		-0.82/0.74
JET_Pileup_OffsetNPV		0.89/-1.45
JET_Pileup_PtTerm		0.37/-0.54
JET_Pileup_RhoTopology	1.13/-3.82	5.31/-5.54
JET_RelativeNonClosure_AFII	-0.56/0.67	
MUON_ID		-1.30/-0.64
MUON_MS		-0.69/0.48
MUON_SCALE		-0.72/0.48
JET_JER_SINGLE_NP	-3.95/3.95	2.21/-2.21
MET_SoftTrk_ResoPerp		1.10/-1.10

Table 125: The variations of experimental uncertainties on yields of m_X=340 GeV, m_S=155 GeV signal, $V + \gamma$ and promptSS, for $\mu\mu$ channel.

Uncertainty source	Signal	promptSS	Vgam
pileupEventWeight	-1.08/1.63	-1.87/-0.46	39.89/-2.98
MV2c10_70_EventWeight_B0		2.06/-1.98	
MV2c10_70_EventWeight_C0	2.36/-2.36	1.31/-1.31	0.57/-0.57
MV2c10_70_EventWeight_Light0	0.51/-0.51	0.53/-0.53	0.54/-0.54
JVT_EventWeight	0.80/-0.86	0.92/-0.94	1.22/-1.21
lepSFObjTight_EL_SF_ID	0.82/-0.82	0.93/-0.93	0.56/-0.56
lepSFObjTight_MU_SF_ID_SYST	0.63/-0.63	0.71/-0.71	0.65/-0.65
EG_SCALE_ALL		1.27/0.59	
JET_EffectiveNP_1	2.72/-3.22	6.51/-7.63	0.50/0.01
JET_EffectiveNP_2	-0.87/0.98	-3.11/1.51	
JET_EffectiveNP_4		1.01/0.01	
JET_EffectiveNP_6		0.67/0.10	
JET_EffectiveNP_7		-0.57/-0.02	
JET_EffectiveNP_8restTerm		2.02/-0.60	
JET_EtaIntercalibration_Modelling	0.51/-1.05	1.41/-4.17	
JET_EtaIntercalibration_NonClosure	-0.73/0.74	-0.45/-2.45	
JET_EtaIntercalibration_TotalStat	0.90/-0.61	1.68/-3.77	
JET_Flavor_Composition	3.21/-5.81	10.94/-12.31	1.76/-11.37
JET_Flavor_Response	-2.35/1.29	-4.70/2.93	
JET_Pileup_OffsetMu		0.25/-0.85	
JET_Pileup_OffsetNPV		-0.26/-1.83	
JET_Pileup_PtTerm		-0.20/-0.57	
JET_Pileup_RhoTopology	3.90/-3.59	11.66/-10.99	1.37/-10.34
JET_RelativeNonClosure_AFII	-1.65/1.23		
JET_JER_SINGLE_NP	-0.98/0.98	4.86/-4.86	4.99/-4.99
MET_SoftTrk_ResoPara		0.63/-0.63	
MET_SoftTrk_ResoPerp		0.59/-0.59	
MET_SoftTrk_Scale		0.68/-0.04	

Table 126: The variations of experimental uncertainties on yields of m_X=340 GeV, m_S=155 GeV signal, $V + \gamma$ and promptSS, for $e\mu$ channel.

Uncertainty source	Signal	promptSS	Vgam
pileupEventWeight		5.21/-2.07	-8.69/-1.60
MV2c10_70_EventWeight_B0		1.73/-1.66	
MV2c10_70_EventWeight_B1		0.65/-0.64	
MV2c10_70_EventWeight_C0	2.70/-2.70	1.69/-1.69	
MV2c10_70_EventWeight_Light0	0.50/-0.50	0.60/-0.60	0.74/-0.73
JVT_EventWeight	0.93/-1.00	0.88/-0.93	
lepSFObjTight_EL_SF_ID	1.66/-1.65	1.72/-1.71	2.12/-2.10
EG_RESOLUTION_ALL		-0.08/3.65	
EG_SCALE_ALL	0.54/-1.00	0.84/-0.11	
JET_EffectiveNP_1	1.24/-2.23	6.12/0.87	97.30/-0.50
JET_EffectiveNP_2	-0.57/0.74	-0.05/1.03	
JET_EffectiveNP_3		0.68/-0.03	
JET_EffectiveNP_6		0.73/-0.04	
JET_EffectiveNP_7		0.01/0.62	
JET_EtaIntercalibration_Modelling	0.08/-0.81	4.11/2.91	
JET_EtaIntercalibration_NonClosure		-1.00/0.75	
JET_EtaIntercalibration_TotalStat		0.92/0.05	
JET_Flavor_Composition	6.01/-7.13	9.60/0.25	104.60/-11.43
JET_Flavor_Response	-1.44/0.78	1.87/4.99	6.01/0.32
JET_Pileup_OffsetMu		-0.10/0.98	
JET_Pileup_OffsetNPV	0.40/-1.64	0.91/3.07	0.00/6.01
JET_Pileup_PtTerm		-0.04/1.84	0.00/6.04
JET_Pileup_RhoTopology	3.68/-4.76	6.19/0.79	118.95/-5.26
JET_RelativeNonClosure_AFII	-0.70/0.82		
JET_JER_SINGLE_NP	3.71/-3.71	-2.18/2.18	-12.97/12.97
MET_SoftTrk_Scale	0.59/0.40		

Table 127: The variations of experimental uncertainties on yields of m_X=340 GeV, m_S=165 GeV signal, $V + \gamma$ and promptSS, for ee channel.

Uncertainty source	Signal	promptSS
pileupEventWeight	-1.60/2.40	-2.74/0.16
MV2c10_70_EventWeight_B0		1.67/-1.61
MV2c10_70_EventWeight_B1		0.50/-0.50
MV2c10_70_EventWeight_C0	2.56/-2.56	1.75/-1.75
MV2c10_70_EventWeight_C1	-0.59/0.59	
JVT_EventWeight	0.69/-0.75	0.57/-0.60
lepSFObjTight_MU_SF_ID_SYST	1.30/-1.29	1.38/-1.37
JET_BJES_Response		1.53/0.08
JET_EffectiveNP_1	1.72/-1.83	4.68/-4.86
JET_EffectiveNP_2	-0.28/0.58	-2.67/1.46
JET_EtaIntercalibration_Modelling	0.55/-0.61	1.88/-2.29
JET_EtaIntercalibration_NonClosure		0.73/1.76
JET_EtaIntercalibration_TotalStat	0.30/-0.51	0.48/-2.09
JET_Flavor_Composition	4.51/-4.98	6.79/-11.63
JET_Flavor_Response	-0.97/1.47	-2.87/3.77
JET_Pileup_OffsetMu	-0.49/0.61	-0.82/0.74
JET_Pileup_OffsetNPV	0.66/-0.56	0.89/-1.45
JET_Pileup_PtTerm		0.37/-0.54
JET_Pileup_RhoTopology	3.08/-2.99	5.31/-5.54
JET_RelativeNonClosure_AFII	-0.78/0.33	
MUON_ID		-1.30/-0.64
MUON_MS		-0.69/0.48
MUON_SCALE		-0.72/0.48
JET_JER_SINGLE_NP	-1.41/1.41	2.21/-2.21
MET_SoftTrk_ResoPara	-0.68/0.68	
MET_SoftTrk_ResoPerp	-0.73/0.73	1.10/-1.10

Table 128: The variations of experimental uncertainties on yields of m_X=340 GeV, m_S=165 GeV signal, $V + \gamma$ and promptSS, for $\mu\mu$ channel.

Uncertainty source	Signal	promptSS	Vgam
pileupEventWeight	-1.90/1.22	-1.87/-0.46	39.89/-2.98
MV2c10_70_EventWeight_B0		2.06/-1.98	
MV2c10_70_EventWeight_C0	2.43/-2.43	1.31/-1.31	0.57/-0.57
MV2c10_70_EventWeight_C1	-0.56/0.56		
MV2c10_70_EventWeight_Light0	0.52/-0.51	0.53/-0.53	0.54/-0.54
JVT_EventWeight	0.91/-0.96	0.92/-0.94	1.22/-1.21
lepSFObjTight_EL_SF_ID	0.77/-0.77	0.93/-0.93	0.56/-0.56
lepSFObjTight_MU_SF_ID_SYST	0.62/-0.62	0.71/-0.71	0.65/-0.65
EG_SCALE_ALL		1.27/0.59	
JET_EffectiveNP_1	3.63/-2.13	6.51/-7.63	0.50/0.01
JET_EffectiveNP_2	-0.69/0.54	-3.11/1.51	
JET_EffectiveNP_4		1.01/0.01	
JET_EffectiveNP_6		0.67/0.10	
JET_EffectiveNP_7		-0.57/-0.02	
JET_EffectiveNP_8restTerm		2.02/-0.60	
JET_EtaIntercalibration_Modelling	0.33/-0.82	1.41/-4.17	
JET_EtaIntercalibration_NonClosure		-0.45/-2.45	
JET_EtaIntercalibration_TotalStat		1.68/-3.77	
JET_Flavor_Composition	6.25/-3.06	10.94/-12.31	1.76/-11.37
JET_Flavor_Response	-1.21/1.52	-4.70/2.93	
JET_Pileup_OffsetMu	-0.59/0.12	0.25/-0.85	
JET_Pileup_OffsetNPV	0.64/0.00	-0.26/-1.83	
JET_Pileup_PtTerm		-0.20/-0.57	
JET_Pileup_RhoTopology	4.67/-2.38	11.66/-10.99	1.37/-10.34
JET_RelativeNonClosure_AFII	-0.93/0.83		
JET_JER_SINGLE_NP	-3.05/3.05	4.86/-4.86	4.99/-4.99
MET_SoftTrk_ResoPara		0.63/-0.63	
MET_SoftTrk_ResoPerp		0.59/-0.59	
MET_SoftTrk_Scale		0.68/-0.04	

Table 129: The variations of experimental uncertainties on yields of m_X=340 GeV, m_S=165 GeV signal, $V+\gamma$ and promptSS, for $e\mu$ channel.

1023 # I NP plots

1024 The plots of NP checks for resonance searches are shown through Fig. 22 to Fig. 65.

1025 ## I.1 The NP plots for $X \rightarrow hh$ searches

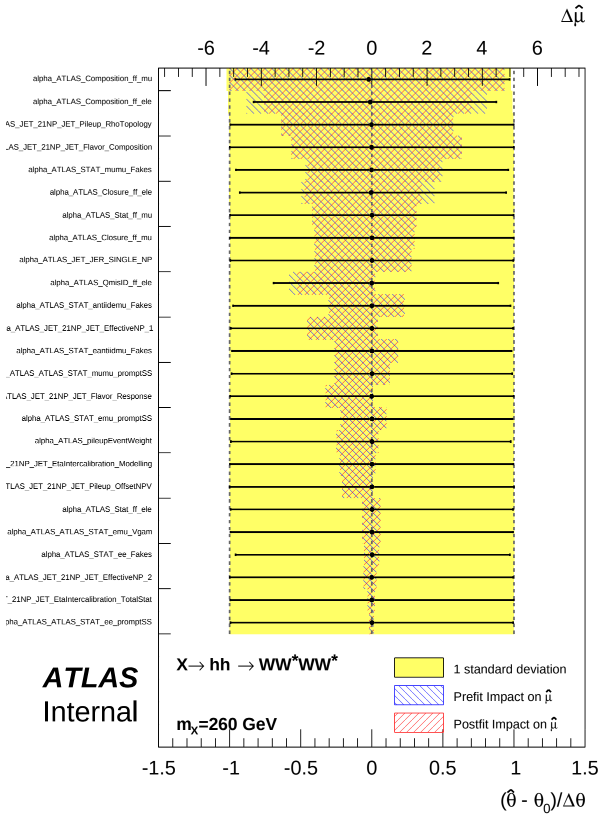

Figure 22: The ranking of NP impact on μ for the search of mX=260 GeV.

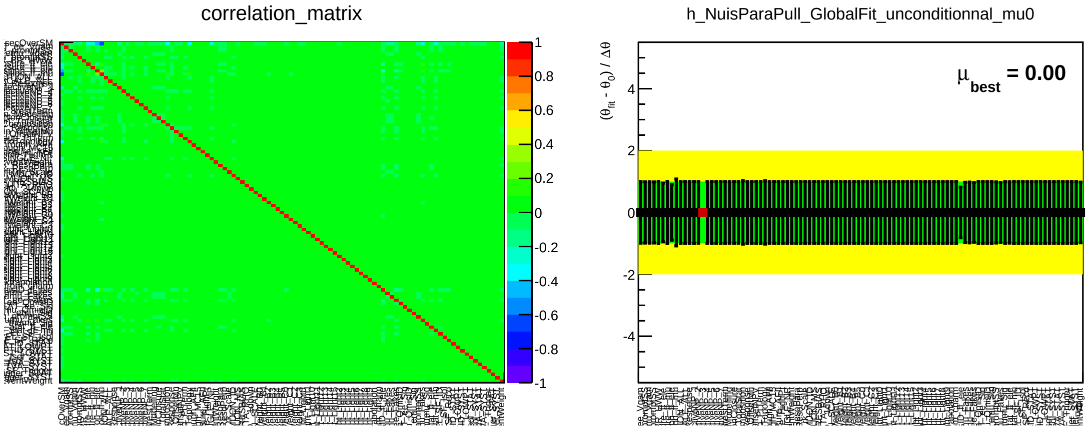

Figure 23: The correlations of NPs and pull checks for the search of mX=260 GeV with an unconditional fit to expected backgrounds only.

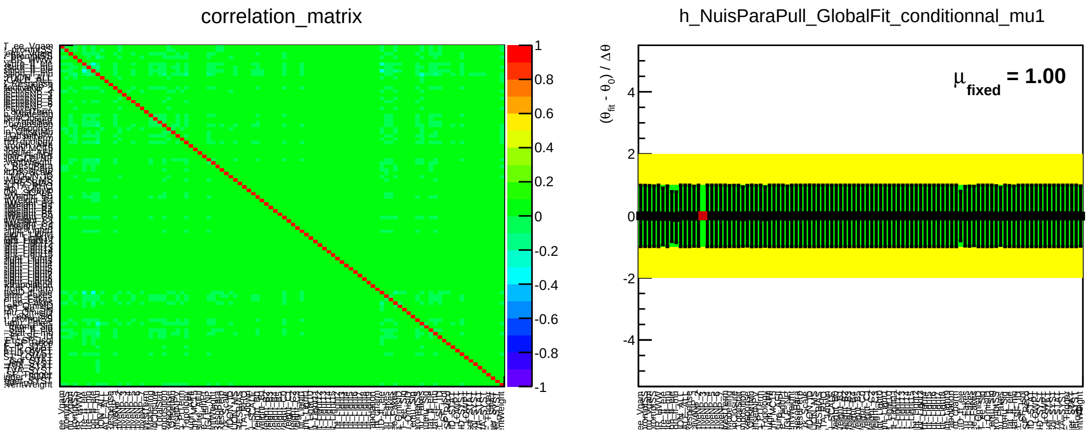

Figure 24: The correlations of NPs and pull checks for the search of mX=260 GeV with a conditional fit to expected signal plus backgrounds.

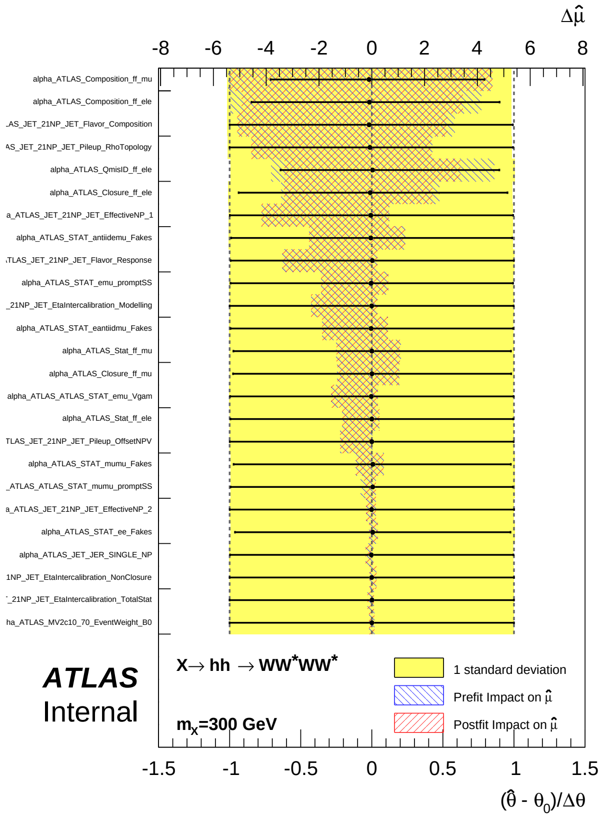

Figure 25: The ranking of NP impact on μ for the search of mX=300 GeV.

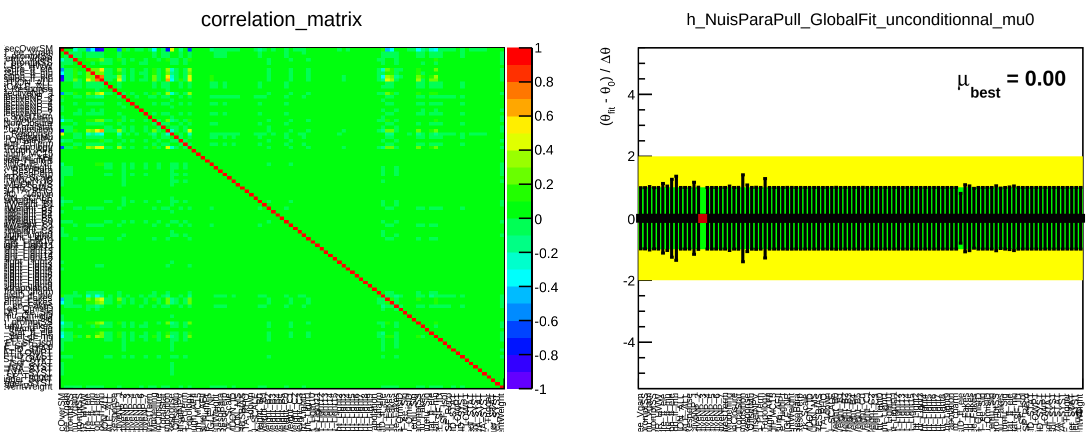

Figure 26: The correlations of NPs and pull checks for the search of mX=300 GeV with an unconditional fit to expected backgrounds only.

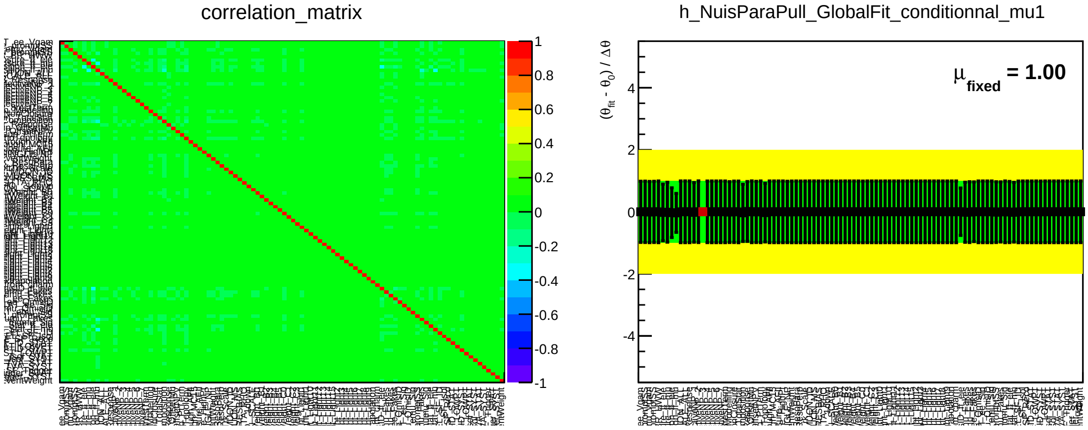

Figure 27: The correlations of NPs and pull checks for the search of mX=300 GeV with a conditional fit to expected signal plus backgrounds.

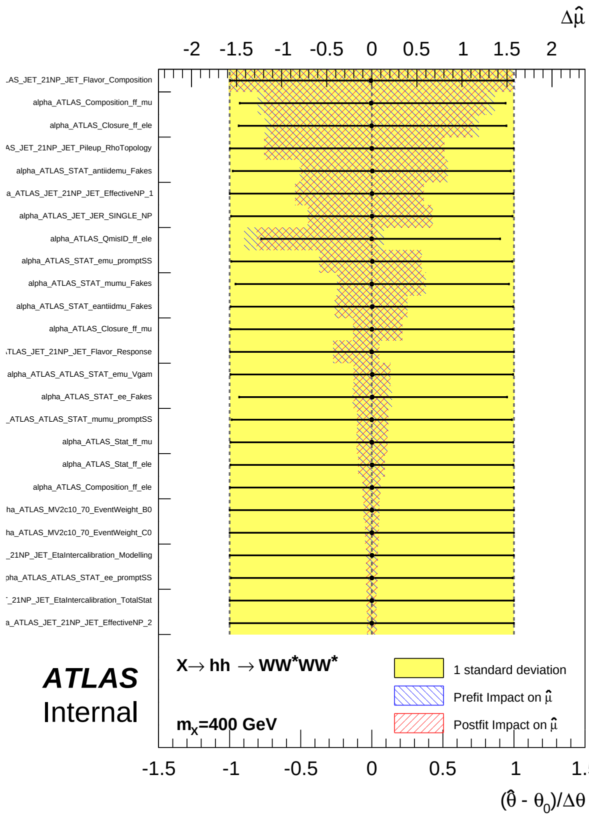

Figure 28: The ranking of NP impact on μ for the search of mX=400 GeV.

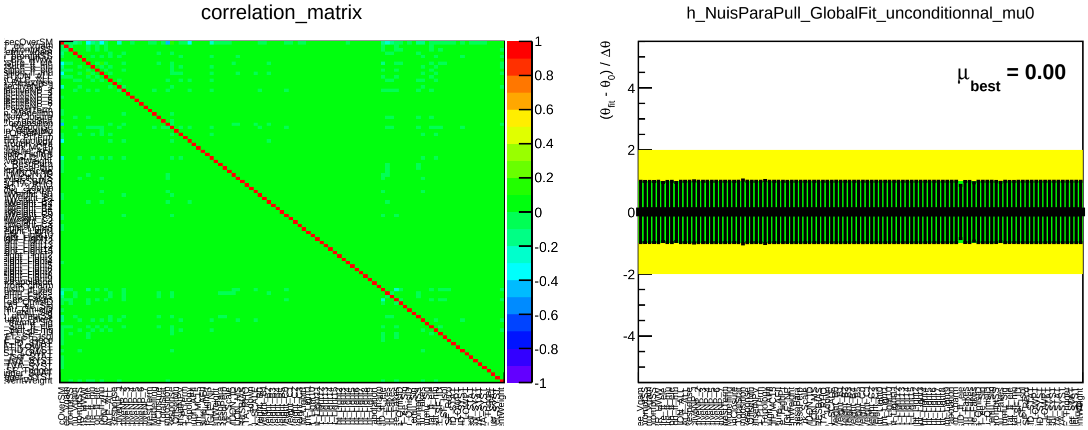

Figure 29: The correlations of NPs and pull checks for the search of mX=400 GeV with an unconditional fit to expected backgrounds only.

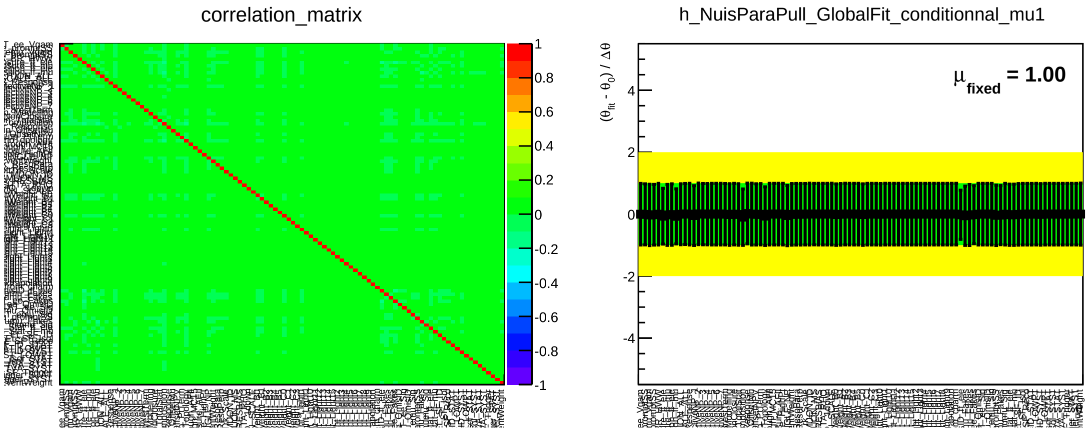

Figure 30: The correlations of NPs and pull checks for the search of mX=400 GeV with a conditional fit to expected signal plus backgrounds.

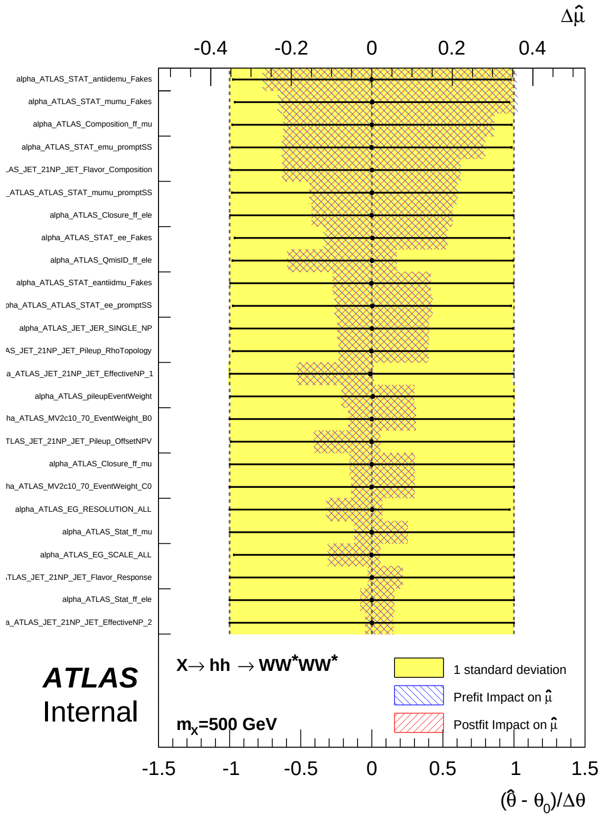

Figure 31: The ranking of NP impact on μ for the search of mX=500 GeV.

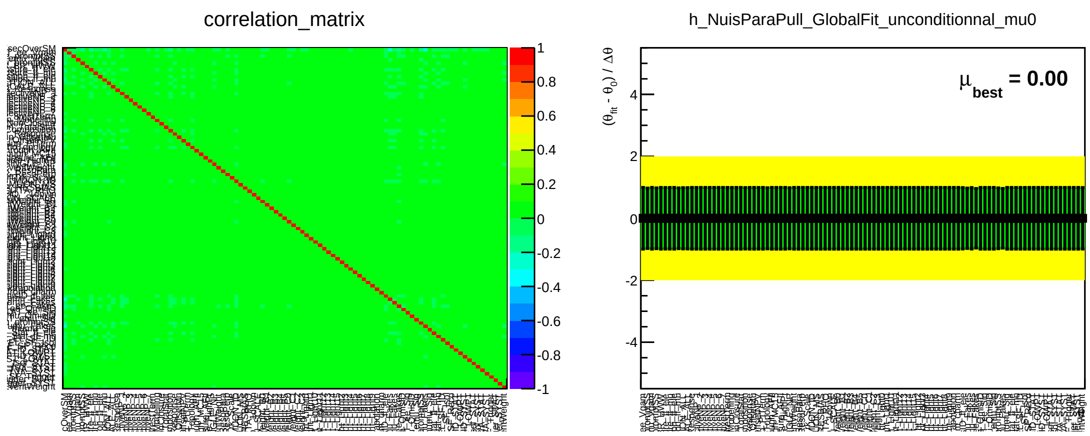

Figure 32: The correlations of NPs and pull checks for the search of mX=500 GeV with an unconditional fit to expected backgrounds only.

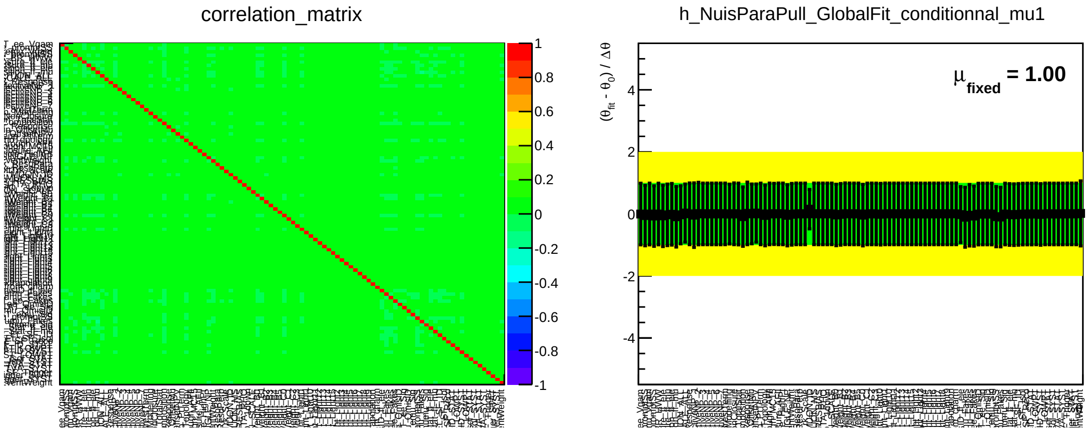

Figure 33: The correlations of NPs and pull checks for the search of mX=500 GeV with a conditional fit to expected signal plus backgrounds.

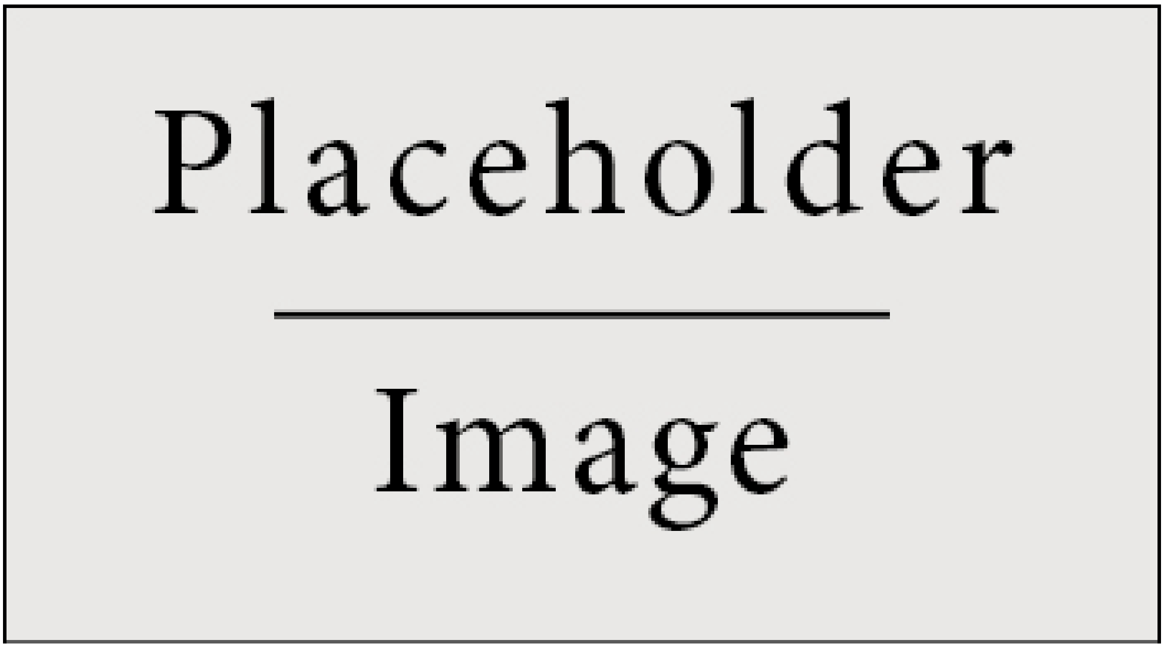

Figure 34: The correlations of NPs and pull checks for the search of mX=260 GeV with a fit to observed data.

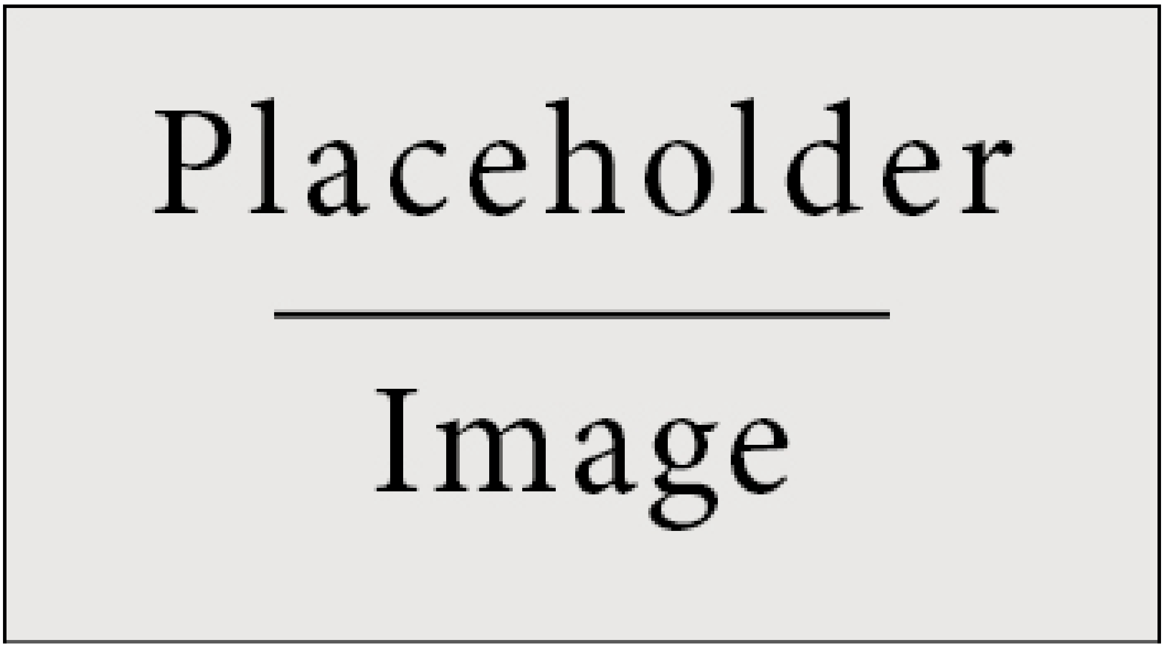

Figure 35: The correlations of NPs and pull checks for the search of mX=300 GeV with a fit to observed data.

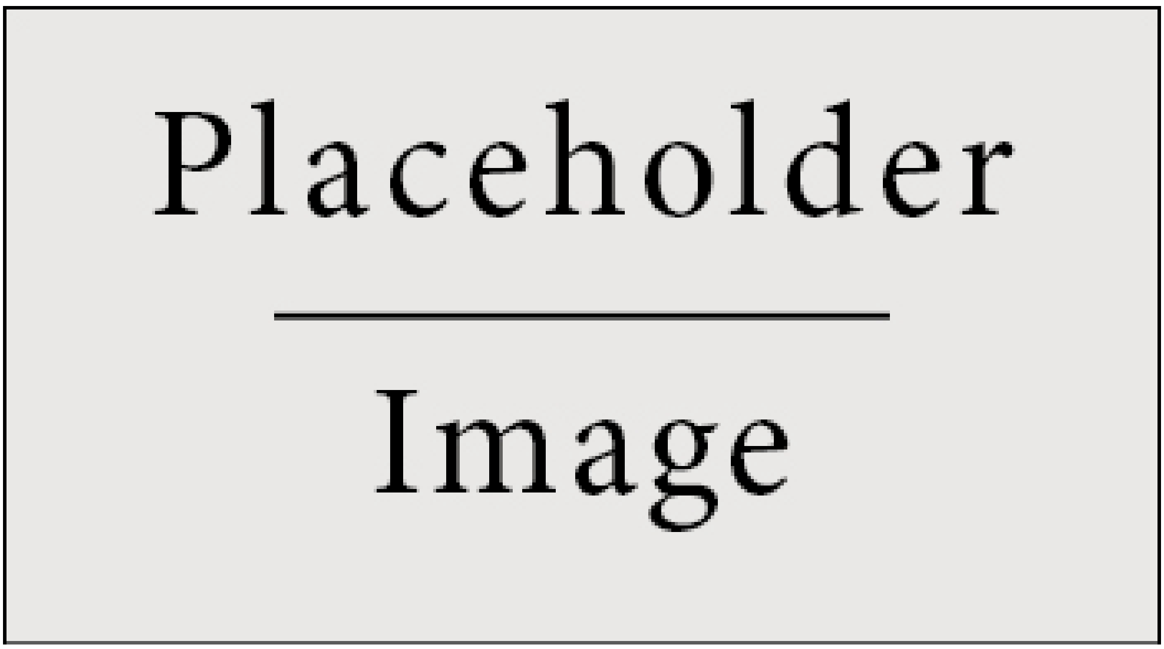

Figure 36: The correlations of NPs and pull checks for the search of mX=400 GeV with a fit to observed data.

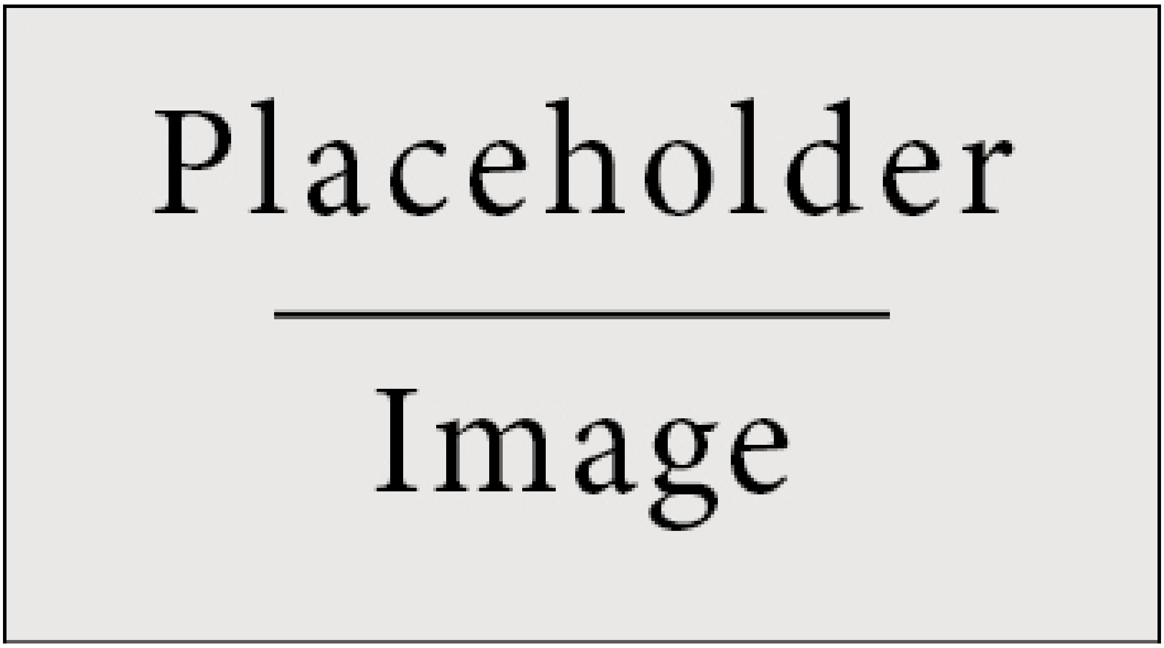

Figure 37: The correlations of NPs and pull checks for the search of mX=500 GeV with a fit to observed data.

I.2 The NP plots for $X \rightarrow SS$ searches

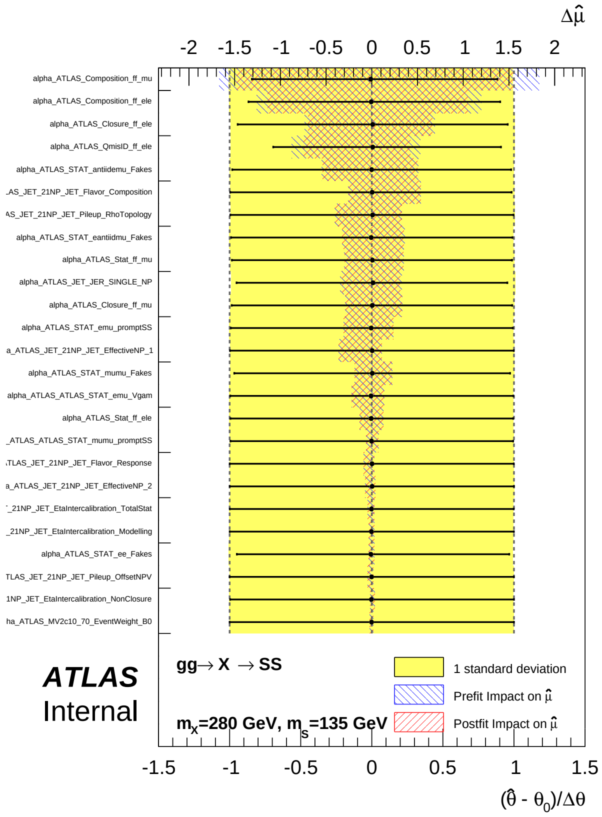

Figure 38: The ranking of NP impact on μ for the search of mX=280 GeV, mS=135 GeV.

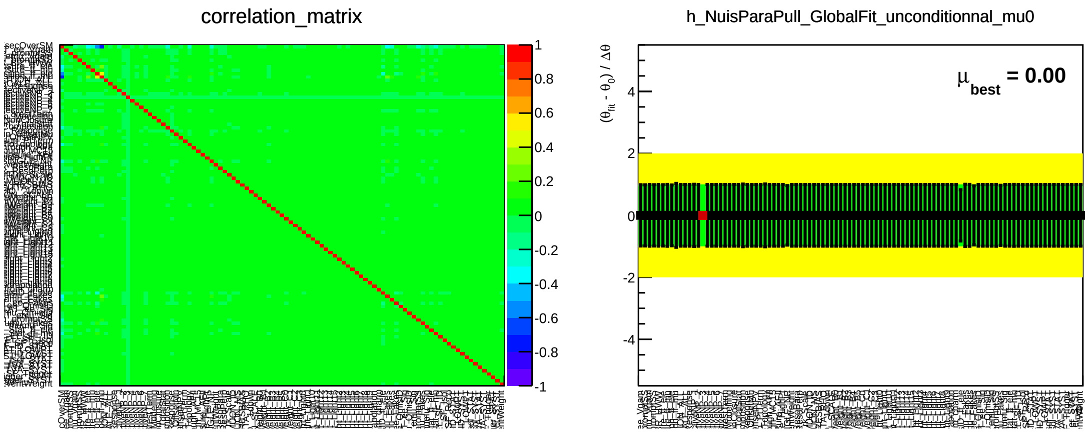

Figure 39: The correlations of NPs and pull checks for the search of mX=280 GeV, mS=135 GeV with a unconditional fit to expected backgrounds only.

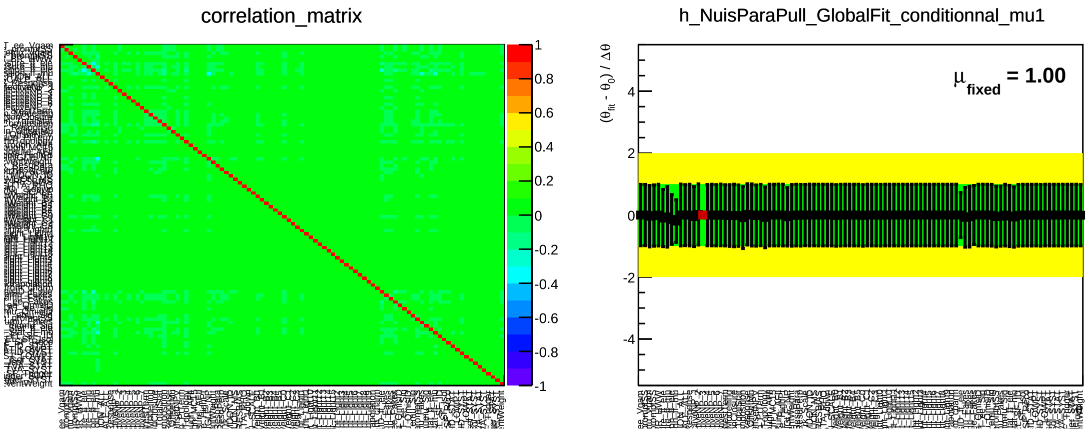

Figure 40: The correlations of NPs and pull checks for the search of mX=280 GeV, mS=135 GeV with a conditional fit to expected signal plus backgrounds.

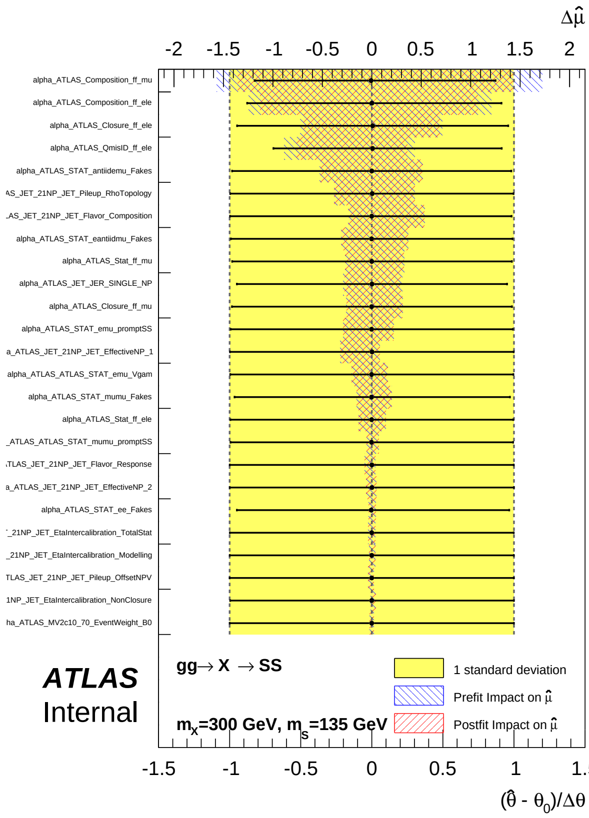

Figure 41: The ranking of NP impact on μ for the search of mX=300 GeV, mS=135 GeV.

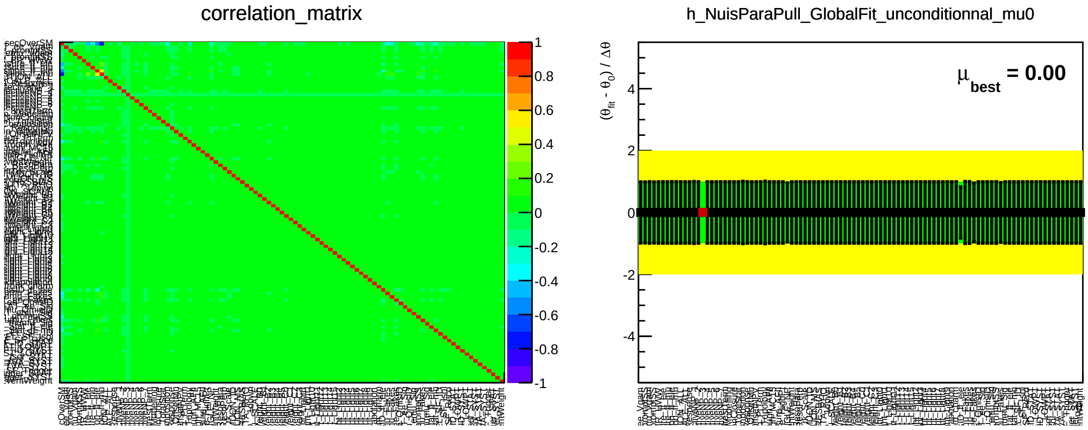

Figure 42: The correlations of NPs and pull checks for the search of mX=300 GeV, mS=135 GeV with a unconditional fit to expected backgrounds only.

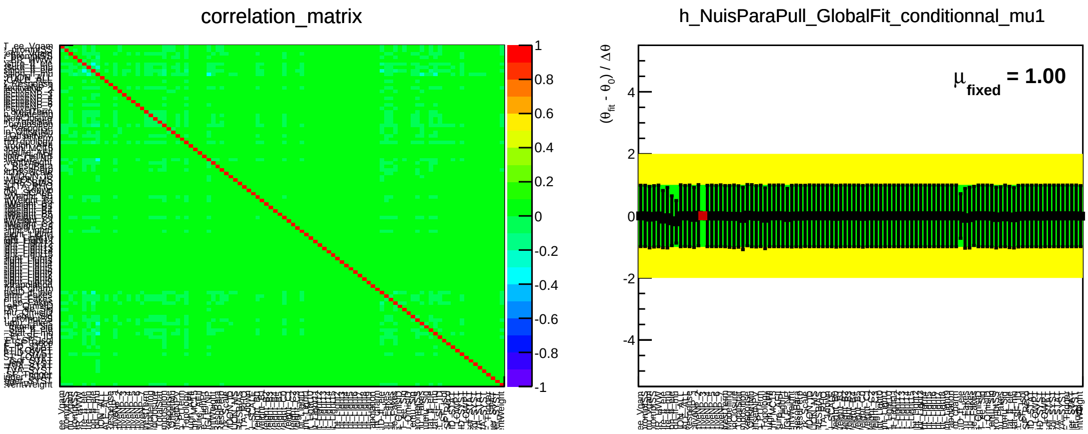

Figure 43: The correlations of NPs and pull checks for the search of mX=300 GeV, mS=135 GeV with a conditional fit to expected signal plus backgrounds.

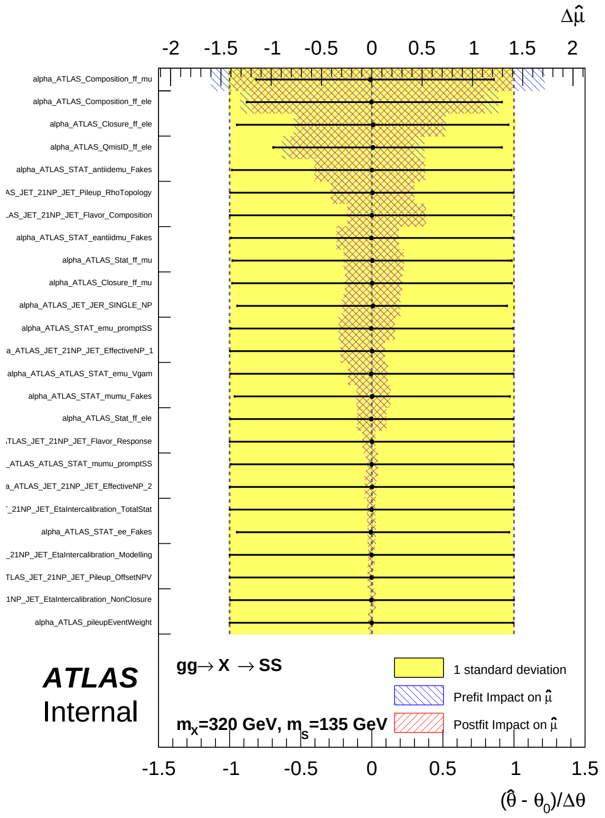

Figure 44: The ranking of NP impact on μ for the search of mX=320 GeV, mS=135 GeV.

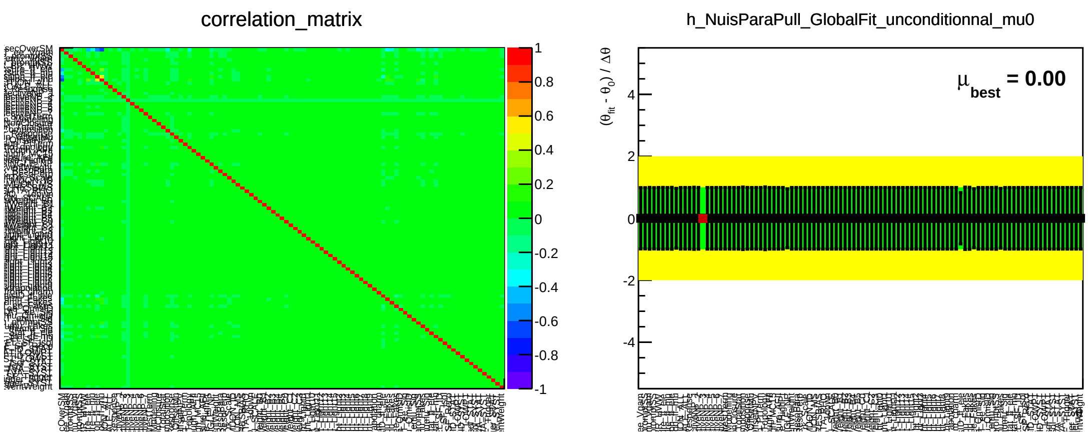

Figure 45: The correlations of NPs and pull checks for the search of mX=320 GeV, mS=135 GeV with a unconditional fit to expected backgrounds only.

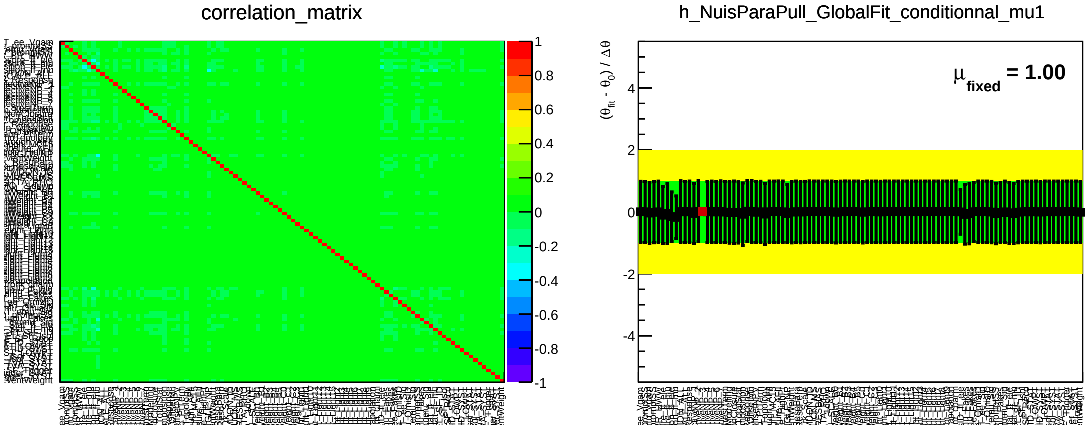

Figure 46: The correlations of NPs and pull checks for the search of mX=320 GeV, mS=135 GeV with a conditional fit to expected signal plus backgrounds.

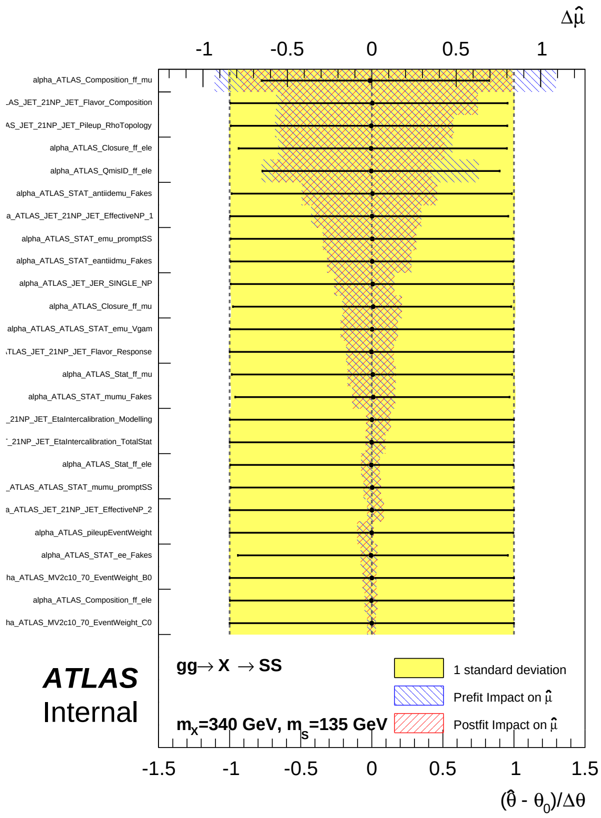

Figure 47: The ranking of NP impact on μ for the search of mX=340 GeV, mS=135 GeV.

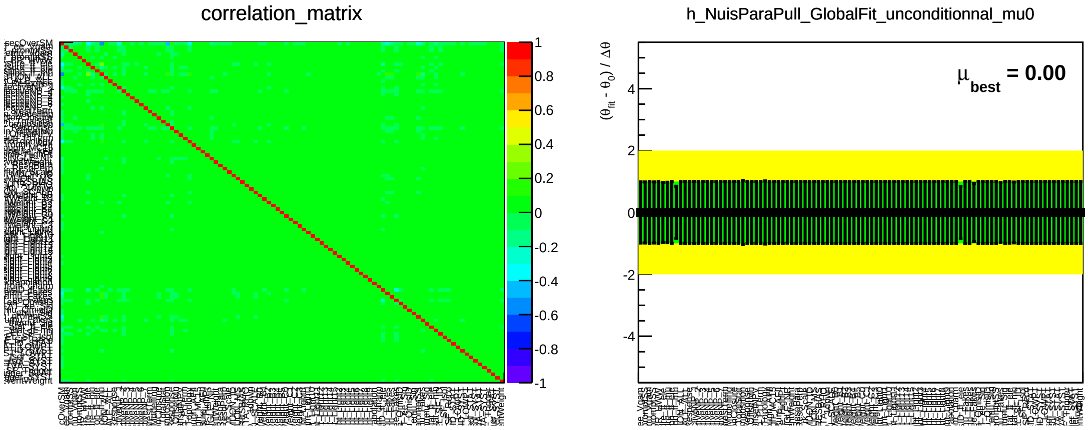

Figure 48: The correlations of NPs and pull checks for the search of mX=340 GeV, mS=135 GeV with a unconditional fit to expected backgrounds only.

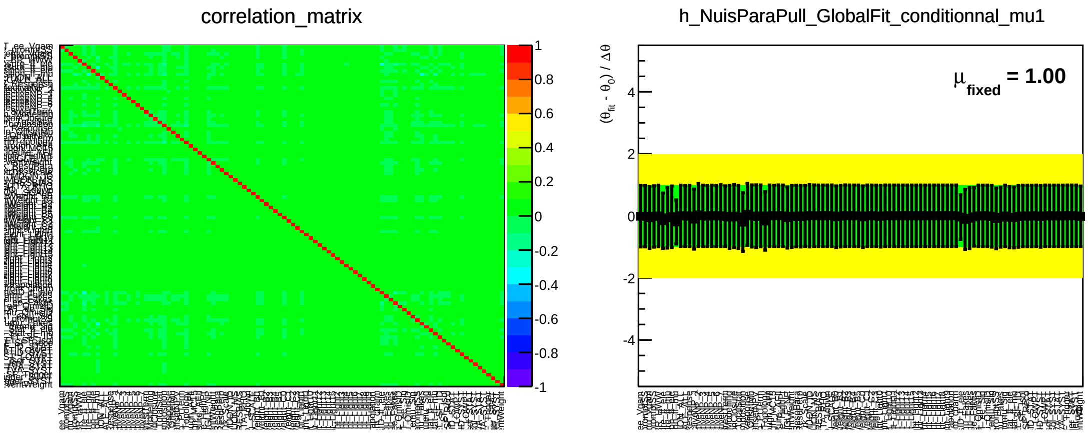

Figure 49: The correlations of NPs and pull checks for the search of mX=340 GeV, mS=135 GeV with a conditional fit to expected signal plus backgrounds.

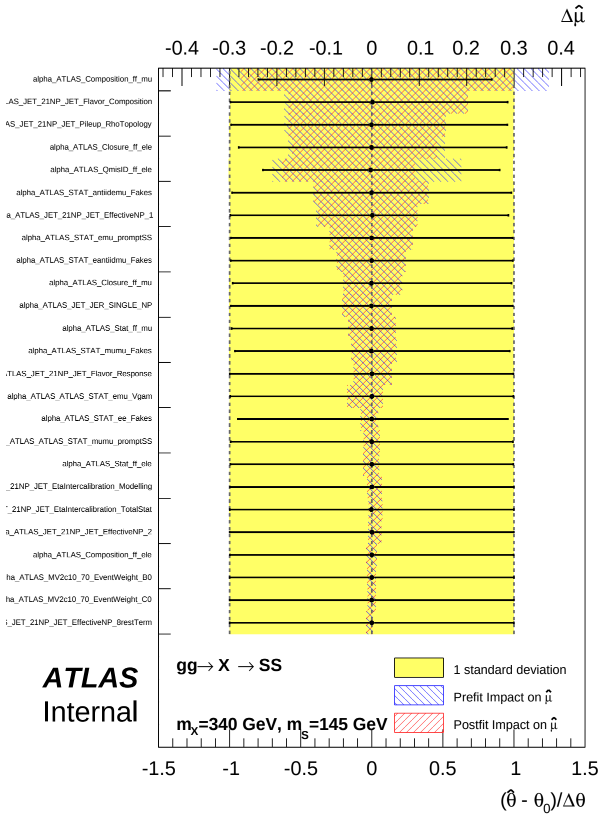

Figure 50: The ranking of NP impact on μ for the search of mX=340 GeV, mS=145 GeV.

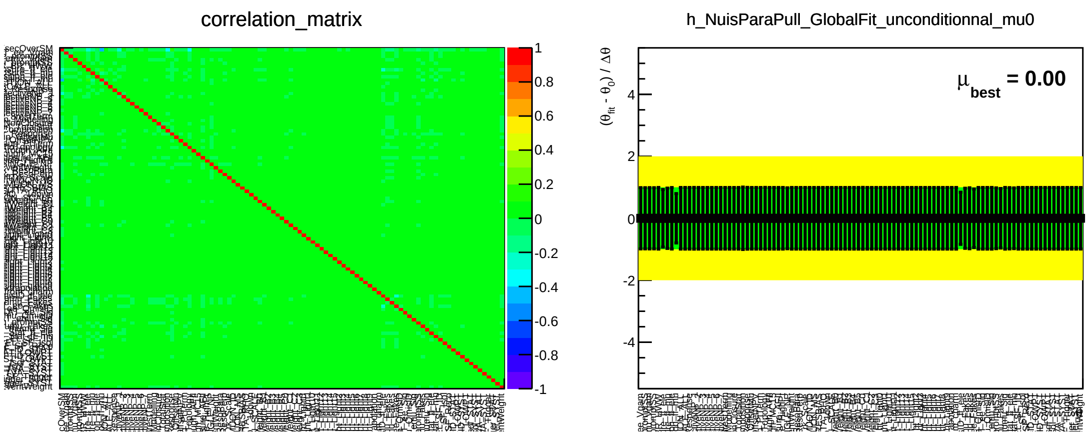

Figure 51: The correlations of NPs and pull checks for the search of mX=340 GeV, mS=145 GeV with a unconditional fit to expected backgrounds only.

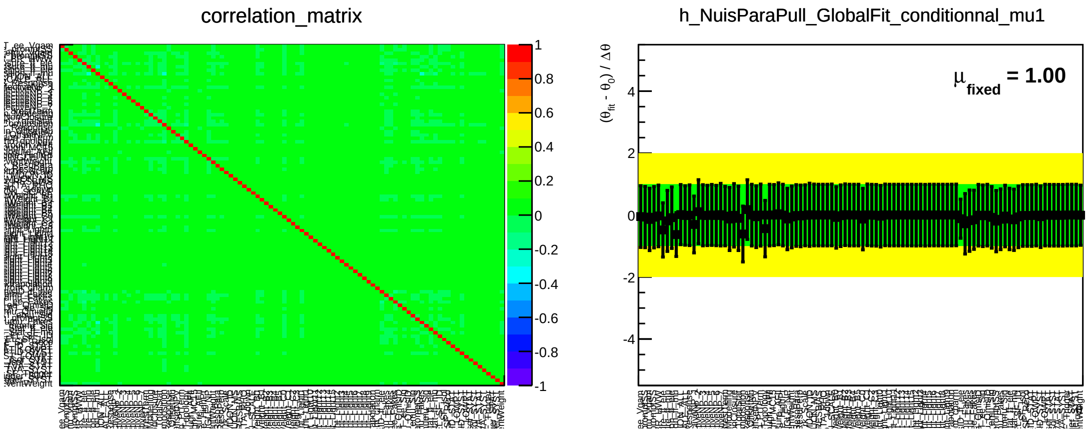

Figure 52: The correlations of NPs and pull checks for the search of mX=340 GeV, mS=145 GeV with a conditional fit to expected signal plus backgrounds.

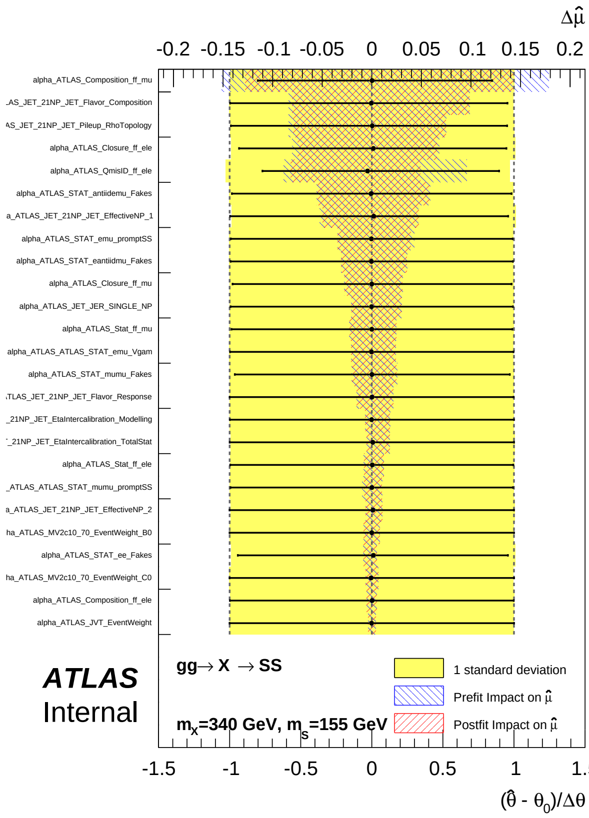

Figure 53: The ranking of NP impact on μ for the search of mX=340 GeV, mS=155 GeV.

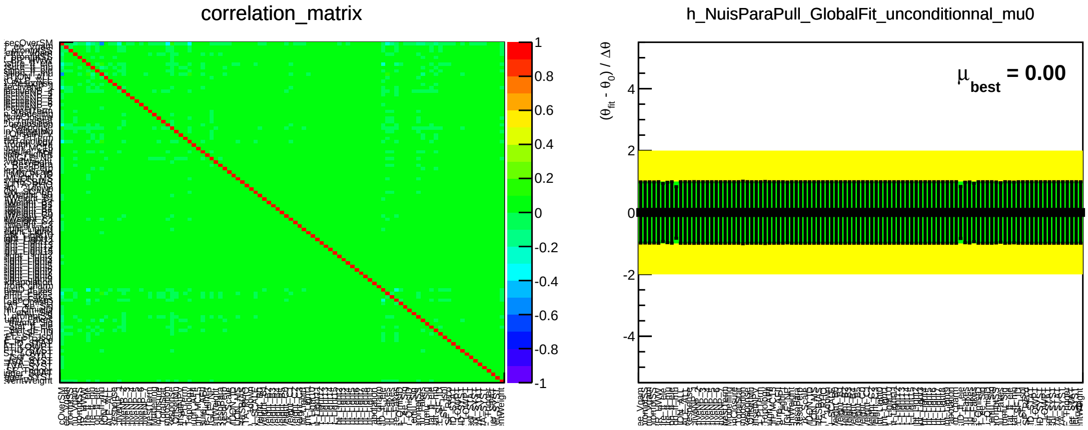

Figure 54: The correlations of NPs and pull checks for the search of mX=340 GeV, mS=155 GeV with a unconditional fit to expected backgrounds only.

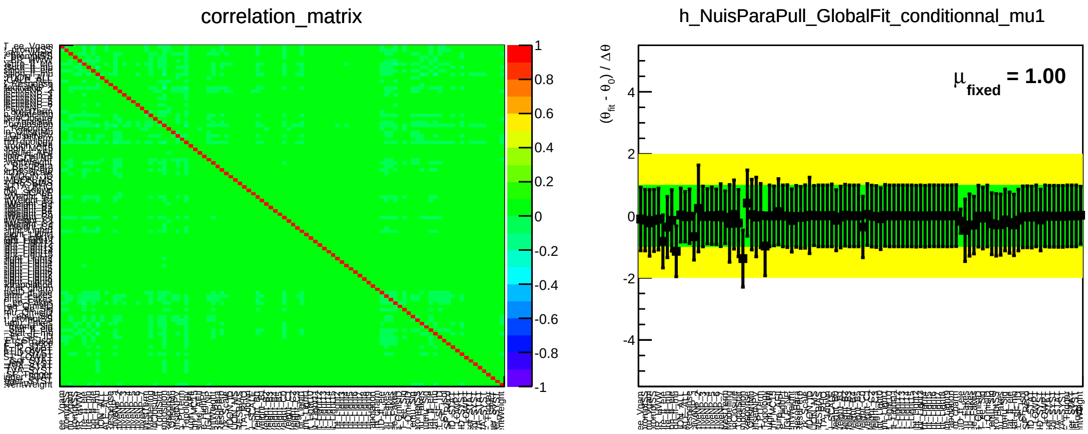

Figure 55: The correlations of NPs and pull checks for the search of mX=340 GeV, mS=155 GeV with a conditional fit to expected signal plus backgrounds.

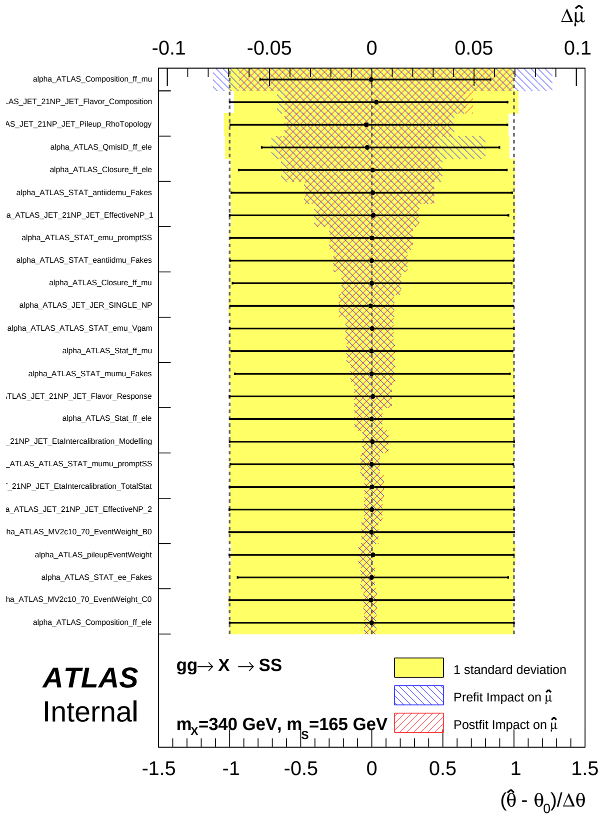

Figure 56: The ranking of NP impact on μ for the search of mX=340 GeV, mS=165 GeV.

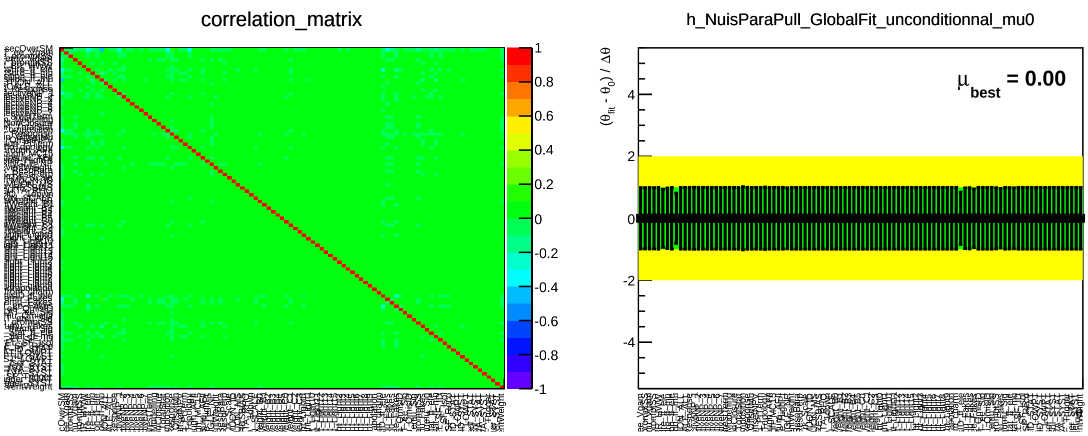

Figure 57: The correlations of NPs and pull checks for the search of mX=340 GeV, mS=165 GeV with a unconditional fit to expected backgrounds only.

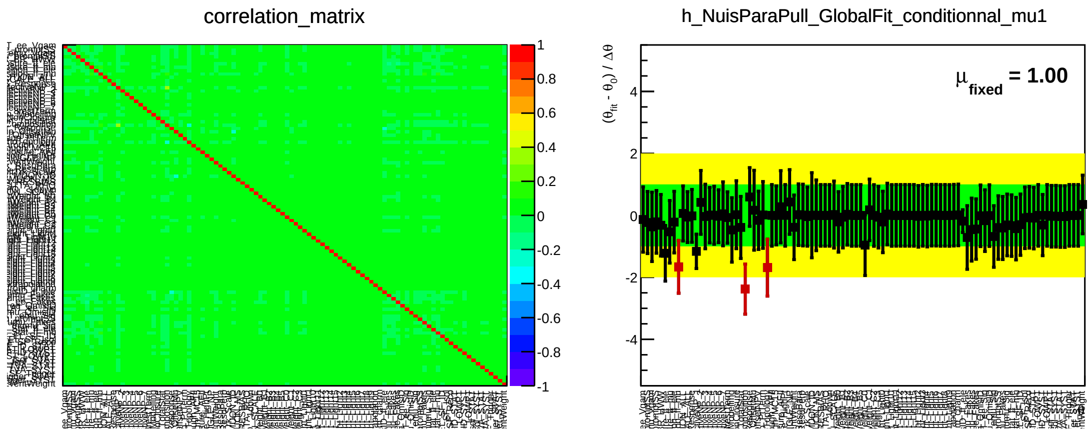

Figure 58: The correlations of NPs and pull checks for the search of mX=340 GeV, mS=165 GeV with a conditional fit to expected signal plus backgrounds.

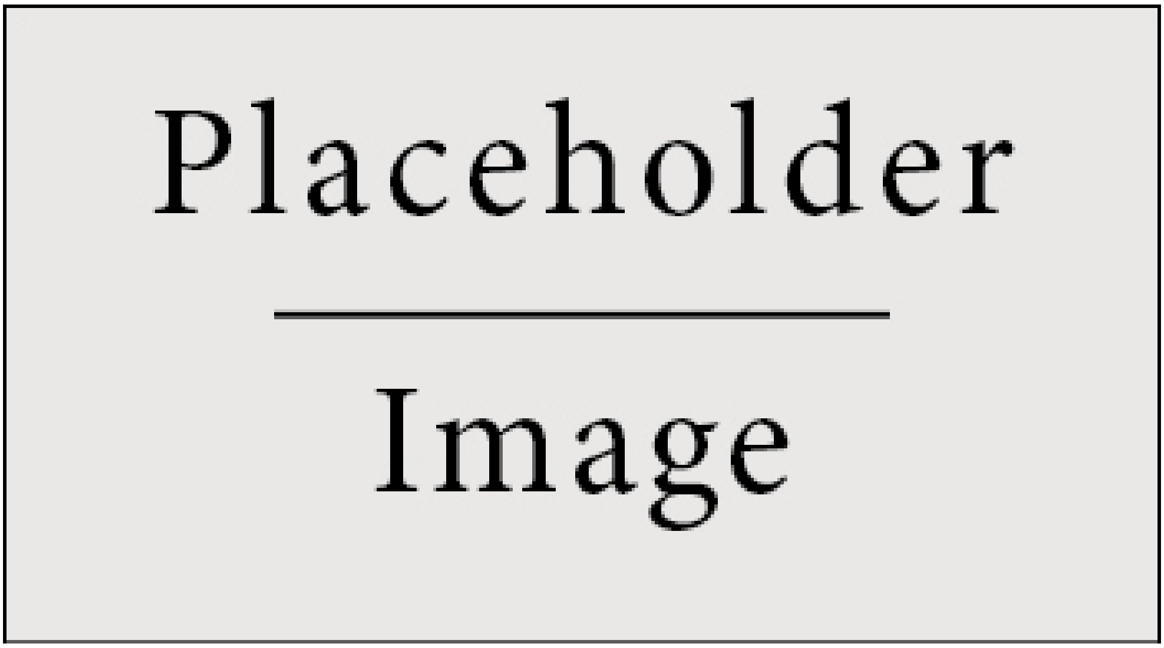

Figure 59: The correlations of NPs and pull checks for the search of mX=280 GeV, mS=135 with a fit to observed data.

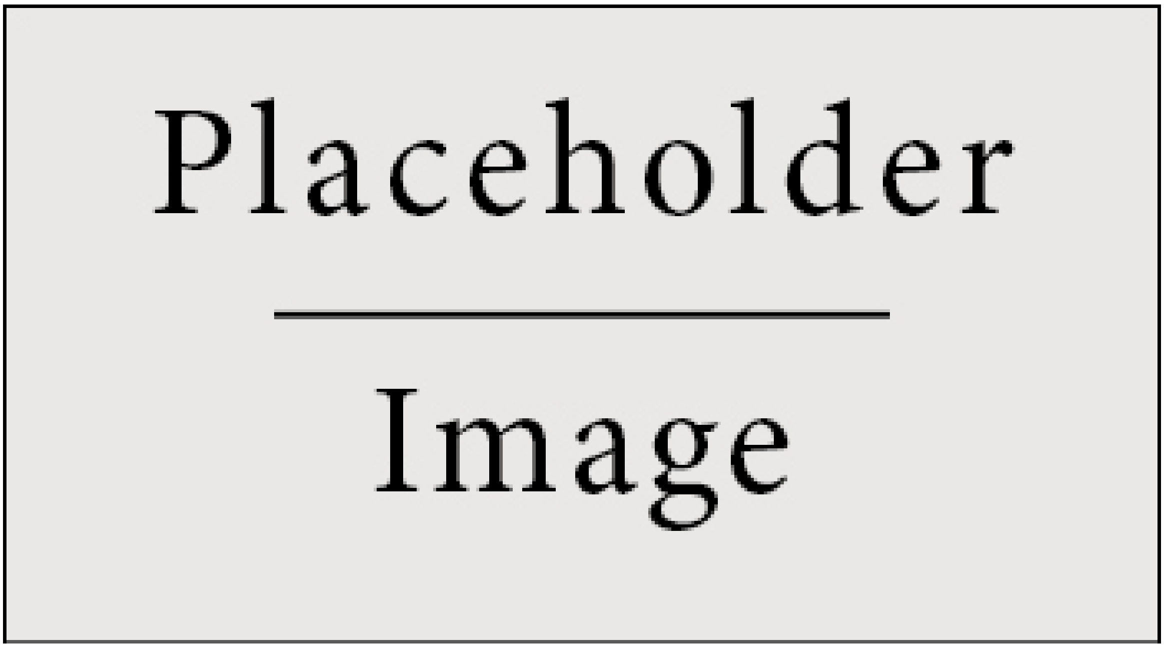

Figure 60: The correlations of NPs and pull checks for the search of mX=300 GeV, mS=135 with a fit to observed data.

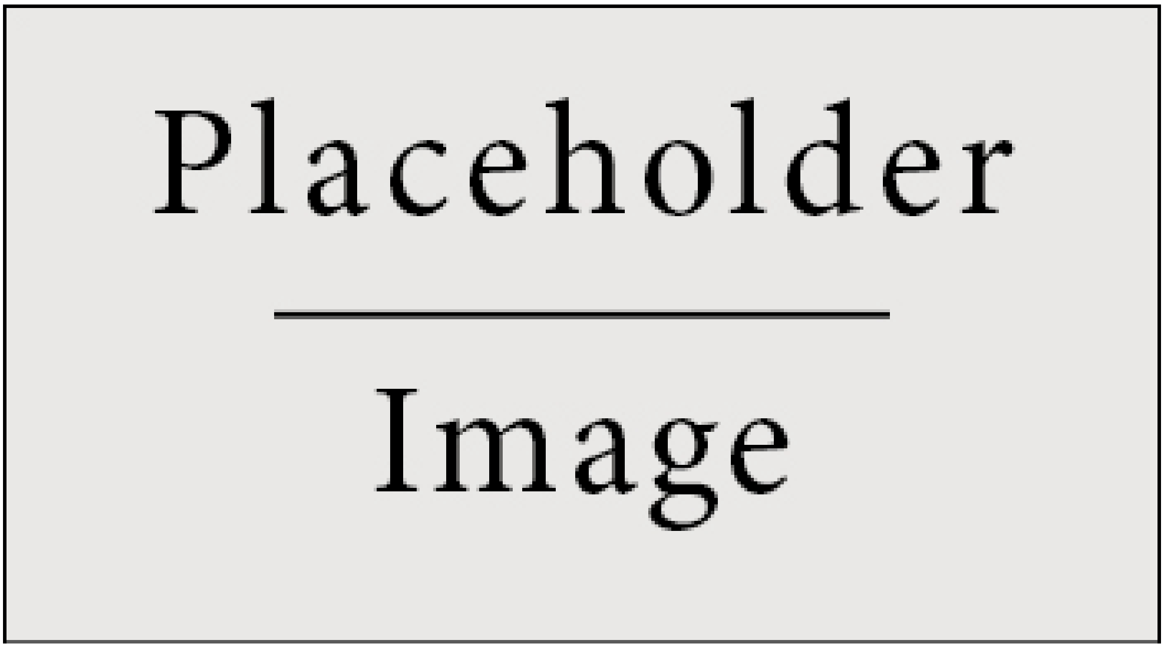

Figure 61: The correlations of NPs and pull checks for the search of mX=320 GeV, mS=135 with a fit to observed data.

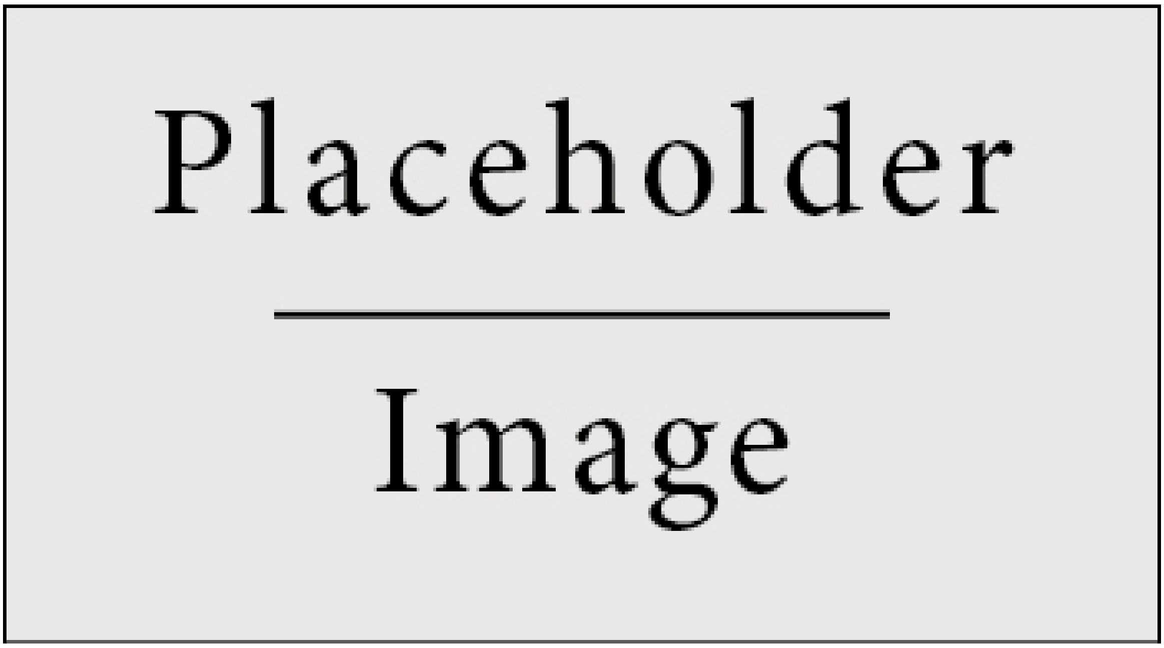

Figure 62: The correlations of NPs and pull checks for the search of mX=340 GeV, mS=135 with a conditional fit to observed data.

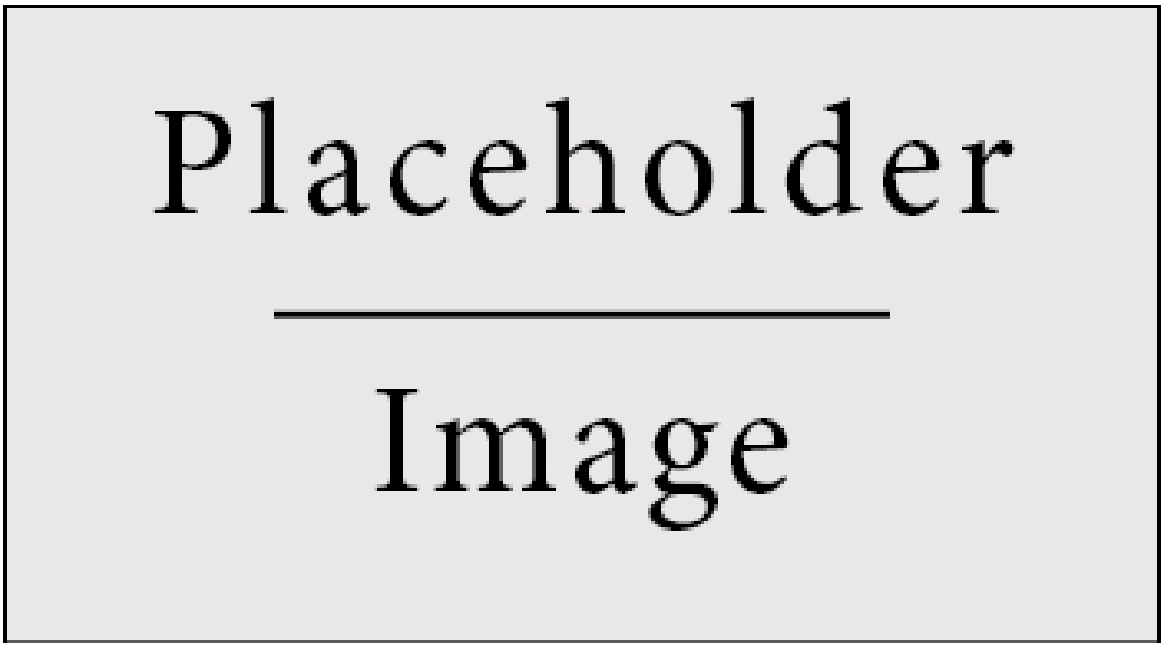

Figure 63: The correlations of NPs and pull checks for the search of mX=340 GeV, mS=145 with a fit to observed data.

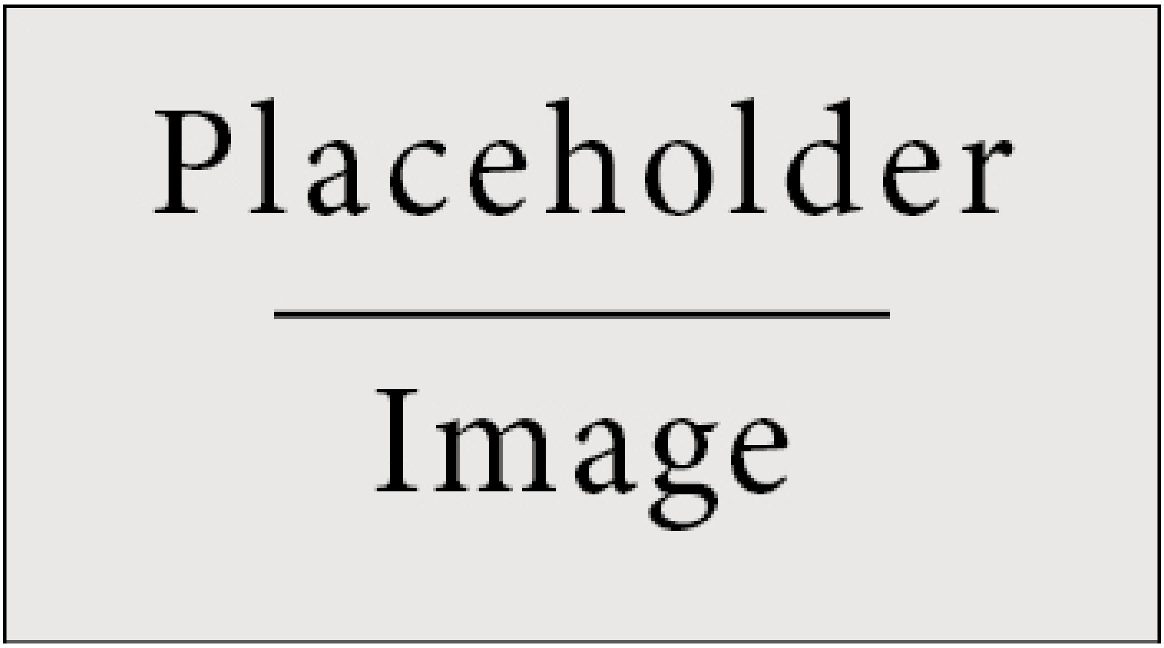

Figure 64: The correlations of NPs and pull checks for the search of mX=340 GeV, mS=155 with a fit to observed data.

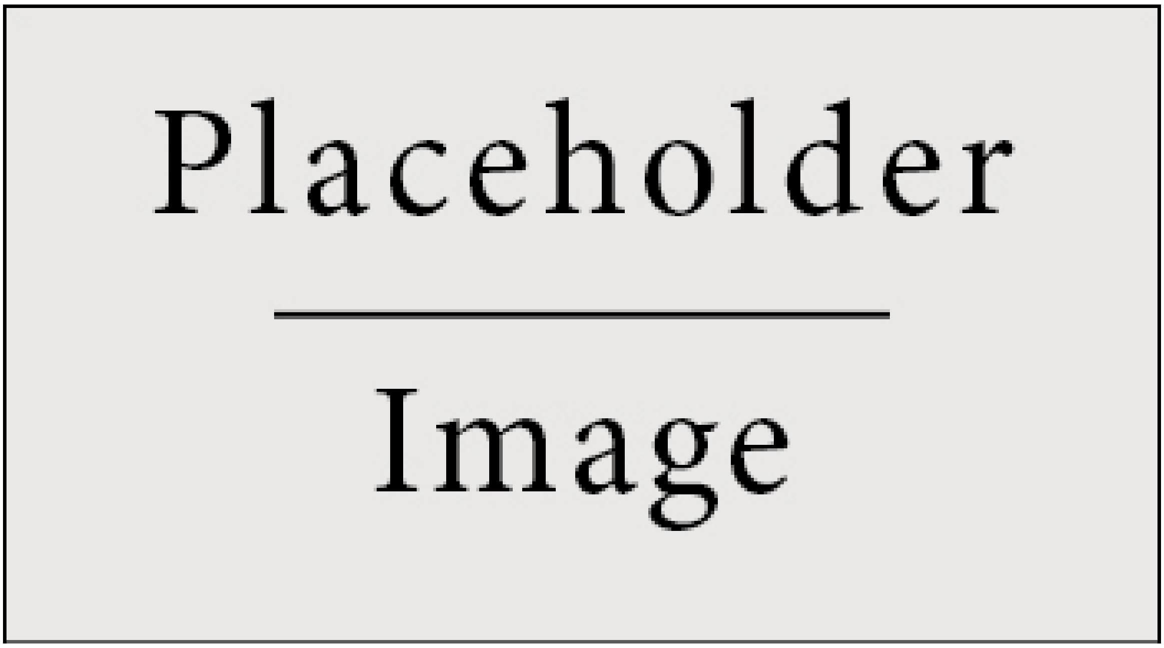

Figure 65: The correlations of NPs and pull checks for the search of mX=340 GeV, mS=165 with a fit to observed data.

List of contributions

Xinchou Lou	Supervisor of Maosen.
Yaquan Fang	Supervisor of Maosen.
Weiming Yao	Discussions on fakes estimations, supervisor of Maosen.
Liang Li	Supervisor of Xingguo Li.
Xiaohu Sun	Discussions on statistics, coordinate signal production
Xingguo Li	Technichal cross check on cut flow and fakes estimations.
Maosen Zhou	Sample production, design, optimization, statistical interpretations.